Aus der Chirurgischen Klinik
der Medizinischen Fakultät Charité – Universitätsmedizin Berlin

DISSERTATION

Enhancing Engineered Vascular Networks *in vitro* and *in vivo* Using Stem Cells and Growth Factors

zur Erlangung des akademischen Grades
Doctor medicinae (Dr. med.)

vorgelegt der Medizinischen Fakultät
Charité – Universitätsmedizin Berlin

von

Claudia C. Friedrich, M.Sc.
aus Berlin

Datum der Promotion: 06.03.2020

INHALTSVERZEICHNIS

1 Zusammenfassung der Dissertation

1.1 Abstract (abgefasst in englischer Sprache)

Introduction

Creating functional vasculature remains one important goal to improve or restore human tissue function in disease or after trauma. However, mechanisms and pleotropic effects involved, especially with regard to osteogenic regeneration, remain poorly understood. We here hypothesized, that angiogenic human umbilical vein endothelial cells (HUVEC) combined with stabilizing, proangiogenic properties of multipotent mesenchymal stem cells (MSC) might enhance vascular network formation. Using different *in vitro* and *in vivo* models, we here addressed aspects of vasculogenesis, vascular functionality and network formation in the context of bone formation.

Methods

We developed two vascularization protocols, one for angiogenesis in a collagen-fibronectin matrix using MSC and HUVEC and one for vascularizing bone grafts using additionally pre-induced and non-induced MSC from human bone marrow. We then tested the impact of recombinant insulin-like growth factor 1 (IGF1) protein and IGF1 expressing HEK293 cells upon vasculogenesis *in vitro* and as subcutaneous implants within immunodeficient mice to investigate anastomoses with the host vessels and functionality. Subsequently we performed morphometric analysis. Thereafter, we harvested bone marrow stromal cells from alpha-smooth muscle actin GFP (α-SMA-GFP) transgenic mice, sorted them by Fluorescence-activated cell sorting (FACS) and applied 3D cell culture model to test their ability to support vascularization.

Results

Endothelial cells formed stable vascular networks *in vitro* and throughout bone scaffolds implanted into NOD SCID mice, when co-cultured with MSC ($p < 0.05$ vs. controls, Objective 1). MSC induced with osteogenic medium showed enhanced bone formation and mineralization after 8 weeks as evidenced by van Kossa and Alizarin red staining (Objective 2). We significantly enhanced *de novo* vasculogenesis *in vitro* and *in vivo* by using IGF1 ($p < 0.05$, Objective 3). Anastomosis occurred by day 11 as visualized by fluorescent labeling of cells and by visualization of blood flow using Quantum dots thereby proving functionality of the engineered vascular networks (Objective 4). α-SMA-GFP positive cells were confirmed as a subpopulation of pericytes that stimulated tube-formation of endothelial cells (Objective 5).

Conclusion

Our data provide first evidence that the use of cellular components yields higher-quality grafts and enables perfusion within the bone scaffolds upon anastomosis. Furthermore, the use of MSC differentiated into vascular lineages results in longer lasting, viable autologous vascularized bone grafts, and osteogenic induction of MSC enhances bone formation and mineralization within the scaffold. Moreover, we were able to show that IGF1 further enhances engineered capillary-like vasculature, which

we attribute to its pleiotropic effects, and by visualizing blood flow in a SCID mouse model *in vivo* through the anastomosed host and graft vessels we were able to testify the functionality of anastomoses and engineered vessels. Finally, we were able to further characterize the relation of MSC and pericytes. The strategies combined suggest a promising approach to engineer *de novo* vasculature to support tissue regeneration. Confirmatory future experiments are urgently needed with a focus on vascular remodeling and long-term results of engineered vessels.

1.2 Abstrakt (abgefasst in deutscher Sprache)

Einleitung

Die Züchtung funktionsfähiger Gefäße aus patienteneigenen Stammzellen und Endothelzellen scheint essentiell, um menschliche Gewebsfunktion nach Unfällen oder infolge von Krankheiten zu verbessern oder wiederherzustellen. Jedoch sind zugrundeliegende Mechanismen und pleiotrope Effekte, insbesondere im Kontext der Knochenregeneration, unzureichend verstanden. Wir postulieren, dass die Kombination menschlicher gefäßbildender Endothelzellen der Umbilikalvene (HUVEC) mit multipotenten, mesenchymalen Stammzellen (MSC) die Bildung kapillarähnlicher Gefäße verbessern kann. Im vorliegenden Manuskript diskutieren wir anhand von *in vitro* und *in vivo* durchgeführten Versuchsreihen verschiedene Aspekte der Vaskulogenese, der Funktionalität gezüchteter Gefäße auch hinsichtlich der Knochenregeneration.

Methoden

Zunächst etablierten wir zwei Vaskularisierungs-Protokolle. Im ersten Modell kombinierten wir eine kollagen-fibrogenhaltige Matrix mit MSC und HUVEC, im zweiten Modell setzen wir zusätzlich osteogen induzierte MSC von Knochenmarksspenden ein, um die Bildung vaskularisierter Knochentransplantate zu simulieren. Wir testeten dann den Einfluss rekombinanten insulin-like growth factor 1 (IGF1) Proteins sowie einer IGF1 exprimierenden HEK293 Zelllinie auf die Vaskulogenese *in vitro* und als subkutane Implantate in einem NOD SCID Mausmodell, um die Anastomosenbildung mit den Wirtsgefäßen und ihre Funktionsfähigkeit zu untersuchen, die wir anschließend morphometrisch analysierten. Zusätzlich wurden Stromazellen des Knochenmarks alpha-smooth muscle actin GFP (α-SMA-GFP) positiver transgener Mäuse gewonnen, mittels Fluorescence-activated cell sorting (FACS) sortiert und in einem dreidimensionalen Zellkultur-Modell bezüglich ihrer Effekte auf die Gefäßneubildung untersucht.

Ergebnisse

Die Endothelzellen bildeten stabile, dichte kapillarähnliche Netzwerke *in vitro* und in der gesamten subkutan implantierten, zellbeschickten Knochenmatrix im NOD SCID Mausmodell im Gegensatz zur Kontrollgruppe unter Standardbedingungen ($p < 0.05$ vs. Kontrollgruppen, Zielstellung 1). Induzierte MSC verbesserten die Knochenbildung und -mineralisierung nach 8 Wochen, wie wir histologisch mittels van Kossa und Alizarinrotfärbung zeigen konnten (Zielstellung 2). Die Anreicherung mit IGF1

verbesserte die *de novo* Vaskulogenese signifikant *in vitro* und *in vivo* ($p < 0.05$, Zielstellung 3). Anastomosenbildung begann ab Tag 11, wie anhand von Fluoreszenzfärbungen der Zellen gezeigt werden konnte. Durch Visualisierung des Blutflusses mittels Quantum dots konnten wir auch die Funktionalität der gezüchteten vaskulären Netzwerke bestätigen (Zielstellung 4). Darüberhinaus konnten wir α-SMA-GFP positive Zellen als Subpopulation von Perizyten nachweisen (Zielstellung 5).

Diskussion

Die Strategien in Kombination zeigen einen vielversprechenden Ansatz auf, die *de novo* Züchtung von Blutgefäßen zu verbessern, um die Regeneration von funktionellem Gewebe zu unterstützen. Zukünftige Experimente sollten die Langzeiteffekte und Re-Modellierung gezüchteter Gefäße untersuchen.

1.3 Introduction with Objectives

For more than a decade, ischemic diseases have been the leading cause of death globally according to Global Health Observatory data (WHO, 2017a). Ischemic heart disease alone led to 8.8 million deaths in 2015 (WHO, 2017b). Despite well-established therapies, ischemic diseases in advanced stages are life-threatening and led to 8.8 million deaths in 2015 (Bonaros et al., 2005; WHO, 2017b). Hence, new strategies need to be developed and implemented to address this situation. Various approaches for vascular graft tissue engineering have been investigated using technologies in cell engineering, stem cell biology, materials science and medicine (Li et al., 2014). While autologous grafts are known to lead to yet the best clinical outcome, their availability is limited and associated with a risk of morbidity and mortality to both donor and recipient (Berner et al., 2013). Therefore, creating functional and durable engineered blood vessels is an important goal within the field of regenerative medicine. In particular, engineered biological vasculature has the potential to improve or restore human tissue function substantially (Au et al., 2008; Melero-Martin et al., 2008; Shepherd et al., 2004; Silvestre et al., 2013).

Clinical protocols have utilized bone marrow to improve, restore or even to correct tissue function (Hsiao et al., 2012; Joensuu et al., 2015; Muscari et al., 2010). Hence, we aimed to investigate how bone grafts enhance scaffold function, promote vascularization and vascular remodeling (Cao and Li, 2015; Guyette et al., 2014; Hanley, 2015). Bone marrow contains vital cells, growth factors and cytokines that are known to improve human tissue function and repair as marrow-derived cytokines induce host neovascularization at the graft surface, however not yet sufficiently at the core, where hypoxic conditions cause significant cell death (Liu et al., 2015). We looked into using human multipotent mesenchymal stem cells (MSC) and to co-culture them with the angiogenic human umbilical cord endothelial cells (HUVEC) that would both stimulate each other to form new blood vessels (de novo vasculogenesis). While MSC have the ability to differentiate into various mesenchymal tissues like bone, cartilage, muscle tissue and adipose tissue, we aimed to use their stabilizing proangiogenic properties to support endothelial tube formation and maturation by paracrine signaling of growth factors like vascular endothelial growth

factor (VEGF), a potent stimulant of de novo vasculogenesis. In parallel, we intended to investigate the effects of pericytes on blood vessel formation when coculture with HUVEC as they are interdependent for pericyte differentiation and endothelial cell maturation mediated by Angiopoietin 1, Tie-2, transforming growth factor beta (TGF-β) and platelet-derived growth factor (PDGF).

1.3.1 Objective 1: High-quality Grafts

Cellular components are well-known to generate extensive primitive plexus-like vascular networks which may potentially enable perfusion of the entire scaffold upon anastomosis. Therefore, we hypothesized that the addition of cellular components might yield high-quality grafts and reduced hypoxia within larger grafts.

1.3.2 Objective 2: Osteogenic Induction of MSC to Enhance Scaffold Mineralization

The ability of MSC to differentiate in vascular and bone lineages could lead to potentially novel therapeutic strategies due to the stabilizing effect of MSC resulting in longer lasting, viable autologous vascularized bone grafts (Fransson et al., 2015; Weinand et al., 2007). Therefore, we hypothesized, that osteogenic induction of MSC would enhance bone formation and mineralization within the scaffolds.

1.3.3 Objective 3: Sustained IGF1 Delivery to Enhance Vasculogenesis

Endothelial progenitor cells are crucially needed for tube formation, maintenance, and anastomoses with the host vasculature (Amini et al., 2012). We hypothesized, that besides the co-culture of HUVEC and MSC with culture medium containing the well-established VEGF the pleiotropic effects of insulin-like growth factor 1 (IGF1) would enhance the engineered capillary-like vasculature. In particular, we aimed to compare the effects of the recombinant IGF1 protein with genetically engineered IGF1 expressing immortalized HEK cells for sustained IGF1 delivery.

1.3.4 Objective 4: Functionality and Anastomosis with Host Vasculature

We aimed to investigate the vascularization setups for functionality and anastomoses with the capillaries of the host. We set up a NOD SCID mouse model to investigate vasculogenesis of human cells *in vivo*. Since SCID mice do not display immunity, this allowed us to study vasculogenesis of human cells *in vivo* without interaction with the host immune system.

1.3.5 Objective 5: Investigation of Relation of Pericytes and MSC

Although it has been established, that stromal cells like pericytes or MSC are essential to vascularization (Bergers and Song, 2005), the relation of pericytes and MSC still remains unclear (Quattrocelli et al., 2012; Tonlorenzi et al., 2017). Hence, we aimed to further characterize their specific role and relation in vasculogenesis. As part of this investigation, we aimed to study the characteristics of smooth muscle actin alpha (α-SMA) positive cells and their effects on endothelial cells (Crisan et al., 2012), and how they impact vasculogenesis.

Parts of the present manuscript have been published in:

1. Friedrich C, Lin Y, Krannich A, Wu Y, Vacanti JP, Neville CM. Enhancing engineered vascular networks *in vitro* and *in vivo*: The effects of IGF1 on vascular development and durability. Cell Prolif. 2017 Nov 7. doi: 10.1111/cpr.12387.
2. Tsigkou O, Pomerantseva I, Spencer JA, Redondo PA, Hart AR, O'Doherty E, Lin Y, Friedrich C, Daheron L, Lin CP, Sundback CA, Vacanti JP, Neville C. Engineered vascularized bone grafts. Proc Natl Acad Sci U S A. 2010 Feb 23;107(8):3311-6. doi: 10.1073/pnas.0905445107. Epub 2010 Feb 2. PMID: 20133604
3. Cai X, Lin Y, Friedrich C, Neville C, Pomerantseva I, Sundback CA, Zhang Z, Vacanti JP, Hauschka PV, Grottkau BE. Bone marrow derived pluripotent cells are pericytes which contribute to vascularization. Stem Cell Rev. 2009 Dec;5(4):437-45. doi: 10.1007/s12015-009-9097-6. Erratum in: Stem Cell Rev. 2009 Dec;5(4):435-6. PMID: 20058207

1.4 Materials and Methods

1.4.1 Materials

We first engineered 3D porous bone scaffolds from the copolymer poly-DL-lactide-co-glycolidic acid (85/15) using the sucrose leaching technique resembling native bone structure. The scaffolds served as a matrix for stem cell attachment differentiating into the osteoblastic lineage and for tube formation in 3D by endothelial cells. We purchased HUVEC derived from pooled umbilical veins (Lonza) as HUVEC represent a standard model system to study angiogenesis and endothelial cell function. We obtained MSC from the bone marrow of patients undergoing hip replacement surgery with the consent of the patients and approval of the Institutional Review Board of Massachusetts General Hospital. We established MSC cultures as previously described (Cai et al., 2009). We used flow cytometry to characterize the presence of established surface

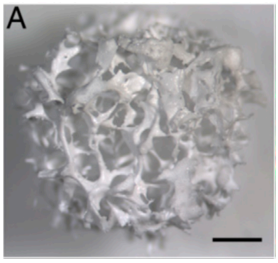

Fig. 1: Bone scaffold prototype consisting of poly-DL-lactide-co-glycolidic acid. Figure derived from previous work (Tsigkou et al., 2010)

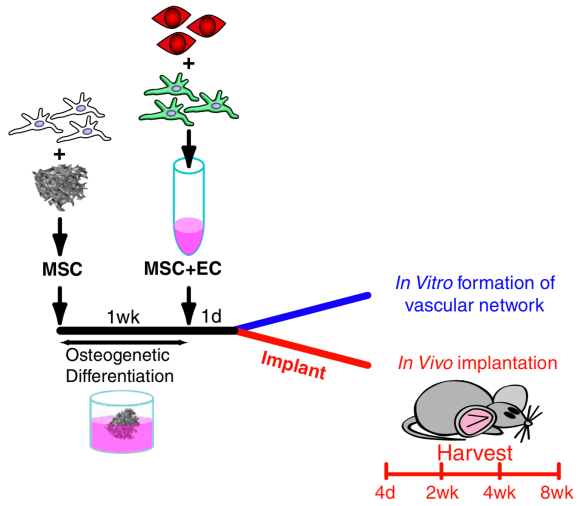

Fig. 2: Experimental Setup MSC seeded on a bone scaffold are cultured in osteogenic medium for one week to promote osteogenic differentiation. HUVEC co-cultured with MSC are added and either cultivated *in vitro* or implanted *in vivo*. Formation of bone and vasculature is observed and analyzed at various time points. Figure derived from previous work (Tsigkou et al., 2010)

markers (FACsort, Becton Dickinson, Franklin Lakes NJ). We harvested mouse MSC from bone marrow of α-SMA-GFP transgenic mice (Jackson Lab), followed by standard culturing, assessed and sorted them for α-SMA-GFP expression at various passages by Fluorescence-activated cell sorting (FACS). We analyzed their proliferative characteristics and multi-lineage differentiation ability to determine whether MSC are a subpopulation of pericytes. All animal procedures were approved by the Institutional Animal Care and Use Committee of the Massachusetts General Hospital and performed according to the National Institutes of Health Guidelines for the Care and Use of Laboratory Animals.

1.4.2 Cell Culture, Maintenance, and Labeling of Cells

We set up cell cultures of HUVEC, MSC and pericytes in an incubator at 37°C in humidified atmosphere with 5% CO_2, covered in EGM-2 (HUVEC), DMEM (MSC) or a-MEM (Pericytes) with 10% fetal bovine serum. We replaced medium twice weekly. We performed expansion at 75% (HUVEC) or 70% confluency (MSC, Pericytes). We fluorescently labeled the HUVEC with tdTomato (red), and MSC with eGFP (green) using Lentivirus.

1.4.3 Generation of Cell Line for Sustained IGF1 Delivery

We used the GateWay system to create a lentivirus plasmid vector for constitutive expression of IGF1 (Esposito et al., 2009). We amplified the protein-encoding region of a rat IGF1 cDNA (Adamo et al., 1991) by PCR. We cloned the resulting DNA fragment directionally in the pENTR/D TOPO vector (Invitrogen, Carlsbad CA) to create an IGF1 entry vector. We used a fast-growing subclone of a HEK293 cell line (HEK293FT, Invitrogen) derived from human embryonic kidney cells (Graham et al., 1977), that expresses the gene of SV40 T antigen. We transduced the cell line with pLB/UbCp(IGF1) and selected the IGF1-expressing cells, HEK-IGF1, with the drug blasticidin, for sustained IGF1 delivery. We adjusted the dosage by using a fraction of engineered cells included in the co-cultures of HUVEC and MSC. We measured IGF1 synthesis levels by HEK-IGF1 cells using the Mouse/Rat IGF-I Quantikine ELISA Kit (R&D Systems, Minneapolis MN), following manufacturer's protocol. We generated a standard curve using the included rIGF1 protein. We formed standard co-cultures that included HEK293 or low, medium, or high levels of HEK-IGF1 cells in triplicate using the collagen-fibronectin gel protocol. After 72 h, we gently homogenized and centrifuged the hydrogels at 16000 g/2 min. We collected and diluted the supernatant 10- and 100-fold before measuring IGF1 concentrations by ELISA.

1.4.4 Hydrogel Setup for Vasculogenesis

We then applied a 3D culture model to test the ability of our protocol to support vascularization. Therefore, we developed hydrogels as a matrix for HUVEC and MSC to attach and provide a 3D structure for the tube formation. Each 1 mL of collagen-fibronectin gel contained 385 µL EGM-2 medium, 25 µL 1 M HEPES buffer, 500 µL 3 mg/mL bovine collagen l (PureCol, Advanced BioMatrix, San Diego CA), and 90 µL 1 mg/mL fibronectin (#33016-015, Invitrogen). Co-culture studies involving the IGF1 expression vector included 0.125 x 10^6 HEK293 cells in the co-culture cell suspension before

pelleting. Three concentrations of HEK-IGF1 cells were evaluated, 1.25 x 10^3 cells (low), 12.5 x 10^3 cells (medium), 125 x 10^3 cells (high). Additional HEK293FT cells were added to the control (no HEK-IGF1 cells), low and medium levels to maintain constant cell numbers across all conditions. Cultures supplemented with recombinant protein contained 0 ng (control (standard)), 4 ng (low), 20 ng (medium), or 40 ng (high) rIGF1 (#100-11, PeproTech, Rocky Hill NJ) per 0.5 mL collagen-fibronectin gel. We pelleted cell suspensions at 500g/10 min and suspended in 0.5 mL ice-cold collagen-fibronectin gel before transfer to a glass-bottom 24-well plate and incubation at 37°C in a 5% CO_2 incubator.

1.4.5 Preinduction of MSC and Vascularization of Bone Scaffolds

We preinduced unlabeled MSCs into osteoblasts in separate multiwell plates using an osteoinductive medium for five days, and during the 1-week culture period, we omitted osteogenic inducers like TGF-β from the culture medium. After that, we added the fibronectin-containing collagen gels containing HUVEC and MSC and implanted in the following day. We compared four setups for the vascular network formation of scaffolds preseeded with HUVEC alone, HUVEC and MSC pre-treated with the standard medium, MesenPro, a medium that specifically supports MSC growth and maintains the multipotential phenotype of MSC, or a TGF-β containing medium. We added collagen-fibronectin gel with HUVEC and MSC to the engineered decellular bone scaffolds and cultured them with osteoinductive medium (MSCGM with 50 μg⁄mL L-ascorbic acid 2-phosphate, 10 mM β-glycerol phosphate, and 10−8 M dexamethasone).

1.4.6 Morphometrics to Determine Vascularization Parameters

We conducted morphometric analysis on the vascular networks that formed in 4 concentrations of IGF1 at several time points throughout the experiments. Therefore, we performed confocal imaging and quantification at mid-depth of the gel, the region of highest cell density. We measured time points initiating at day 1 and continuing through day 40 to assess vessel density, length, diameter, and bifurcations per image field and normalized for reporting in international units of measurement (e.g., μm or mm^2).

1.4.7 Immunohistochemical Analysis of Hydrogels and Scaffolds

We excised samples derived from central regions of hydrogels, fixed them in 4% paraformaldehyde solution overnight at 4°C, dehydrated them, and embedded them in paraffin. We then cut them in 10 μm sections and labeled them with primary antibody mouse anti-human CD31 (1:25; #M0823, DAKO, Carpinteria CA), mouse anti-smooth muscle actin (1:50; DAKO), and anti-vimentin (1:50; DAKO), and subsequently detected them with the EnVision+ kit (#K4006, DAKO) using 3,3′-diaminobenzidine before counter-staining with hematoxylin and eosin. We explanted the vascularized bone scaffolds at several time points between two and eight weeks, and prepared frozen sections for immunohistochemical staining using anti-human CD31 to detect 2ndary labeled antibodies, thereby distinguishing between host and

human vasculature. We analyzed scaffolds by von Kossa staining for evidence of calcium production and consequent bone formation. We confirmed Calcium deposition by Alizarin red staining.

1.4.8 Implantation of Hydrogels and Scaffolds into NOD SCID Mouse Model

We utilized a NOD SCID Mice model to study the intravital human vascular formation and to test their functionality *in vivo*. Therefore, we implanted pre-seeded scaffolds subcutaneously in the dorsum of NOD SCID mice to research vascularization *in vivo* between day four and five months after implantation of the pre-seeded scaffolds. Therefore, we anesthetized ten severe immunodeficient mice (NOD.CB17, Jackson Laboratory, Bar Harbor ME) with a Ketamine/Xylazine solution (c = 1 mg/30 g mouse) for pain relief. The animals received four pre-seeded scaffolds, one for each condition. We rotated positions in each mouse to different quadrants (crossover design). The subcutaneous injection protocol used to evaluate the effect of IGF1 *in vivo* (Melero-Martin et al., 2008) gelled when warmed to body temperature. We used cell ratios and concentrations of recombinant protein identical to those used in the *in vitro* studies.

1.4.9 Functional Analysis: Confocal Laser Imaging *in vivo*

For *in vivo* imaging, we tracked the fluorescently labeled HUVEC and MSC in the scaffolds with a custom-built video-rate laser-scanning confocal microscope. We imaged the scaffolds with a 30× 0.9 N.A. water immersion objective (LOMO) and a 60× 1.2 N.A. water immersion objective to visualize eGFP, tdTomato, and Qtracker800 quantum dots (Invitrogen). We used a Nikon A1 confocal microscope for detection and measurements of the vascularized collagen plugs with a 20x objective for imaging vascular networks. We performed an analysis of images in ImageJ using the Vascular Network Toolkit Plug-in.

1.4.10 Measuring Blood Flow using Quantum Dots

We used intravital microscopy at several time points to evaluate the vascular network formation within the scaffolds as well as the anastomoses with the host vessels. To test for permeability of anastomosed vessels, we injected the fluorescent dye Evans blue and in subsequent, additional measurements we used Qtracker 800 quantum dots (Invitrogen) and DiD membrano-labelled blood cells systemically through injection into the tail vein of the mice. At two and eight weeks postimplantation, we evaluated patency, functionality, and maturity by visualizing blood flow through the grafts and the nearby host vasculature and determined the amount of leakiness as an indicator of vessel maturation.

1.4.11 Statistical Analysis

We expressed the data of the vascularized bone grafts as means SEM and evaluated the data by one-way ANOVA; a p-value of < 0.05 indicated strong evidence against the null hypothesis, hence we rejected the null hypothesis when $p < 0.05$. We performed a nonparametric repeated measurement ANOVA for group comparison of the IGF1 supplemented setups and the Mann-Whitney-U Test for comparison of two independent setups per time point (Brunner et al., 2002). We investigated group effect, time effect, and the interactions between group and time, where a p-value < 0.05 was considered to be significant. Due to

the exploratory study design and the weakness of post hoc power analyses, we considered all calculated p-values in a non-confirmatory way. We accounted for missing data by using the last observation carried forward (LOCF) method. For all numerical calculations, we used IBM SPSS Statistics, Ver. 20, and the software package R Project for Statistical Computing, Ver. 3.0.2.

1.5 Results

1.5.1 Vasculogenesis: Enhanced Tube-like Structures in Hydrogel

Endothelial cells formed tube-like structures and subsequently networks throughout the bone scaffold starting at day 4 after implantation (Fig. 3A). MSC were essential for stable vascular network formation (Fig. 5A – D, Fig. 7E – 7F). Without co-culturing of MSC, the tube-like structures gradually degraded (data not shown). Vasculature exposed to the medium designed to maintain a proliferative, non-differentiated state (Fig. 5B) formed extensively when compared to MSC, which were pre-conditioned with a TGF-β-induced smooth muscle cell phenotype (Fig. 7C).

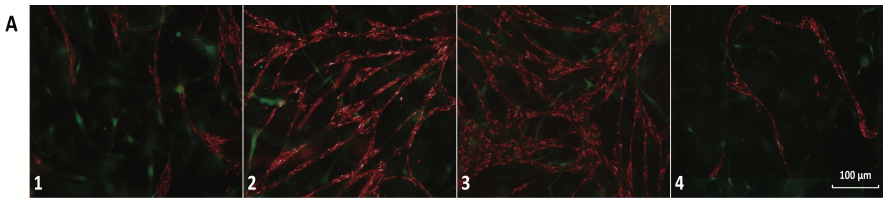

Fig. 3: Enhanced vascular network formation *in vitro* using HEK-IGF1 in low (2), medium (3) and high (4) concentration versus control (1). Vascularization was most extensive when co-cultured with IGF1 in low or medium levels (2,3) compared to the control group (1). IGF1 in high levels showed detrimental to the vasculogenesis. Figure derived from previous work (Friedrich et al., 2018)

1.5.2 Enhanced Bone Formation and Scaffold Mineralization

Scaffolds explanted after eight weeks showed significant mineralization (Fig. 4B), however less than the samples pretreated with osteoinductive medium (Fig. 4A). Controls of scaffolds that we had not preseeded with primary cells produced a modest staining for calcium (Fig. 4C). Calcium phosphate deposition was mainly attached to the surface of the scaffold pores (Fig. 4A – 4B). Co-culture of EC with MSC for vascularization of the bone scaffolds significantly enhanced bone formation (Fig. 4A – 4B).

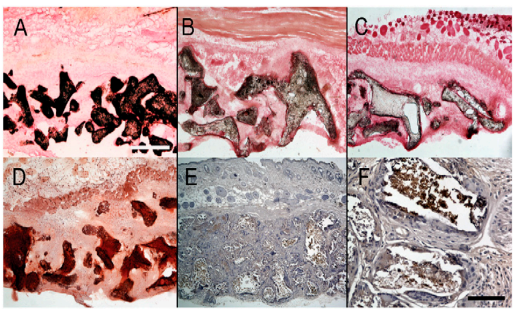

Fig. 4: Bone formation and scaffold mineralization *in vivo* Extensive bone formation observed in the vascularized bone scaffolds with osteogenic induction (A) Vascularized bone scaffolds without osteogenic induction (B) Avascular bone scaffolds (C). Calcium deposition within the bone scaffolds confirmed by Alizarin red staining (D). Counterstaining with H&E revealed osteocalcin within bone scaffolds (3E, 3F). A – E = 500µm, F = 100µm. Figure derived from previous work (Tsigkou et al., 2010)

1.5.3 Impact of Exogenous IGF1 on Vasculogenesis

Vascular network formation was apparent in hydrogel setups containing HUVEC, MSC and genetically engineered HEK293 cells that constitutively expressed IGF1 (Fig. 3, Fig. 5A – 5B). Of the three different HEK-IGF1 concentrations compared to the control that had no IGF1, the hydrogel setups containing low

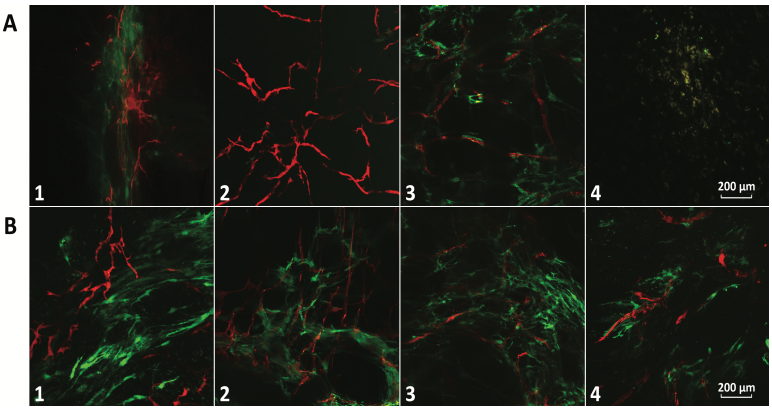

Fig. 5: Enhanced capillary-like net-works *in vivo* (A) Setups cultured with HEK-IGF1 in low (2), medium (3) and high (4) concentration in comparison to control without IGF1 treatment (1). (B) Capillary-like networks *in vivo* enhanced with recombinant IGF1 in low (2), medium (3) and high (4) concentration in comparison to control (1). Figure derived from previous work (Friedrich et al., 2018)

and medium IGF1 levels formed the most extensive (measured as network density, vessel length, and diameter) and longest lasting networks, measured up to 40 days (Fig. 5A – 5B, Fig. 7, Fig. 9 – 10). Control cultures without IGF1-expressing HEK cells maintained their viability for three weeks, however rapidly declined thereafter in contrary to the setups containing HEK-IGF1 in low or medium concentrations. The highest levels of IGF1 tested were either ineffective or even deleterious (Fig. 5A – 5B). To determine whether recombinant IGF1 (rIGF) would have similar effects of vasculogenesis, we replaced the genetically engineered cells and used rIGF in similar concentrations as beforehand measured and confirmed by ELISA. While results using rIGF were comparable for *in vitro* and *in vivo* setups, network density, diameters and branching were inferior compared to setups that contained the constitutively expressing HEK-IGF1 cells (Fig. 9 – 11). In low and medium containing rIGF setups, network survival was superior compared to the co-cultures without rIGF supplementation that served as controls (Fig. 10 – 11).

1.5.4 The Functionality of Vasculature, Anastomoses with Host Vasculature and Blood Flow

We visualized human CD31+ cells and the pericyte markers smooth muscle actin and calponin (Fig. 6I – 6L, Fig. 6Q – 6T) using immunohistology and detected lumina of the engineered vascular networks (Fig. 6J – 6L). At day four, no erythrocytes could be detected indicating that the vascular networks were not yet functional. At day 11, multiple erythrocytes were visible within the lumina of CD31+ cells indicating

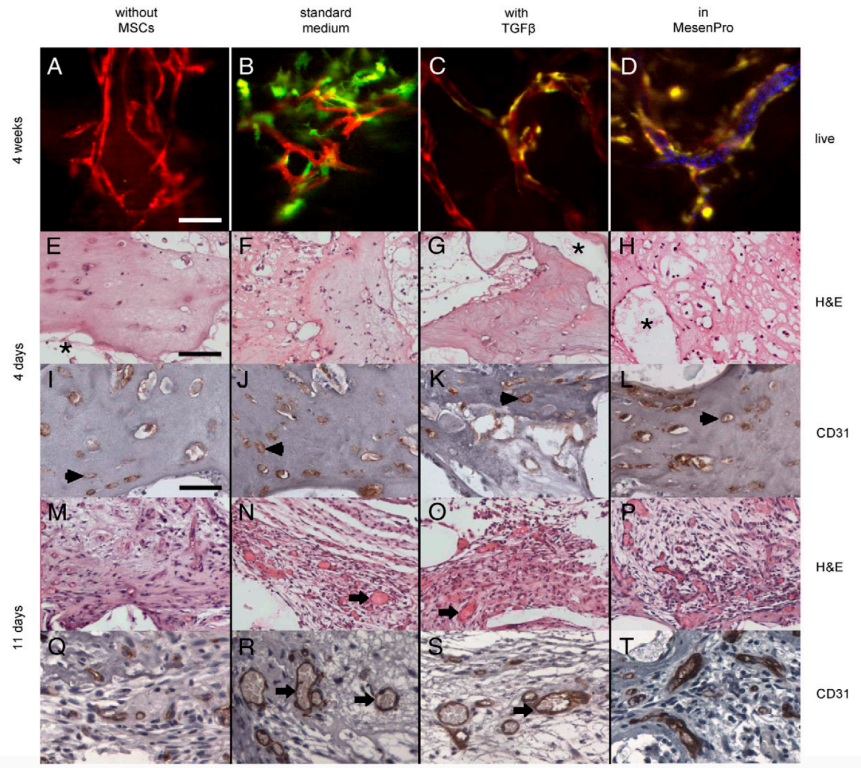

Fig. 6: Formation of human vascular networks in 3D matrices *in vivo* and histology Vascular networks *in vivo* with HUVEC labeled in tdTomato, MSC labeled in eGFP showing the stem cells in close alignment to the vascular tube structures (A-D), histological proof of human vasculature *in vivo* using antibody staining (E-T), blood flow through human vessels (C-D). Figure derived from previous work (Tsigkou et al., 2010)

patency and functionality of the engineered vasculature Fig. 6Q – 6T).

Analysis of vascularization in 3D with osteoinductive cultured MSC *in vivo* showed that anastomosis with host vasculature (Fig. 7C) occurred by day 11 with most human MSC flattened and with stellate processes attached to or in proximity with the network. Using fluorescently labeled HUVEC and MSC together with Quantum dots Qtracker 800 injected into the tail vein of anesthetized NOD SCID mice to visualize blood flow, fluorescent microscopy using a confocal laser microscope confirmed the presence of vascular tube formation, the alignment or close proximity of MSC to the vascular networks *in vivo* as well as blood flow through both the host vasculature and engineered vascular networks (Fig. 7A – 7C, Fig. 8).

Although

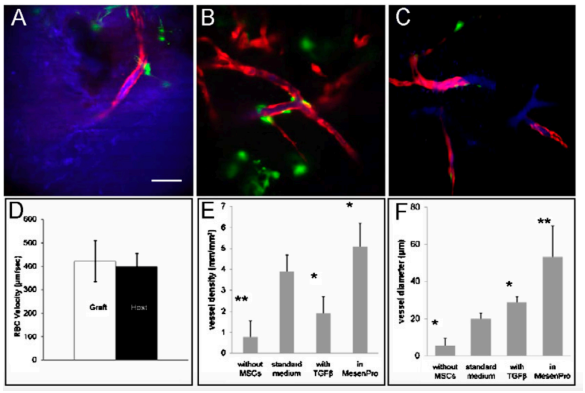

Fig. 7: Anastomosis and maturation of human vascular networks *in vivo*, (A) Immature vasculature with high leakiness after several minutes post injection of Qdots 800, (B) Mature vasculature with blood flow visible in lumina and MSC in close alignment to tubes, (C) Anastomoses of host vasculature with human engineered vasculature (D) Velocity of erythrocytes within host vasculature in comparison to engineered vasculature, resembling a similar velocity ($p > 0.05$), (E) Depending on the medium, the diameter of the engineered vasculature increases significantly when using MesenPro and decreases when using TGF-β in comparison to the control with standard medium, (F) Vessel density significantly increased in MesenPro and declined with TGF-β or without MSC present. Figure derived from previous work (Tsigkou et al., 2010)

initially immature and highly permeable, fluorescence microscopy using Qtracker 800 visualized blood flow through engineered vascular networks (Fig. 7A – 7C), however, in the vascular networks younger than four weeks, significant blue fluorescence could be detected in the extravascular space (Fig. 7A). At four weeks, however, blue fluorescence resembling blood flow through both host and engineered vascular networks was mainly visible intravascularly, serving as evidence, that the networks were mature (Fig. 6D, Fig. 7B – 7C). Several engineered vessels were still present at five months. However, the majority of the graft vasculature had been functionally remodeled with host cells (data not shown).

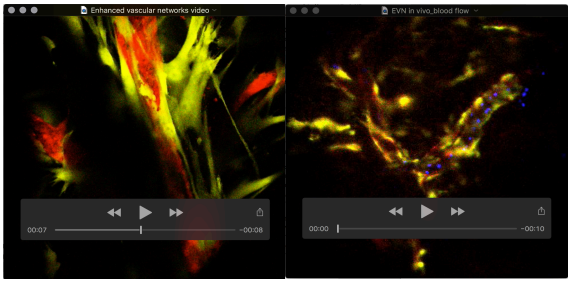

Fig. 8: Video sequences showing enhanced engineered vascular networks *in vitro* (A) MSC have elongated with stellate processes and reside in proximity to the tube-forming HUVEC resembling microvascular networks (B) Engineered vascular systems with Evans blue dye visible in the lumina proofing patency and maturity of the engineered vasculature. Figure derived from previous work (Tsigkou et al., 2010).

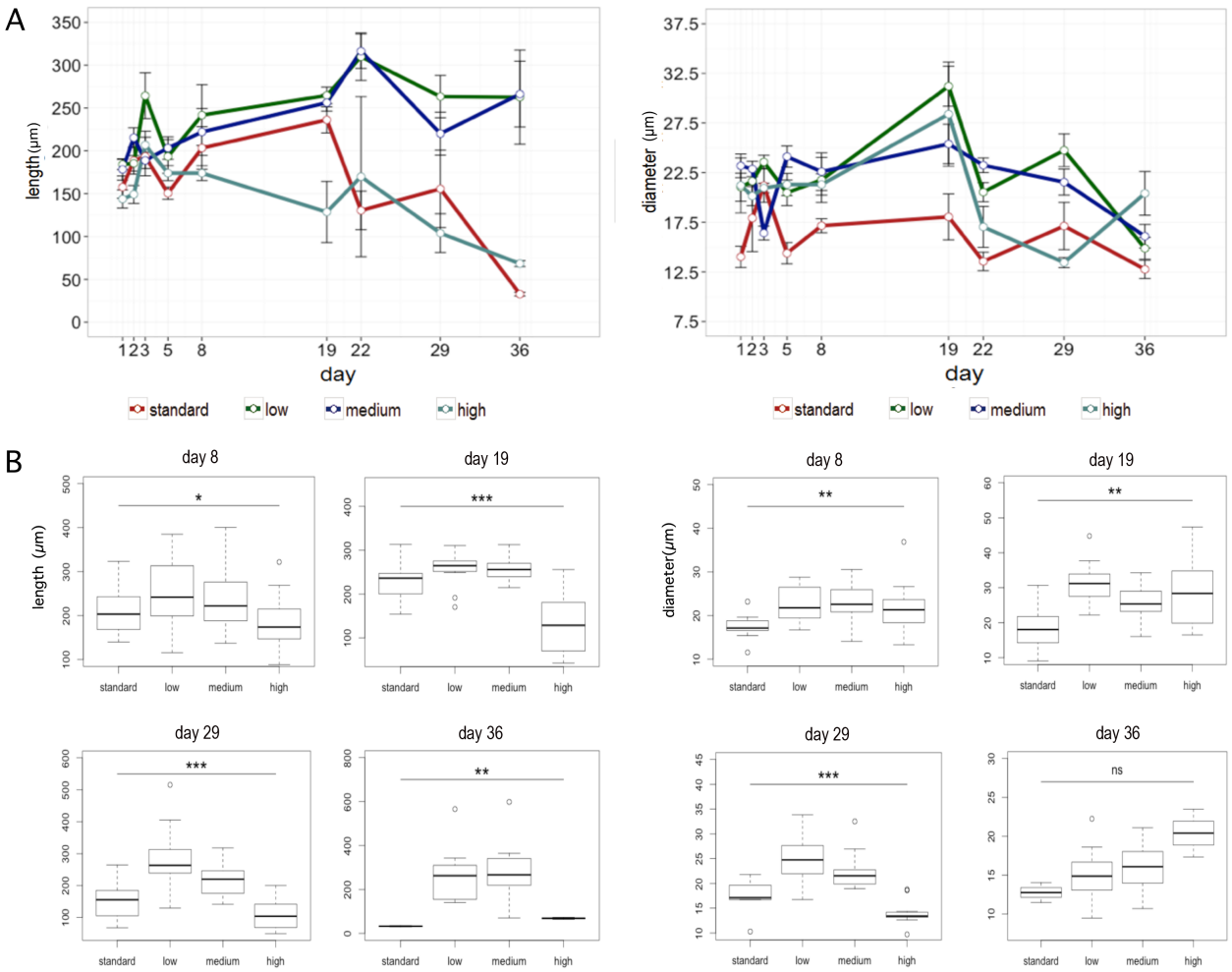

Fig. 9: Statistical comparison of enhanced vascular network formation using HEK-IGF1 *in vitro* Co-cultures of HUVECs and MSCs seeded with varying numbers of HEK-IGF1 showed increased length (A) and diameter (B) *in vitro*. Cell setups were incubated for 40 days and imaged at the indicated times. Box and whisker plots below present the statistical distribution of data for selected subsets of time points. p values for this and subsequent figures: NS = not significant, * <0.05, **<0.01, *** <0.001. Figure derived from previous work (Friedrich et al., 2018)

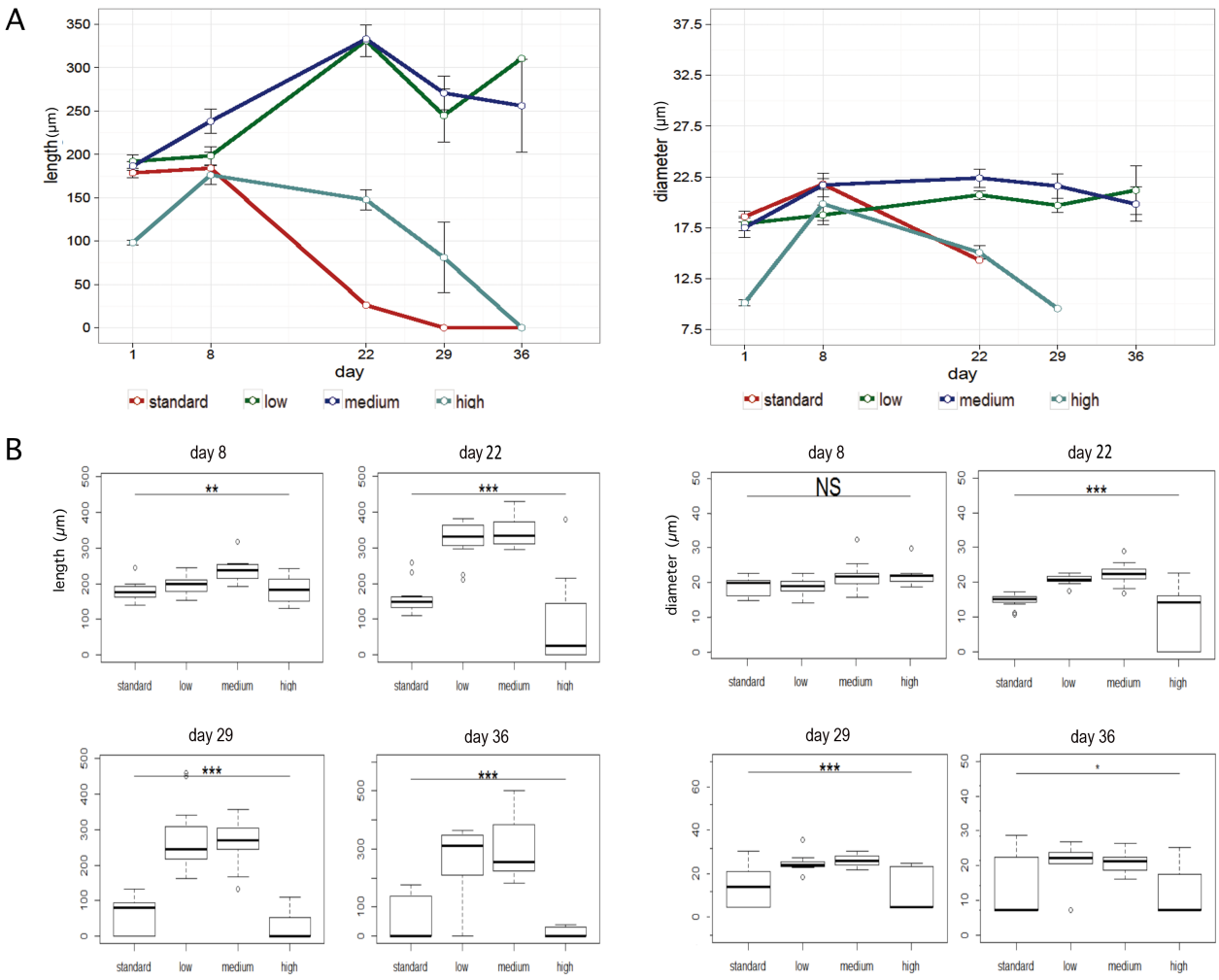

Fig. 10: Statistical analysis of enhanced vas-cular network formation using recombinant IGF1 *in vitro*. rIGF1 promotes increased length and diameter of setups *in vitro* in comparison to the control. Co-cultures with varying concentrations of rIGF1 protein were incubated for 36 days (A) and imaged at the indicated times. The average vessel length was calculated using ImageJ. (B) Box and whisker plots show the statistical distribution of data for a selected subset of time points. Figure derived from previous work (Friedrich et al., 2018)

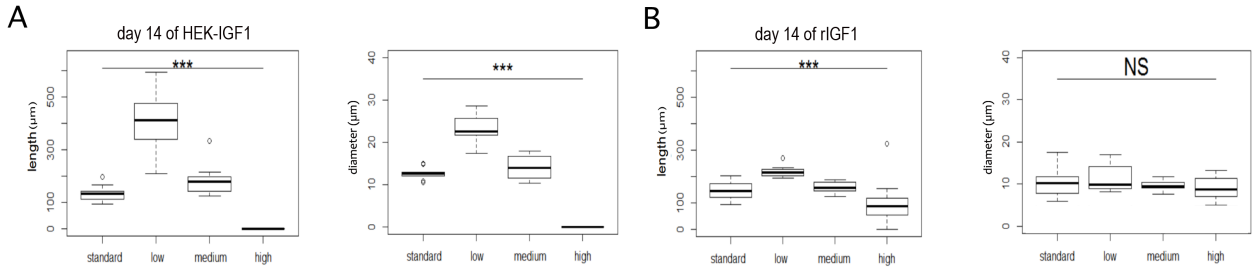

Fig. 11: Statistical analysis of vascular network formation using rIGF or HEK-IGF1 respectively. As measured by length and diameter of vessels, network formation was best in low or medium concentrations (A, B). However, a difference in diameter was not significant for the setups using rIGF1. Figure derived from previous work (Friedrich et al., 2018)

1.5.5 MSC as a Subpopulation of Pericytes

Finally, the results showed that the α-SMA-GFP positive bone marrow stromal cells are larger and of flat morphology in comparison to the α-SMA-GFP negative cells, that appear smaller and spindle-like. The GFP positive cells consisted of pericytes and smooth muscle cells and expressed α-SMA. When sorted and analyzed by FACS, the percentage of α-SMA positive cells increased faster than the α-SMA negative cells. α-SMA-GFP positive cells expressed α-SMA during differentiation into the adipogenic, chondrogenic and osteogenic lineages suggesting that MSC are a subpopulation of pericytes (Fig. 10 – 11). Further, α-SMA-GFP positive cells stimulated the endothelial cells to form tube-like structures and subsequently to form robust vascular networks in 3D culture. Both the phenotype and the relative number of pericytes influenced inherent microvascular properties, i.e., the leakiness, degree of branching, and vessel density, which are essential parameters for the construction of functional vasculature in engineered tissue. In our model, network formation occurred rapidly, and anastomosis was first detected eleven days post-implantation for all MSC-containing scaffolds in concurrence with our previous findings. When cultured in adipogenic medium for seven days, the α-SMA-GFP positive cells changed their morphology towards a rounded shape with lipid drop accumulation as demonstrated by Oil Red O staining in comparison to the control group that had been cultured in α-MEM with 10% FBS. Further, RT-PCR revealed, that the adipogenic markers PPAR-γ, LPL were expressed in α-SMA-GFP positive cells only. When cultured in chondrogenic medium for seven days, the α-SMA-GFP positive cells changed their morphology into a flat and multi-angled shape. RT-PCR revealed expression of the chondrogenic genes SOX 9 and COL-II in the α-SMA-GFP positive cells only. When cultured in osteogenic medium for 21 days, the α-SMA-GFP positive cells adopted an osteoblast-like shape. RT-PCR revealed expression of OSX and OSC as osteogenic specific genes in α-SMA-GFP positive cells in opposite to the control. Mineralization was confirmed using Alizarin Red-S staining. Using morphometrics and RT-PCR, we were able to prove directly, that the bone-marrow derived pluripotent MSC express α-SMA-GFP, which is a marker of perivascular cells. We, therefore, conclude, that MSC derive from perivascular cells and pericytes.

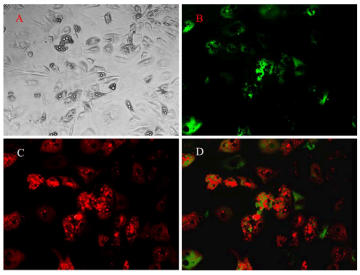

Fig. 12: Adipogenic differentiation of α-SMA-GFP positive cells Cells were derived from bone marrow and incubated in osteoinductive medium for two weeks. Microscopic images revealed adipogenic differ-rentiated α-SMA-GFP positive cells. Figure derived from previous work (Cai et al., 2009)

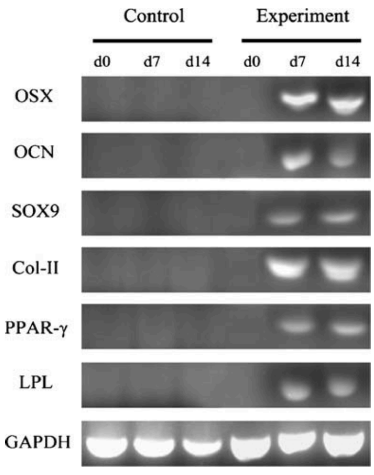

Fig. 13: RT-PCR of multilineage differentiation of genes Genes involved in osteogenic, chondrogenic or adipogenic differentiation showed upregulation of specific markers (osteogenic - OSX, OCN, chondrogenic - SOX9, Col-IIα1, adipogenic - PPAR-γ, LPL) at various time points in comparison to α-SMA-GFP positive cells cultured in control medium (Cai et al., 2009)

1.6 Discussion

1.6.1 Higher-quality grafts using MSC

In our earlier work, we demonstrated that MSC are a subset of pericytes that are crucial to improve vascularization, as nascent vascular networks require mural cells to mature and form functioning vasculature (Cai et al., 2009; Jain, 2003). It has recently become evident, that there are different classes of pericytes with heterogeneous morphology, protein expression and different degrees of contraction during ischemia, leading to vastly different outcomes (Attwell et al., 2016). Here, we studied whether pre-vascularized structures in a 3D collagen-fibronectin matrix seeded onto an engineered bone scaffold can enhance vasculogenesis *in vivo*, when implanted into NOD-SCID mice (Tsigkou et al., 2010). We therefore assessed by confocal laser microscopy, whether the vasculogenic setups survived implantation and anastomosed with the host vasculature. We tested murine embryonic fibroblasts, 10T1/2 fibroblasts and NIH/3T3 cells as established previously by other groups (Reznikoff et al., 1973; Todaro and Green, 1963), however, due to our previous findings we decided to utilize MSC for enhanced vasculogenesis.

1.6.2 Osteogenic Induction of MSC for Enhanced Scaffold Mineralization

We then developed a novel bone scaffold seeding protocol based on findings of other groups (Au et al., 2008; Melero-Martin et al., 2008; Shepherd et al., 2004). We used MSC to derive osteoblasts, and subsequently seeded a second co-culture of MSC and HUVEC to generate a vascular network (Tsigkou et al., 2010). To further enhance vascular network formation, we shifted a separate setup of MSC towards a smooth muscle phenotype using TGF-β as this had been shown to induce both changes in shape and expression of SMC markers in the presence of endothelial cells thereby contributing to the forming vessel wall *in vivo* (Hirschi et al., 1998). However, the results of bone formation using TGF-β were significantly behind the experiments with undifferentiated MSC. We attribute this effect to the essential trophic factors released by the undifferentiated MSC. In future experiments, the combination of both TGF-β treated and undifferentiated MSC along with HUVEC should be investigated. Also, evidence suggests MSC playing a role in reducing immunological rejection (Pober and Tellides, 2012).

1.6.3 Exogenous IGF1 Delivery for Enhanced Vasculogenesis

In order to shorten the time upon anastomosis, we considered various strategies such as the use of exogenous IGF1. Although almost no research is suggesting the role of IGF1 as an angiogenic growth factor, we tested IGF1 in various concentrations and co-cultured the growth factor in low, medium and high concentrations with our vasculogenesis protocol in comparison to the control. We showed IGF1 significantly promoted vasculogenesis both *in vitro* and *in vivo*. Since IGF1 can be used to produce neovasculature with significantly enhanced network density and durability, this indicates a promising methodology for engineering *de novo* vasculature to support the regeneration of functional tissue. However, as IGF1 leads to proliferative and anti-apoptotic effects, careful regulations of IGF1 administration are mandatory as well as investigating its autocrine, paracrine and endocrine effects. While

angiogenesis is controlled by a local balance between endogenous stimulators and inhibitors, in tumorigenesis, there is an imbalance leading to an 'angiogenic switch' (Ribatti, 2014). This is especially important as tumors at different stages of development may require different concentrations of angiogenic factors for tumor vasculogenesis (Ribatti, 2008).

1.6.4 Potential Impact of Confirmed Functionality and Anastomosis with Host Vasculature

Next, we aimed to study the anastomosis of the engineered vessels with the host vasculature as it had been hypothesized that endothelial cells and perivascular cells could potentially create functional connections with the host vessels (Jain et al., 2005). In our experiments, anastomoses occurred by day 11 after implantation, which was evidenced by blood-filled human-CD31 expressing networks in paraffin sections. Therefore, vascularized bone grafts and vascularized tissues using human cells can contribute to restoring oxygenation and removal of metabolites thereby potentially alleviating hypoxia and improving tissue function when injected into ischemic tissues.

1.6.5 Potential Future Role of α-SMA-GFP positive cells in Vasculogenesis

Bone marrow-derived α-SMA-GFP positive stromal cells like MSC and pericytes enhanced the process of vasculogenesis and its maintenance. Without the contribution of pericytes or MSC, the tube-like structures built by HUVEC fell apart within days (Tsigkou et al., 2010). α-SMA-GFP positive cells reside in proximity to the vascular tubes suggesting MSC-mediated paracrine mediators (Gnecchi et al., 2016) support HUVEC to form and maintain vascular networks. They, therefore, fulfil two crucial roles in supporting vasculogenesis: formation of the mural wall of new blood vessels and synthesis of growth factors (Cai et al., 2009). The extracellular environment influences MSC paracrine activity. Hence, adjusting for oxygen tension, growth factor composition and mechanical properties may alter the gene regulation underlying the MSC-mediated paracrine actions. Factors secreted by MSC referred to as the secretome may therefore be crucial for developing clinical MSC applications (Kusuma et al., 2017).

1.6.6 Outlook and Limitations

Blood vessel generation is a critical issue in the field of tissue engineering, as it holds the potential to improve or recover organ performance after trauma or illness. Future experiments might well likely focus on the acceleration of anastomoses between the engineered blood vessels and the vessels of the host to further reduce ischemia and impaired tissue function as early as possible. Future studies should also investigate how the sizes of the bone scaffolds can be increased while further reducing the hypoxic core as the latter still represents a main limitation of engineered vascularized bone grafts. Novel techniques like 3D bioprinting may be able to accelerate functional replacement of body parts, taking into consideration the scaffolds biocompatibility, biodegradability, interconnectivity, porosity, and mechanical properties (Do et al., 2015), which were previously difficult to address. A hybrid approach using both natural and synthetic materials may be essential to create ECM-like scaffolds, thereby providing a microenvironment for cell attachment and proliferation. Therefore, bio-functional scaffolds could

contribute to address and reduce the shortage of donated organs or parts of them (Lee and Dai, 2017). We are in the need to investigate the process and effectiveness of vascular remodeling of the engineered vascular networks over time with capillaries by the host. While every effort has been undertaken to maximize the comparability of statistics across institutions, setups and over time, data may differ regarding the definitions, data-collection methods, population coverage and estimation methods used. Besides, non-autologous bone grafts are still limited in size due to metabolic demands and limited gas exchange within the grafts. Hence, future protocols should focus on how to expand scaffold sizes to achieve larger custom-built transplants for potential use in a clinical setting. Further, the strength of bio-printed scaffolds may vary depending on product quality and properties, which may affect the outcome and scaffold functionality. Finally, sensible regulations and ethical agreements i.e., concerning misuse should be considered and updated continuously.

1.6.7 Summary

The ability to promote rapid vascularization for clinically relevant settings could vastly expand the utility of synthetic bone grafts and re-vascularization in ischemic tissues. Vascularized bone grafts utilizing human stromal cells as mesenchymal stem cells or pericytes co-cultured with human endothelial cells proliferate best when enhanced using MesenPro medium, , or DMEM. Using DMEM, MSC and HUVEC seeded together onto a collagen-fibronectin matrix develop stronger networks regarding vessel length and diameter, when exposed to the growth factor IGF1. IGF1 in low and medium supplementation created vascular network structures superior to high IGF1 or no IGF1 exposure. When provided continuously with genetically engineered HEK293 cells, setups with low or medium IGF1 concentration generated better vascular networks *in vitro* and *in vivo*, when compared to recombinant IGF1 exposure. Vascular and bone graft engineering pertain to a promising technology that addresses a critical issue in regenerative biology. It holds the potential to significantly improve translational models *in vitro* and *in vivo* primarily in bone, skeletal muscle, and liver engineering. Further research should focus on the acceleration of anastomoses, functionality in larger constructs and long-term results after remodelling, an important topic, which has been briefly addressed, yet would have been beyond the scope of discussion.

1.7 List of Abbreviations

a-MEM	Minimum Essential Medium Eagle - Alpha Modification
α-SMA-GFP	α-Smooth Muscle Actin GFP Reporter
C3H/10T1/2	Fibroblast Cell Line, Strain C3H
DiD	Lipophilic Fluorescent Red Dye
DMEM	Dulbecco's Modified Eagle Medium
eGFP	Enhanced Green Fluorescent Protein
ELISA	Enzyme-linked Immunosorbent Assay
EGM-2	Endothelial Cell Growth Medium-2
FACS	Fluorescence-activated Cell Sorting
FBS	Fetal Bovine Serum
HEK293	Human Embryonic Kidney 293 Cell Line
HUVEC	Human Umbilical Vein Endothelial Cells
IGF1	Insulin-like Growth Factor 1
MSC	Mesenchymal Stem Cells
MEF	Murine Embryonic Fibroblasts
NIH/3T3 cells	Standard Fibroblast Cell Line, 3-day transfer, inoculum 3×10^5 cells
NOD	Non-obese Diabetic
SCID	Severe Combined Immune Deficiency
PLGA	Poly-DL-Lactide-Co-Glycolic Acid
tdTomato	Tandem Dimer (td) Tomato Red Fluorescent Protein
TGF-β	Transforming Growth Factor Beta

1.8 List of Figures

1.9 References

1. Adamo, M.L., Ben-Hur, H., LeRoith, D., and Roberts, C.T., Jr. (1991). Transcription initiation in the two leader exons of the rat IGF-I gene occurs from disperse versus localized sites. Biochem Biophys Res Commun *176*, 887-893.
2. Amini, A.R., Laurencin, C.T., and Nukavarapu, S.P. (2012). Differential analysis of peripheral blood- and bone marrow-derived endothelial progenitor cells for enhanced vascularization in bone tissue engineering. Journal of orthopaedic research : official publication of the Orthopaedic Research Society *30*, 1507-1515.
3. Attwell, D., Mishra, A., Hall, C.N., O'Farrell, F.M., and Dalkara, T. (2016). What is a pericyte? J Cereb Blood Flow Metab *36*, 451-455.
4. Au, P., Tam, J., Fukumura, D., and Jain, R.K. (2008). Bone marrow-derived mesenchymal stem cells facilitate engineering of long-lasting functional vasculature. Blood *111*, 4551-4558.
5. Bergers, G., and Song, S. (2005). The role of pericytes in blood-vessel formation and maintenance. Neuro Oncol *7*, 452-464.
6. Berner, A., Reichert, J.C., Woodruff, M.A., Saifzadeh, S., Morris, A.J., Epari, D.R., Nerlich, M., Schuetz, M.A., and Hutmacher, D.W. (2013). Autologous vs. allogenic mesenchymal progenitor cells for the reconstruction of critical sized segmental tibial bone defects in aged sheep. Acta Biomater *9*, 7874-7884.
7. Bonaros, N., Bernecker, O., Ott, H., Schlechta, B., and Kocher, A.A. (2005). Cell- and gene therapy for ischemic heart disease. Minerva Cardioangiol *53*, 265-273.
8. Brunner, E., Domhof, S., and Langer, F. (2002). Nonparametric analysis of longitudinal data in factorial experiments (New York, NY: Wiley).
9. Cai, X., Lin, Y., Friedrich, C.C., Neville, C., Pomerantseva, I., Sundback, C.A., Zhang, Z., Vacanti, J.P., Hauschka, P.V., and Grottkau, B.E. (2009). Bone marrow derived pluripotent cells are pericytes which contribute to vascularization. Stem Cell Rev *5*, 437-445.
10. Cao, W., and Li, P. (2015). Effectiveness and Safety of Autologous Bone Marrow Stromal Cells Transplantation After Ischemic Stroke: A Meta-Analysis. Med Sci Monit *21*, 2190-2195.
11. Crisan, M., Corselli, M., Chen, W.C., and Peault, B. (2012). Perivascular cells for regenerative medicine. J Cell Mol Med *16*, 2851-2860.
12. Do, A.V., Khorsand, B., Geary, S.M., and Salem, A.K. (2015). 3D Printing of Scaffolds for Tissue Regeneration Applications. Adv Healthc Mater *4*, 1742-1762.
13. Esposito, D., Garvey, L.A., and Chakiath, C.S. (2009). Gateway cloning for protein expression. Methods Mol Biol *498*, 31-54.
14. Fransson, M., Brannstrom, J., Duprez, I., Essand, M., Le Blanc, K., Korsgren, O., and Magnusson, P.U. (2015). Mesenchymal stromal cells support endothelial cell interactions in an intramuscular islet transplantation model. Regenerative medicine research *3*, 1.

15. Friedrich, C.C., Lin, Y., Krannich, A., Wu, Y., Vacanti, J.P., and Neville, C.M. (2018). Enhancing engineered vascular networks in vitro and in vivo: The effects of IGF1 on vascular development and durability. Cell Prolif *51*.
16. Gnecchi, M., Danieli, P., Malpasso, G., and Ciuffreda, M.C. (2016). Paracrine Mechanisms of Mesenchymal Stem Cells in Tissue Repair. Methods Mol Biol *1416*, 123-146.
17. Graham, F.L., Smiley, J., Russell, W.C., and Nairn, R. (1977). Characteristics of a human cell line transformed by DNA from human adenovirus type 5. J Gen Virol *36*, 59-74.
18. Guyette, J.P., Gilpin, S.E., Charest, J.M., Tapias, L.F., Ren, X., and Ott, H.C. (2014). Perfusion decellularization of whole organs. Nat Protoc *9*, 1451-1468.
19. Hanley, P.J. (2015). Therapeutic mesenchymal stromal cells: where we are headed. Methods Mol Biol *1283*, 1-11.
20. Hirschi, K.K., Rohovsky, S.A., and D'Amore, P.A. (1998). PDGF, TGF-beta, and heterotypic cell-cell interactions mediate endothelial cell-induced recruitment of 10T1/2 cells and their differentiation to a smooth muscle fate. J Cell Biol *141*, 805-814.
21. Hsiao, S.T., Asgari, A., Lokmic, Z., Sinclair, R., Dusting, G.J., Lim, S.Y., and Dilley, R.J. (2012). Comparative analysis of paracrine factor expression in human adult mesenchymal stem cells derived from bone marrow, adipose, and dermal tissue. Stem cells and development *21*, 2189-2203.
22. Jain, R.K. (2003). Molecular regulation of vessel maturation. Nature medicine *9*, 685-693.
23. Jain, R.K., Au, P., Tam, J., Duda, D.G., and Fukumura, D. (2005). Engineering vascularized tissue. Nat Biotechnol *23*, 821-823.
24. Joensuu, K., Uusitalo, L., Alm, J.J., Aro, H.T., Hentunen, T.A., and Heino, T.J. (2015). Enhanced osteoblastic differentiation and bone formation in co-culture of human bone marrow mesenchymal stromal cells and peripheral blood mononuclear cells with exogenous VEGF. Orthopaedics & traumatology, surgery & research : OTSR.
25. Kusuma, G.D., Carthew, J., Lim, R., and Frith, J.E. (2017). Effect of the Microenvironment on Mesenchymal Stem Cell Paracrine Signaling: Opportunities to Engineer the Therapeutic Effect. Stem cells and development *26*, 617-631.
26. Lee, V.K., and Dai, G. (2017). Printing of Three-Dimensional Tissue Analogs for Regenerative Medicine. Ann Biomed Eng *45*, 115-131.
27. Li, S., Sengupta, D., and Chien, S. (2014). Vascular tissue engineering: from in vitro to in situ. Wiley Interdiscip Rev Syst Biol Med *6*, 61-76.
28. Liu, Y., Chan, J.K., and Teoh, S.H. (2015). Review of vascularised bone tissue-engineering strategies with a focus on co-culture systems. J Tissue Eng Regen Med *9*, 85-105.
29. Melero-Martin, J.M., De Obaldia, M.E., Kang, S.Y., Khan, Z.A., Yuan, L., Oettgen, P., and Bischoff, J. (2008). Engineering robust and functional vascular networks in vivo with human adult and cord blood-derived progenitor cells. Circ Res *103*, 194-202.

30. Muscari, C., Gamberini, C., Basile, I., Bonafe, F., Valgimigli, S., Capitani, O., Guarnieri, C., and Caldarera, C.M. (2010). Comparison between Culture Conditions Improving Growth and Differentiation of Blood and Bone Marrow Cells Committed to the Endothelial Cell Lineage. Biological procedures online *12*, 9023.
31. Pober, J.S., and Tellides, G. (2012). Participation of blood vessel cells in human adaptive immune responses. Trends Immunol *33*, 49-57.
32. Quattrocelli, M., Palazzolo, G., Perini, I., Crippa, S., Cassano, M., and Sampaolesi, M. (2012). Mouse and human mesoangioblasts: isolation and characterization from adult skeletal muscles. Methods Mol Biol *798*, 65-76.
33. Reznikoff, C.A., Bertram, J.S., Brankow, D.W., and Heidelberger, C. (1973). Quantitative and qualitative studies of chemical transformation of cloned C3H mouse embryo cells sensitive to postconfluence inhibition of cell division. Cancer Res *33*, 3239-3249.
34. Ribatti, D. (2008). Judah Folkman, a pioneer in the study of angiogenesis. Angiogenesis *11*, 3-10.
35. Ribatti, D. (2014). History of research on angiogenesis. Chem Immunol Allergy *99*, 1-14.
36. Shepherd, B.R., Chen, H.Y., Smith, C.M., Gruionu, G., Williams, S.K., and Hoying, J.B. (2004). Rapid perfusion and network remodeling in a microvascular construct after implantation. Arterioscler Thromb Vasc Biol *24*, 898-904.
37. Silvestre, J.S., Smadja, D.M., and Levy, B.I. (2013). Postischemic revascularization: from cellular and molecular mechanisms to clinical applications. Physiological reviews *93*, 1743-1802.
38. Todaro, G.J., and Green, H. (1963). Quantitative studies of the growth of mouse embryo cells in culture and their development into established lines. J Cell Biol *17*, 299-313.
39. Tonlorenzi, R., Rossi, G., and Messina, G. (2017). Isolation and Characterization of Vessel-Associated Stem/Progenitor Cells from Skeletal Muscle. Methods Mol Biol *1556*, 149-177.
40. Tsigkou, O., Pomerantseva, I., Spencer, J.A., Redondo, P.A., Hart, A.R., O'Doherty, E., Lin, Y., Friedrich, C.C., Daheron, L., Lin, C.P.*, et al.* (2010). Engineered vascularized bone grafts. Proc Natl Acad Sci U S A *107*, 3311-3316.
41. Weinand, C., Gupta, R., Huang, A.Y., Weinberg, E., Madisch, I., Qudsi, R.A., Neville, C.M., Pomerantseva, I., and Vacanti, J.P. (2007). Comparison of hydrogels in the in vivo formation of tissue-engineered bone using mesenchymal stem cells and beta-tricalcium phosphate. Tissue engineering *13*, 757-765.
42. WHO (2017a). Cardiovascular diseases (CVDs) (World Health Organization). Accession June 17, 2017.
43. WHO (2017b). The top 10 causes of death (World Health Organization), Accession April 11, 2018.

2 Eidesstattliche Versicherung

„Ich, Claudia Friedrich, versichere an Eides statt durch meine eigenhändige Unterschrift, dass ich die vorgelegte Dissertation mit dem Thema „Enhancing engineered vascular networks *in vitro* and *in vivo* using stem cells and growth factors" selbstständig und ohne nicht offengelegte Hilfe Dritter verfasst und keine anderen als die angegebenen Quellen und Hilfsmittel genutzt habe.
Alle Stellen, die wörtlich oder dem Sinne nach auf Publikationen oder Vorträgen anderer Autoren beruhen, sind als solche in korrekter Zitierung (siehe „Uniform Requirements for Manuscripts (URM)" des ICMJE -www.icmje.org) kenntlich gemacht. Die Abschnitte zu Methodik (insbesondere praktische Arbeiten, Laborbestimmungen, statistische Aufarbeitung) und Resultaten (insbesondere Abbildungen, Graphiken und Tabellen) entsprechen den URM (s.o) und werden von mir verantwortet.
Mein Anteil an der ausgewählten Publikation entspricht dem, der in der untenstehenden Erklärung, angegeben ist.

Die Bedeutung dieser eidesstattlichen Versicherung und die strafrechtlichen Folgen einer unwahren eidesstattlichen Versicherung (§156,161 des Strafgesetzbuches) sind mir bekannt und bewusst."

Datum
20. Juni 2019

_____
Unterschrift

3 Ausführliche Anteilserklärung an den erfolgten Publikationen

Publikation 1:

Friedrich C, Lin Y, Krannich A, Wu Y, Vacanti JP, Neville CM. Enhancing engineered vascular networks in vitro and in vivo: The effects of IGF1 on vascular development and durability. Cell Prolif. 2017 Nov 7. doi: 10.1111/cpr.12387.

Impact Factor 2017: 4.112 (current impact factor)

Beitrag im Einzelnen:

- Planung und Entwicklung des Versuchsaufbaus in vitro und *in vivo*
- Hauptverantwortlicher Beitrag zur Entwicklung des Studienprotokolls
- Selbständige Durchführung der Versuche *in vitro* und *in vivo*, aus der die Figures 3, 5, 7, 9, 10 und 11 hervorgegangen sind
- Selbständige Datenverarbeitung und Datenauswertung
- Beitrag zur statistischen Analyse
- Erstellen von Diagrammen und Graphiken für die Publikation
- Selbständiges Verfassen des Manuskripts
- Korrespondenz mit den Editoren und Gutachtern des Journals

Publikation 2:

Tsigkou O, Pomerantseva I, Spencer JA, Redondo PA, Hart AR, O'Doherty E, Lin Y, Friedrich C, Daheron L, Lin CP, Sundback CA, Vacanti JP, Neville C, Engineered vascularized bone grafts, Proc Natl Acad Sci U S A. 2010 Feb 23;107(8):3311-6. doi: 10.1073/pnas.0905445107. Epub 2010 Feb 2. PMID: 20133604

Impact Factor 2016: 9.661 (Impact Factor 2010: 9.771)

Beitrag im Einzelnen:

- Mitarbeit bei der Durchführung der Versuche:
  - Selbständige Durchführung von Messreihen *in vitro*
  - Selbständige Durchführung von Implantationen im NOD SCID Mausmodell *in vivo*
  - Assistenz bei der Durchführung der Analgosedierung der Versuchstiere
  - Assistenz bei der Durchführung des Live-Imagings *in vivo,* aus der die Figures 6, 7 und 8 hervorgegangen
- Beitrag zur Datenverarbeitung und Datenauswertung
  - Erstellen photomikrographischer Aufnahmen *in vitro*
  - Erstellen photomikrographischer Aufnahmen *in vivo*

- Assistenz zur Visualisierung der Anastomosen mit den Wirtsgefäßen
- Assistenz zur Visualisierung des Blutflusses und damit der Funktionalität der gezüchteten Gefäße

- Erstellen von Diagrammen und Graphiken für die Publikation
  - Assistenz bei der Herstellung immunohistochemischer Präparate, aus der Figure 4 A – F und Figure 6 E – T hervorgegangen sind
- Beitrag zum Verfassen des Manuskripts

Publikation 3:

Cai Y, Lin Y, Friedrich C, Neville C, Pomerantseva I, Sundback CA, Zhang Z, Vacanti JP, Hauschka PV, Grottkau BE, Bone marrow derived pluripotent cells are pericytes which contribute to vascularization, Stem Cell Review, 2009 Dec;5(4):437-45. doi: 10.1007/s12015-009-9097-6. Erratum in: Stem Cell Rev. 2009 Dec;5(4):435-6. PMID: 20058207

Impact Factor 2016/2017: 2.967 (Impact Factor 2009: 3,766)

Beitrag im Einzelnen:

- Mitarbeit bei der Durchführung der Versuche
  - Selbständige Durchführung von Messreihen *in vitro*
  - Assistenz bei der Analyse von Perizyten und MSC mittels FACS
  - Assistenz bei der RNA-Isolation mittels RT-PCR, aus der Figure 13 hervorgegangen ist
  - Assistenz bei der Herstellung dreidimensionaler Hydrogele
- Beitrag zur Datenverarbeitung und Datenauswertung
  - Erstellen photomikrographischer Aufnahmen *in vitro*
- Beitrag zur Ausformulierung des Manuskripts

_____

Unterschrift, Datum und Stempel des betreuenden Hochschullehrers/der betreuenden Hochschullehrerin

_____

Unterschrift des Doktoranden/der Doktorandin

4 Druckexemplare der ausgewählten Publikationen

Received: 30 May 2016 | Accepted: 21 July 2017

DOI: 10.1111/cpr.12387

ORIGINAL ARTICLE

WILEY Cell Proliferation

Enhancing engineered vascular networks in vitro and in vivo: The effects of IGF1 on vascular development and durability

Claudia C. Friedrich[1,2,5] | Yunfeng Lin[1,3,4] | Alexander Krannich[6] | Yinan Wu[6] | Joseph P. Vacanti[1,2] | Craig M. Neville[1,2,3]

[1]Center for Regenerative Medicine, Massachusetts General Hospital, Boston, MA, USA

[2]Department of Surgery, Massachusetts General Hospital, Boston, MA, USA

[3]Department of Orthopaedics, Massachusetts General Hospital, Harvard Medical School, Boston, MA, USA

[4]State Key Laboratory of Oral Diseases, West China College of Stomatology, Sichuan University, Chengdu, China

[5]Department of Anesthesiology and Intensive Care Medicine, Campus Virchow Klinikum and Campus Charité Mitte, Charité Universitätsmedizin Berlin, Berlin, Germany

[6]Department of Biostatistics, Clinical Research Unit, Charité Universitätsmedizin Berlin, Berlin, Germany

Correspondence
Claudia C. Friedrich, Department of Anesthesiology and Intensive Care Medicine, Charité Universitätsmedizin Berlin, Berlin, Germany.
Email: claudia.friedrich@charite.de

Funding information
Stanley H. Durwood Foundation; Harvard Stem Cell Institute; Charité – Universitätsmedizin Berlin; Biomedical Sciences Exchange Program of the International Academy of Life Sciences

Abstract

Objectives: Creation of functional, durable vasculature remains an important goal within the field of regenerative medicine. Engineered biological vasculature has the potential to restore or improve human tissue function. We hypothesized that the pleotropic effects of insulin-like growth factor 1 (IGF1) would enhance the engineering of capillary-like vasculature.

Materials and methods: The impact of IGF1 upon vasculogenesis was examined in in vitro cultures for a period of up to 40 days and as subcutaneous implants within immunodeficient mice. Co-cultures of human umbilical vein endothelial cells and human bone marrow-derived mesenchymal stem cells in collagen-fibronectin hydrogels were supplemented with either recombinant IGF1 protein or genetically engineered cells to provide sustained IGF1. Morphometric analysis was performed on the vascular networks that formed in four concentrations of IGF1.

Results: IGF1 supplementation significantly enhanced de novo vasculogenesis both in vitro and in vivo. Effects were long-term as they lasted the duration of the study period, and included network density, vessel length, and diameter. Bifurcation density was not affected. However, the highest concentrations of IGF1 tested were either ineffective or even deleterious. Sustained IGF1 delivery was required in vivo as the inclusion of recombinant IGF1 protein had minimal impact.

Conclusion: IGF1 supplementation can be used to produce neovasculature with significantly enhanced network density and durability. Its use is a promising methodology for engineering de novo vasculature to support regeneration of functional tissue.

1 | INTRODUCTION

Vasculature assures oxygen delivery and nutrient supply for all organs in vertebrates. It allows for carbon dioxide and metabolite removal, which is crucial to maintain health. An injured, flow-limited, or occluded vascular system can lead to organ malfunction and tissue necrosis. According to the WHO, ischemic diseases are among the leading causes of death globally—for example, ischemic heart disease alone killed 8.8 million people in 2015.[1] In the advanced stages, ischemic diseases are life threatening despite well-established therapies. New strategies need to be developed and implemented to address this situation.

In addition, vascularization of engineered tissue designed for eventual clinical implantation for therapeutic purposes remains a major challenge. Angiogenesis, vasculature formed from pre-existing host vessels, has a maximum ingrowth rate of approximately 1 mm/day, much too slow to be able to support the significant tissue masses often required. Vasculogenesis, the de novo formation of blood vessels, is now being developed to create tissues ex vivo with pre-formed

This research was performed at the Center for Regenerative Medicine, Massachusetts General Hospital.

vascular networks that rapidly anastomose with host vessels and become functional soon after implantation.

Studies using clinically relevant progenitor sources for pericytes and endothelial cells (ECs) show that they can generate functional microvascular networks.[2-5] These networks, however, are typically immature and may rapidly regress. Vascular development and remodelling is dependent on several growth factors, the best known of which are Vascular Endothelial Growth Factor (VEGF) A, and Fibroblast Growth Factor (FGF) 2.[6-9] Improved engineered vasculature would allow ischemic and traumatic tissue defects to be treated more effectively and efficiently.[9-13]

The insulin super-family is composed of 10 members in mammals, insulin, 2 insulin-like growth factors, 3 relaxin proteins, and 4 insulin-like peptides. Sequence conservation is minimal; the major commonality is structural, as they all have 3 characteristic disulfide bonds. They also have diverse physiological roles. Among its many functions, insulin-like growth factor 1 (IGF1) is recognized as an angiogenic factor, along with specific members of the VEGF, FGF, Bone Morphogenetic Protein (BMP), Tissue Growth Factor (TGF), and Hepatocyte Growth Factor (HGF) families.[14-17] However, the normal regulatory role of IGF1 in promoting angiogenesis is not particularly well understood as most research has focused upon its possible pathogenic participation in promoting aberrant vascularization during retinopathy and tumour growth. In addition, many reports are highly contradictory, perhaps reflecting the importance of the precise context of the studies and the pleiotropic nature of the growth factor and its receptor.[18,19]

IGF1 is an effective FDA-approved therapy for children with short stature as it has a beneficial effect upon the entire musculoskeletal system. In addition to its anabolic properties, IGF1 enhances tissue repair by promoting angiogenesis and attenuating inflammation, necrosis, and apoptosis. Systemic IGF1 is largely synthesized by the liver. Its expression is controlled by Growth Hormone (GH) and mediates much of its growth-promoting activity. IGF1 is a small peptide and is rapidly cleared by the kidneys (t1/2 = 15 minute) if not in a binary complex with a member of the IGF1-binding protein family (IGFBP) or ternary complex with an additional acid labile subunit.[20] However, being complexed appears to most often reduce the bio-availability of systemic IGF1 as it cannot bind receptor. In addition, ternary complexes are unable to transit capillary walls. Although total IGF1 levels are typically in the 175-260 ng/mL in young adults,[21] only 0.2-0.6 ng/mL in serum and 3.6-10 ng/mL in interstitial fluid is free and bioavailable. Because IGF1 binding proteins are in vast excess to their ligand,[21] simply increasing total levels of system IGF1 has minimal impact on free levels. An engineered version of human IGF1, LR3IGF-I, was generated by inserting the first 11 amino acids of methionyl porcine growth hormone followed by the dipeptide VN and mutating the third codon encoding the mature human IGF1 peptide (E3R); this created a protein that can no longer be sequestered by IGFBPs yet can still bind and activate the IGF1 receptor.[22] However, like native unbound IGF1, LR3IGF-I is also rapidly cleared. IGF1 is also synthesized locally by most tissues through activation of an alternative transcriptional promoter. Local synthesis is GH independent, but is modulated by a variety of other soluble factors. Mural cells produce relatively high levels of IGF1 while the expression level in ECs is usually quite low. However, both cell types have high levels of IGF1 receptor and are fully capable of responding to changes in signalling. Clinical trials evaluating IGF1 on various ischaemia and neuropathies have been somewhat disappointing, perhaps because of their reliance on the systemic application regime developed to augment the GH-hepatic IGF1 axis in the treatment of short stature. IGF1 that is produced and acts locally could provide a sustained, spatially restricted signal could offer an effective means of treating such pathologies as avascular necrosis.

2 | MATERIALS AND METHODS

2.1 | Study design

The impact of including exogenous IGF1 on the formation of vascular networks in co-cultures of human umbilical vein endothelial cells (HUVECs) and human bone marrow-derived mesenchymal stem cells (MSCs) was examined. IGF1 was provided by including HEK-293 cells genetically engineered to constitutively secrete IGF1. HEK-293 cells are frequently used to synthesize biologically active, processed recombinant peptides in the pharmaceutical industry. This co-culture format allowed for continuous, localized IGF1 supplementation to cells within the core of the dense hydrogel plugs, even after implantation. The dosage was more readily controlled by adjusting the fraction of engineered cells included in the co-cultures than if HUVECs or MSCs had been engineered to directly express IGF1. Parallel experiments including recombinant IGF1 (rIGF1) protein during the formation of the hydrogel were also performed. Measurement and analysis of network morphometry were performed at several time points throughout the in vitro study period. IGF1-supplemented co-cultures were also evaluated in vivo by subcutaneous implantation in immunodeficient mice.

2.2 | Vascular cell preparations

Bone marrow samples were obtained from patients undergoing hip replacement surgery with the approval of the Institutional Review Board of Massachusetts General Hospital. hMSC cultures were established essentially as previously described.[23] 20 mL samples were diluted 1:1 in Hank's Buffered Salt Solution and the mononuclear fraction was isolated on a 10 mL ficoll gradient (Ficoll-Paque, GE Healthcare Life Sciences, Uppsala Sweden). Cells were plated in 25 mL α-MEM without nucleotides or β-glycerol phosphate supplemented with 20% foetal calf serum (Sigma, St. Louis, MO) and incubated at 37°C with 5% humidified CO_2. Non-adherent cells were discarded in 24 hours. Medium was replaced twice weekly. After 2 weeks, cultures were harvested by trypsin, and cryopreserved at a density of 10^6 cells/mL in complete medium with 5% DMSO. A thawed aliquot of each isolate was used to verify viability, determine colony forming units (cfu), marker expression, and confirm differentiation potential. Standard culture and assay conditions were used to verify that MSC isolations could be induced into adipocyte-, chondrocyte-, and osteocyte-specific lineages.[24] The Human MSC Marker Antibody Panel (R&D Systems, Minneapolis MN) was used to characterize the presence

of established surface markers by flow cytometry (FACsort, Becton Dickinson, Franklin Lakes NJ). A single human bone marrow MSC isolation was used for all experiments reported in this study. The isolation yielded 32 cfu/100 cells when plated at a density of 10 cells/cm^2 and cultured for 2 weeks. Approximately 88% of the cell population was positive for the markers CD90, CD105, CD146, and CD166, and negative for CD45. When plated, the cells stained positive for smooth muscle actin (ACTA2) and PDGF receptor beta (PDGFRβ). Cells were expanded in Mesenchymal Stem Cell Growth Medium (MSCGM) (Cambrex) and used at passage 4.

A pooled culture of HUVECs (Cascade Biologics, Portland, OR) was expanded two passages prior to use. The ECs were cultured in complete Endothelial Growth Medium 2 (EGM-2, PromoCell, Heidelberg, Germany), which contains 0.5 ng/mL VEGF-A, during expansion and in all experiments. MSCs were labelled with enhanced green fluorescent protein (eGFP) and HUVECs with tdTomato using standard lentivirus protocols.[25]

2.3 | Construction of IGF1-expressing cells

The GateWay system was used to create a lentivirus plasmid vector for constitutive expression of IGF1. The protein-encoding region of a rat IGF1 cDNA[26] (kind gift of Derek LeRoith) was amplified by PCR using the oligonucleotides CACCATGGGGAAAATCAGCAGT and CTACATTCTGTAGGTCTTGTTTCCT. The resulting DNA fragment was directionally cloned in the pENTR/D TOPO vector (Invitrogen, Carlsbad, CA) to create an IGF1 entry vector. The leading CACC sequence of the forward oligonucleotide functioned as a ribosome assembly site (Kozak sequence). A Clonase recombination reaction was performed using the plasmid pENTR5′(UbCp) containing the constitutively active human Ubiquitin C promoter, the IGF1 Entry plasmid, and the Destination vector pL6/R4R2V5-DEST (Invitrogen) to generate the plasmid pLB/UbCp(IGF1). The HEK-293 derived cell line used expresses the SV40 T antigen gene and is a fast growing subclone (HEK-293FT, Invitrogen) of the original derived from human embryonic kidney cells.[27] The T antigen allowed the transfected plasmid to be maintained as a stabile epitope. The cell line was transduced with pLB/UbCp(IGF1) and selected with the drug blasticidin to generate the IGF1-expressing cell line, HEK-IGF1.

2.4 | Formation of vascular constructs

The standard protocol for vascularization (control group) was based on previous studies.[2,28] Our prior work indicated a ratio of 2:1 of HUVECS and MSCs was optimal for inducing and maintaining vascular structures in a hydrogel.[3] Here, preliminary experiments were performed to confirm conditions for vasculogenesis with our cell preparations and materials, and to verify that inclusion of unmodified HEK-293FT cells would not be deleterious (data not shown). This information was then used to generate the following protocol. All reagents were maintained on ice prior to use. Each mL of collagen-fibronectin gel contained 385 μL EGM-2 medium, 25 μL 1 mol L^{-1} HEPES buffer, 500 μL 3 mg/mL bovine collagen I (PureCol, Advanced BioMatrix, San Diego, CA), 90 μL 1 mg/mL fibronectin (#33016-015, Invitrogen, Carlsbad, CA). Co-cultures studies involving the IGF1 expression vector included 0.125 × 10^6 HEK-293 cells in the co-culture cell suspension prior to pelleting. Three concentrations of HEK-IGF1 cells were evaluated, 1.25 × 10^3 cells (low), 12.5 × 10^3 cells (medium), 125 × 10^3 cells (high). Additional HEK-293FT cells were added to the control (no HEK-IGF1 cells), low and medium levels to maintain constant cell numbers across all conditions. Recombinant protein supplemented cultures contained 0 ng (control [standard]), 4 ng (low), 20 ng (medium), or 40 ng (high) rIGF1 (#100-11, PeproTech, Rocky Hill, NJ) per 0.5 mL collagen-fibronectin gel.

Cell suspensions containing 0.5 × 10^6 HUVECs, 0.25 × 10^6 MSCs, and optionally HEK-293 cells, were pelleted at 500 g/10 minute. Cell pellets were suspended in 0.5 mL ice-cold collagen-fibronectin gel before transferring to a glass-bottom 24-well plate and incubating at 37°C in a 5% CO_2 incubator. The gels were then overlaid with EGM-2 medium. Medium was replaced twice weekly and cultured for up to 40 days. Although the gel system showed progressive contraction, no conditions induced signs of gel degradation. Confocal imaging and quantification was performed at mid-depth of the gel, the region of highest cell density. Technical replicates were performed in triplicate for each condition, and the in vitro experiment repeated three times. Time points were measured initiating at day 1 and continued through day 40 (Table 1). The measured outcomes of interest were characteristics density, length, diameter, and bifurcations per image field and normalized for reporting in international units of measurement (eg, μm, or mm^2).

2.5 | Quantification of IGF1 release in vitro

IGF1 synthesis levels by HEK-IGF1 cells was measured using the Mouse/Rat IGF-I Quantikine ELISA Kit (R&D Systems, Minneapolis, MN), following manufacturer's protocol. A standard curve was generated using the included murine rIGF1 protein. Standard co-cultures that included HEK-293 or low, medium, or high levels of HEK-IGF1 cells were formed in triplicate using the collagen-fibronectin gel protocol. After 72 hours, the hydrogels were gently homogenized by stirring with a pipette tip, transferred to a 2 mL microfuge tube, and centrifuged at 16 000 g/2 minute. The supernatant was collected and diluted 10- and 100-fold prior to measuring IGF1 concentrations by ELISA.

2.6 | Immunodeficient mouse model

The subcutaneous injection procedure for producing vascularized hydrogel plugs in immunodeficient mice was used to evaluate the effect of IGF1 in vivo,[28] with ice-cold collagen-fibronectin plugs containing co-cultures that gelled when warmed to body temperature.[29] Providing growth factor by HEK-IGF1 and as rIGF1 were both examined. All animal procedures were approved by the Institutional Animal Care and Use Committee of the Massachusetts General Hospital and performed according to the National Institutes of Health Guidelines for the Care and Use of Laboratory Animals. Control, low, medium,

TABLE 1 Vessel parameters

Time point	Setup	Length of vessels (μm)	± SD	Diameter of vessels (μm)	± SD	Bifurcations (per vessel)	± SD	Vessel density (mm^2)
Day 1	Standard	150.23	17.27	14.82	4.38	3.00	1.63	37.47
Day 1	Low IGF-1 concentration	190.97	29.07	21.68	3.54	4.40	0.71	49.95
Day 1	Medium IGF-1 concentration	183.28	15.15	24.34	6.11	4.00	0.94	46.83
Day 1	High IGF-1 concentration	143.77	20.31	20.90	6.32	3.60	1.78	49.95
Day 2	Standard	188.01	13.61	17.91	6.32	2.20	1.03	40.59
Day 2	Low IGF-1 concentration	196.22	20.12	21.81	3.13	3.50	1.27	53.08
Day 2	Medium IGF-1 concentration	215.37	52.27	23.24	4.22	3.80	1.23	65.56
Day 2	High IGF-1 concentration	139.49	14.25	20.26	3.88	2.90	1.10	46.83
Day 3	Standard	223.57	76.20	21.19	6.01	2.70	0.95	53.08
Day 3	Low IGF-1 concentration	264.36	40.25	23.26	2.96	3.90	1.66	93.66
Day 3	Medium IGF-1 concentration	188.90	43.30	16.41	2.46	2.50	1.43	124.88
Day 3	High IGF-1 concentration	225.93	82.05	20.92	1.62	5.60	2.76	84.30
Day 4	Standard	185.70	62.01	22.06	7.12	4.90	1.52	93.66
Day 4	Low IGF-1 concentration	239.28	57.87	23.38	3.51	6.10	1.20	109.27
Day 4	Medium IGF-1 concentration	272.63	61.95	27.40	4.79	5.30	0.82	171.72
Day 4	High IGF-1 concentration	155.52	39.92	13.80	7.84	4.10	1.52	112.40
Day 5	Standard	152.48	32.79	14.21	4.14	3.10	0.86	37.47
Day 5	Low IGF-1 concentration	240.76	124.51	21.79	5.23	3.10	1.33	40.59
Day 5	Medium IGF-1 concentration	209.22	52.50	24.12	3.46	4.40	1.88	46.67
Day 5	High IGF-1 concentration	178.64	55.29	22.80	4.78	4.50	1.98	61.03
After 1 wk = d8	Standard	175.68	61.46	19.24	3.46	3.15	1.88	57.98
After 1 wk = d8	Low IGF-1 concentration	195.56	87.71	16.69	4.14	1.91	1.08	61.03
After 1 wk = d8	Medium IGF-1 concentration	240.45	89.26	22.43	4.80	3.21	1.22	72.24
After 1 wk = d8	High IGF-1 concentration	178.64	55.29	22.80	4.78	4.50	1.98	0.00
After 2.5 wks = d19	Standard	228.19	45.39	18.50	6.82	2.90	0.99	101.14
After 2.5 wks = d19	Low IGF-1 concentration	254.49	42.74	31.21	6.94	4.90	1.45	98.45
After 2.5 wks = d19	Medium IGF-1 concentration	256.24	29.41	25.39	6.02	5.10	1.52	101.14
After 2.5 wks = d19	High IGF-1 concentration	133.48	82.45	28.39	10.74	1.10	0.74	91.89
After 3 wks = d22	Standard	154.00	55.51	14.59	3.99	1.90	0.57	42.95
After 3 wks = d22	Low IGF-1 concentration	314.22	132.60	20.56	3.38	3.30	1.25	62.58
After 3 wks = d22	Medium IGF-1 concentration	325.56	71.02	23.33	3.11	3.40	1.17	74.18
After 3 wks = d22	High IGF-1 concentration	216.59	171.74	17.09	9.45	0.60	0.48	19.56
After 4 wks = d29	Standard	155.65	94.95	17.12	9.30	0.80	0.70	12.21
After 4 wks = d29	Low IGF-1 concentration	287.51	107.81	24.84	5.06	2.80	1.48	52.89
After 4 wks = d29	Medium IGF-1 concentration	220.08	60.12	22.40	4.30	4.60	1.78	59.11
After 4 wks = d29	High IGF-1 concentration	110.15	54.61	14.08	2.73	1.40	0.70	30.52
After 5 wks = d36	Standard	32.65	13.84	12.76	5.41	0.00	0.00	6.10
After 5 wks = d36	Low IGF-1 concentration	262.62	132.56	15.07	3.71	0.80	0.63	45.77
After 5 wks = d36	Medium IGF-1 concentration	278.81	168.41	16.05	5.87	1.20	0.79	27.46
After 5 wks = d36	High IGF-1 concentration	68.23	28.85	20.41	8.73	0.10	0.32	6.10
After 6 wks = d40	Standard	102.86	75.87	22.26	12.10	0.63	0.71	24.41
After 6 wks = d40	Low IGF-1 concentration	268.75	71.28	38.19	16.61	3.90	1.79	36.62
After 6 wks = d40	Medium IGF-1 concentration	231.14	135.50	30.51	18.38	1.50	0.71	27.46
After 6 wks = d40	High IGF-1 concentration	124.23	88.74	30.91	16.38	0.00	0.00	15.26

and high concentrations of HEK-IGF1 and rIGF1 were studied; cell rations and recombinant protein concentrations were identical to those used in the in vitro studies. At least three technical replicates of each of the four conditions for both HEK-IGF1 and rIGF1 were implanted. The cell compositions of the HEK-IGF1 were identical to those used for the in vitro studies.

Ten severe immunodeficient mice (NOD.CB17, Jackson Laboratory, Bar Harbor, ME) were implanted, four samples/mouse. Animals were anesthetized with a Ketamine/Xylazine solution (c = 1 mg/30 g mouse) for pain relief for the implant injections. Collagen-fibronectin gels were created on ice as described above prior to subcutaneous dorsal injection using a 1 mL syringe fitted with a 26 gauge needle. Each mouse received one plug of each of the four conditions; the positions were rotated in each mouse to different quadrants (crossover design). At 2 weeks, the plugs were explanted from sacrificed mice and analyzed via confocal microscopy imaging and histology.

2.7 | Imaging measurements using light microscopy

A Nikon A1 confocal microscope for detection and measurements of the vascularized collagen plugs with a 20× objective was used for imaging vascular networks. Representative regions mid-depth for each sample were imaged. Analysis of images was performed in ImageJ using the Vascular Network Toolkit Plug-in.[30] The red (HUVEC) channel of each image was isolated and the thresholding function used to generate a 2-bit skeletal vascular map from which the network values were quantified. Node analysis was performed, and distance measurements between nodes and density per unit area obtained. Thickness function was used to determine average vessel radius; this value was doubled and data presented as diameter. Vessel density was determined by determining the fractional area incorporated into vessels in the skeletonized images.

2.8 | Histological preparation and analysis

For histological analysis, the collagen-fibronectin plugs were excised from mice and fixed in 4% paraformaldehyde solution overnight at 4°C. Samples were dehydrated and embedded in paraffin by standard conditions. Transverse sections 10 μm thick were cut and processed for immunohistochemistry using primary antibody mouse anti-human CD31 (1:25; #M0823, DAKO, Carpinteria, CA), mouse anti-smooth muscle actin (1:50; DAKO), and anti-vimentin (1:50; DAKO), detected with the EnVision+ kit (#K4006, DAKO) using 3,3′-diaminobenzidine, and counter-stained with hematoxylin and eosin. Sections being probed with the anti-CD31 antibody were first processed for antigen retrieval by heating at 97°C for 30 minutes in 10 mM citrate, pH 6.0.

2.9 | Statistical analysis

To compare four setups at several time points, a non-parametric repeated measurement ANOVA was used for group comparison.[31] The Mann–Whitney-U Test was used for comparison of two independent setups per time point.[31] Group effect, time effect, and the interactions between group and time were investigated. A $P < .05$ was considered to be significant. Due to the exploratory study design and the weakness of post hoc power analysis, all calculated P values were considered in a non-confirmatory way. Missing data was accounted for using the last observation carried forward (LOCF) method. All numerical calculations were performed with IBM SPSS Statistics, Ver. 20, and the software package R Project for Statistical Computing, Ver. 3.0.2.

3 | RESULTS

3.1 | HEK-IGF1 significantly enhanced in vitro vascular network formation

In order to evaluate the impact of IGF1 on vasculogenesis, HEK-293 cells were genetically engineered to constitutively express IGF1. The engineered cells were included with co-cultures of HUVECs and MSCs during the formation of collagen-fibronectin hydrogels. Three HEK-IGF1 concentrations were compared to control co-cultures containing non-engineered HEK-293 cells for up to 40 days in vitro. Although many cultures remained viable, compaction of the hydrogel inhibited further analysis. Average network density, vessel length, and vessel diameter were determined periodically throughout the culture period for each of the experimental conditions.

Control co-cultures with non-IGF1 expressing HEK-293 cells largely maintained good viability to almost 3 weeks, after which they rapidly declined (Figure 1). This was in marked contrast to HUVEC cultures without MSCs, which form transient networks that rapidly fell apart in hours ([32] and data not shown). Supplementation by HEK-IGF1 cells dramatically impacted vascular network formation throughout the experimental period as measured by several metrics, with visible differences readily detectable by the third day. Network density was significantly greater for co-cultures containing low or medium levels of HEK-IGF1 cells (Figure 2). In contrast, high levels of HEK-IGF1 produced inferior networks that were largely indistinguishable or worse than control cultures. These differences were maintained throughout the entire experimental time course.

Co-cultures with low or medium levels of HEK-IGF1 had positive effects upon vessel length relative to controls throughout the experiment (Figure 3A). High levels of HEK-IGF1 produced networks that were initially similar to both control and medium levels. After day 3, networks became dramatically worse than all other conditions. Vessel lengths were consistently shorter at the highest HEK-IGF1 levels for the remainder of the study period.

Control co-cultures displayed the greatest average vessel diameter at day 3, after which it gradually declined (Figure 3B). All 3 HEK-IGF1 concentrations displayed significantly increased average vessel diameter relative to control conditions on day 1. Medium HEK-IGF1 levels consistently caused a significant and reproducible dip in both vessel length and diameter at day 3, after which the cultures rapidly recovered. Unlike average vessel length, the initial

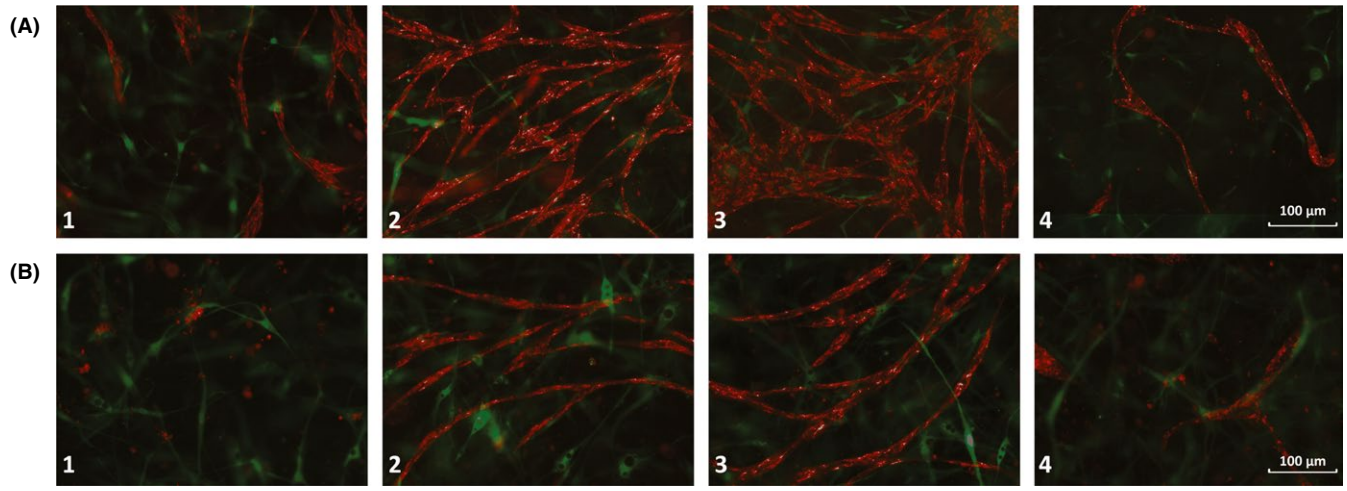

FIGURE 1 HEK-IGF1 promotes durable vascular network formation in vitro. Co-cultures of HUVECs and MSCs seeded with varying numbers of HEK-IGF1 cells were incubated for 40 d. Genetic labelling by lentivirus was used to express tdTomato in HUVECs and eGFP in MSCs. HEK-IGF1 cells were not fluorescently labelled. A, Co-cultures at 22 d. The networks of low (2) and medium (3) levels of HEK-IGF1 were denser than those of control cultures (1) and high levels (4). B, Co-cultures at 40 d. The networks of control cultures (1) and high levels (4) had largely degraded in contrast to those of low (2) and medium (3) levels. Scale bar = 100 microns

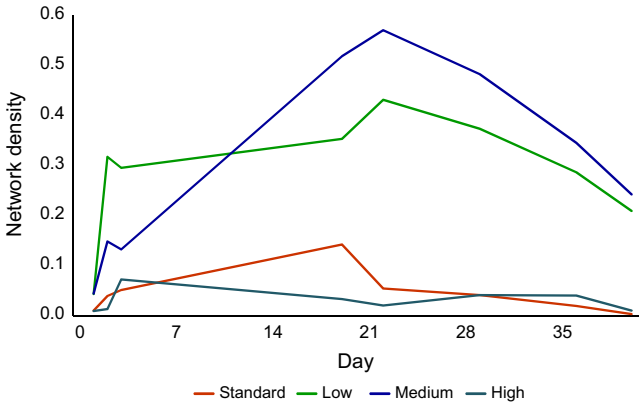

FIGURE 2 HEK-IGF1 promotes denser vascular networks in vitro. Co-cultures of HUVECs and MSCs seeded with varying numbers of HEK-IGF1 cells were incubated for 40 d. Cultures were imaged at the indicated times and average vessel density was calculated and plotted

increase in average vessel diameter for HEK-IGF1 co-cultures was not maintained throughout the study period by any of the tested conditions. Maximum average diameter peaked on day 19 for all cultures that included HEK-IGF1, a few days before the period displaying maximum length. The apparent large diameter of the high-level HEK-IGF1 co-cultures at the final time point was the result of the few surviving HUVECs forming clumps or islands rather than tubes. The number of vessel bifurcations occurring under each condition was also determined, but differences were not statistically significant (data not shown).

3.2 | Quantification of IGF1 release by HEK-IGF1

We wanted to determine if medium supplemented with rIGF1 protein could substitute for that produced by HEK-IGF1. Synthesis levels were assessed using ELISA to measure IGF1 in the medium of co-cultures containing HEK-293, or low, medium, or high levels of HEK-IGF1. Measured IGF1 levels were proportional to a number of HEK-IGF1 cells in the culture, and corresponded to *ca.* 1 ng/10^3 HEK-IGF1 cells/day. Negligible levels of IGF1 were detected from HEK-293 cells in these conditions.

3.3 | rIGF1 protein stabilizes in vitro vascular networks

Co-cultures were prepared with rIGF1 protein replacing HEK-IGF1. Again, three levels of IGF1 supplementation were compared to unsupplemented control cultures. For low and medium cultures, rIGF1 levels were chosen to match those measured in the corresponding HEK-IGF1 setups. Because the highest HEK-IGF1 levels were clearly toxic, a lower concentration of recombinant protein was used in the high-level cultures. Co-cultures were followed until compaction of the hydrogel made imaging difficult (36 days). Supplementation with rIGF1 again dramatically impacted vasculogenesis, with visible differences readily detectable throughout the culture period (Figure 4). Although the resulting networks were similar to those prior, rIGF1 supplementation did not precisely mirror that with HEK-IGF1. For high rIGF1 co-cultures, the reduced growth factor level was still deleterious, and like unsupplemented co-cultures, had few surviving ECs. Both low and medium rIGF1 levels promoted network survival to a similar degree. However, the resulting networks were notably less dense with shorter branches (Figure 5A). In addition, vessel diameters were greatly reduced (Figure 5B).

3.4 | Assessment IGF1 treatment on in vivo vascular networks

To assess potential in vivo functionality of IGF1-enhanced vascular networks, co-cultures containing collagen-fibronectin plugs were

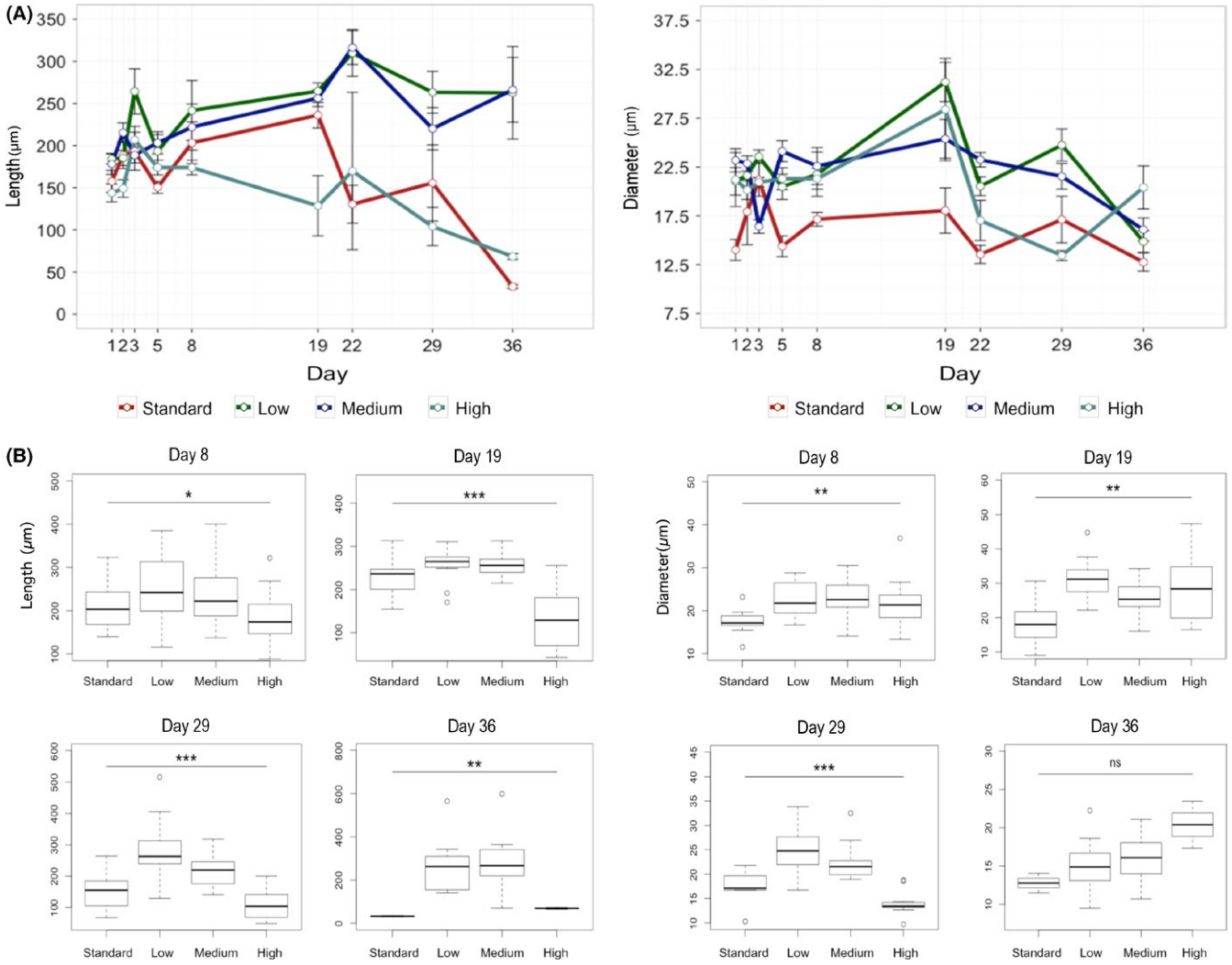

FIGURE 3 HEK-IGF1 promotes vasculature with longer length and greater diameter in vitro. Co-cultures of HUVECs and MSCs seeded with varying numbers of HEK-IGF1 cells were incubated for 40 d. Cultures were imaged at the indicated times. Average length (A) and diameter of the vessels (B) were calculated. Box and whisker plots below show the statistical distribution of data for selected subsets of time points. *P* values for this and subsequent figures: NS = not significant, *<.05, **<.01, ***<.001

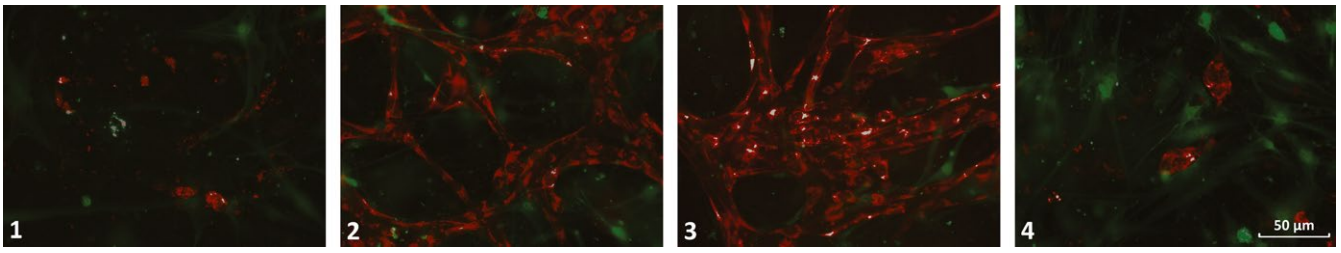

FIGURE 4 rIGF1 protein promotes durable vascular networks in vitro. Co-cultures of HUVECs and MSCs seeded with varying concentrations of rIGF1 protein were imaged at 36 d. Genetic labelling by lentivirus was used to express tdTomato in HUVECs and eGFP in MSCs. The networks of control cultures (1) and high concentration (4) had largely degraded in contrast to those of low (2) and medium (3) concentration. Scale bar = 50 μm

implanted subcutaneously in immunodeficient mice. Both supplementations by HEK-IGF1 and rIGF1 were evaluated. After 14 days the implants were removed for analysis. They were initially imaged by confocal microscopy to assess network survival and morphometry. Vascular networks were readily detectable in control samples for both HEK-IGF1 and rIGF1 containing plugs (Figure 6A, B). Few surviving HUVECs were found in high HEK-IGF1 samples; remaining MSCs were numerous but most appeared pyknotic. Networks in both the low and medium HEK-IGF1 samples were relatively extensive compared to those in controls. Both the average length

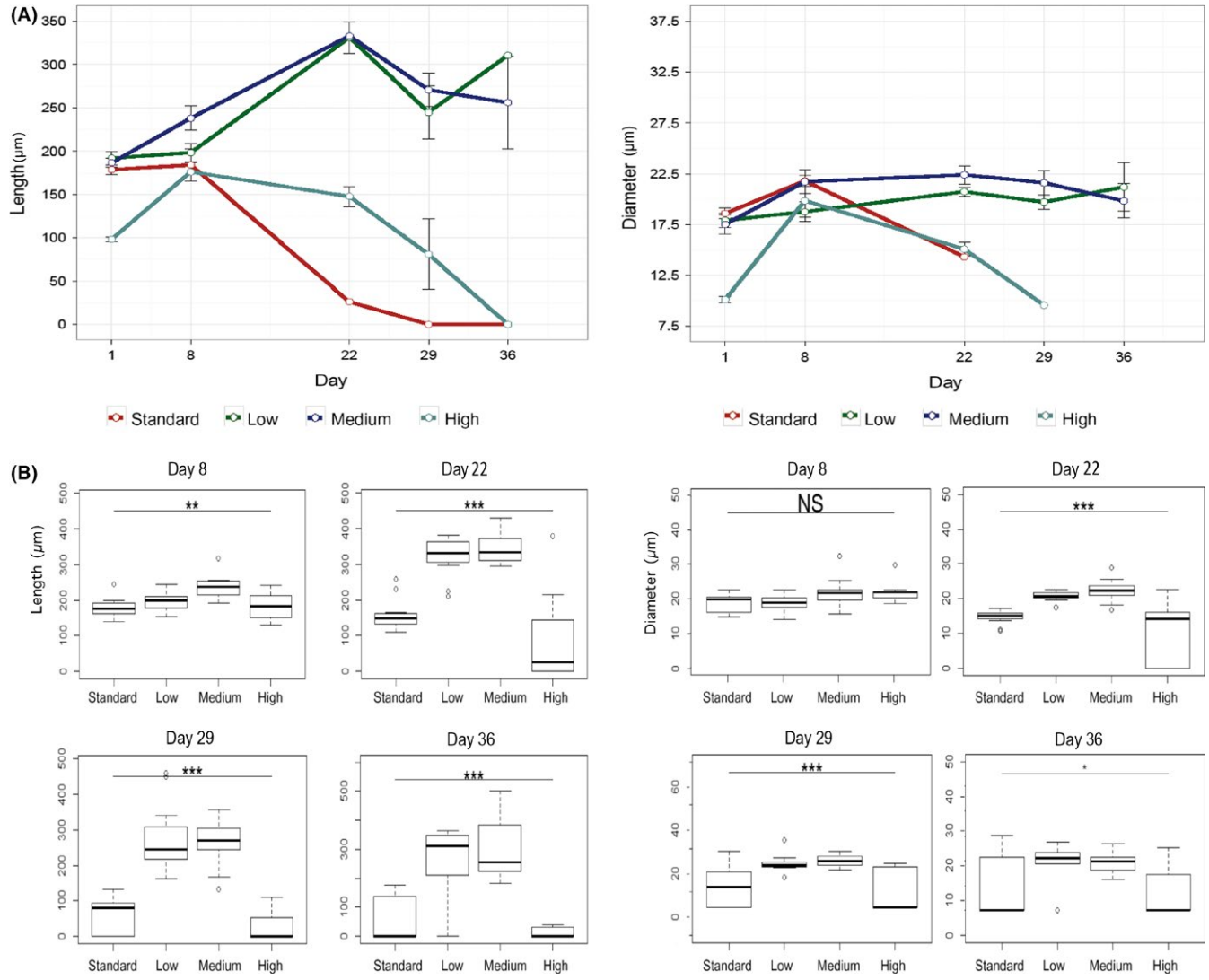

FIGURE 5 rIGF1 promotes vasculature with longer length and greater diameter in vitro. Co-cultures of HUVECs and MSCs seeded with varying concentrations of rIGF1 protein were incubated for 36 d. A, Cultures were imaged at the indicated times and average vessel length was calculated. B, Box and whisker plots show the statistical distribution of data for a selected subset of time points. NS = not significant

and diameter of the low HEK-IGF1 samples were larger than for all other conditions studied (Figure 7A). Although the low HEK-IGF1 produced vessels that were uniform in appearance, they still maintained a degree of tortuous (immature) character. In contrast, vessels in medium HEK-IGF1 samples appeared noticeably more linear. Explants containing rIGF1 supplementation produced networks at all levels. No toxicity was seen at high levels of rIGF1. However, supplementation with rIGF1 caused a small but significant increase in the low dosage only; the highest levels were somewhat detrimental. Average vessel diameters were unchanged at all dosages (Figure 7B). Paraffin sections from embedded samples were probed with a human-specific antibody against the endothelial marker CD31. Numerous HUVEC-derived capillaries were present in both HEK-IGF1 and rIGF1 supplemented implants. The vessels were filled with blood cells, providing evidence of the patency of the vascular lumen and anastomosis of the network (Figure 6C).

4 | DISCUSSION

During angiogenesis and vasculogenesis, interactions between pericytes and ECs promote vessel formation by altering the microenvironment. Both exchange of soluble factors and physical contact are important. In vasculogenesis studies, MSCs are routinely used to serve as mural cells. Indeed, there is evidence that MSCs derive from a subpopulation of mural cells.[16,24] They produce trophic factors that stimulate angiogenesis and subsequent contact significantly stabilizes the resulting networks.[2,3,32] A number of signalling molecules, metalloproteases, and ECM components have been shown to be critical players in the complex process. In spite of the coordinated involvement of several growth factors during growth of normal, functional vasculature, well-timed therapy with a single factor such as VEGF-A or PDGF-BB can also result in mature vessels.[33,34] This may be because most angiogenic growth factors can induce expression of

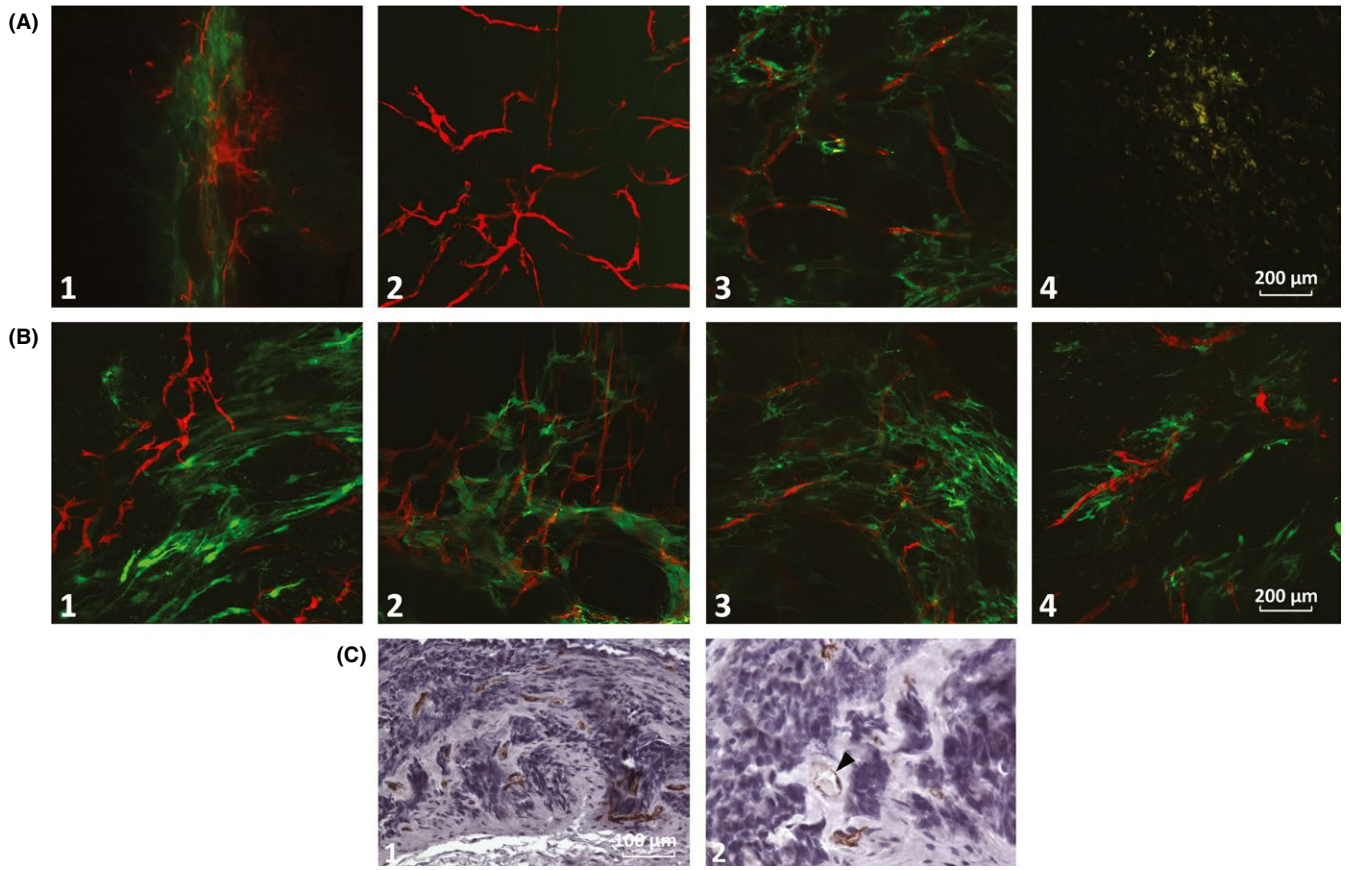

FIGURE 6 IGF1 supplementation promotes extensive vascular networks in vivo. Collagen-fibrinogen plugs with co-cultures of HUVECs and MSCs were implanted subcutaneously in immunodeficient mice. Plugs were explanted at 14 d and imaged by confocal microscopy. A, Varying numbers of HEK-IGF1 cells were included in the co-cultures: control (1), low (2), medium (3), and high (4). B, Varying amounts of recombinant IGF1 protein were included with the co-cultures during hydrogel formation: control (1), low (2), medium (3), and high (4). C, A paraffin section from a medium HEK-IGF supplemented explanted sample was probed with a human-specific anti-CD31 antibody to identify implant derived vessels (enlargement on right). Vascular networks were filled with blood cells, indicating that they anastomosed and are patent and functional. Scale bar for (A, B) = 200 µm

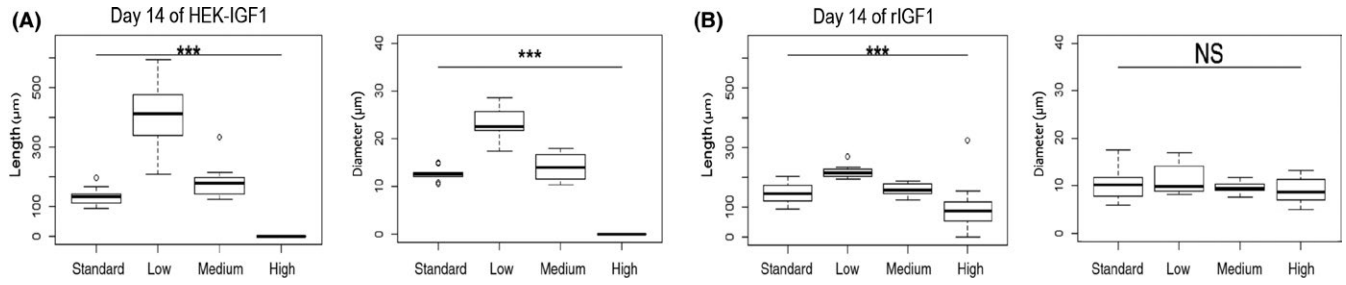

FIGURE 7 HEK-IGF1 but not rIGF1 supplementation promotes extensive vascular networks in vivo. Average vessel lengths and diameters were calculated from images of the explanted plugs and plotted for HEK-IGF1 (A) and rIGF1 (B). NS = not significant

many of the other factors by the target cells. Although IGF1 can upregulate expression of several growth factors including VEGF-A and PDGF-BB, evidence is lacking that any angiogenic factors upregulate IGF1 expression.[35] This may place IGF1 in an apex position in hierarchy of angiogenic signalling. Therapeutic rationale for providing angiogenic factors include limiting endogenous concentrations of a growth factor, augmentation of the response by providing supraphysiological amounts, and overcoming inhibitory conditions.[36]

IGF1 is an attractive candidate as a potential therapeutic factor to promote angiogenesis. Although its angiogenic properties were first recognized three decades ago,[37,38] even very basic studies involving this factor have been quite limited due to fears of retinopathy and coronary artery disease in clinical use.[39,40] However, extensive and prolonged use of IGF1 to treat short stature and numerous recent clinical studies have not born out such fears. Nevertheless, the failure of many of these clinical trials has clearly indicated that systemic

application of the growth factor is often not efficacious for treating localized ailments. IGF1 bio-availability is tightly regulated by both its binding proteins and turnover; specific local applications may need to be developed in order to take advantage of its properties.

IGF1 can potentially mediate angiogenesis through several mechanisms, as both ECs and mural cells express significant levels of IGF1 receptor.[41,42] IGF1 robustly promotes proliferation of vascular smooth muscle cells.[43] Reports of the effect upon EC proliferation vary, and may depend upon the vascular bed being studied.[14,15,35,43] IGF1 stimulates migration of both smooth muscle and ECs.[37,38] It promotes EC migration through phosphatidylinositol 3-kinase (PI3K) activation.[44] Importantly, at moderate levels, it is also a major survival factor for a broad range of cell types, and is able to prevent cell death and apoptosis during normal development, stress, repair, and disease.[45] The role in modulating inflammatory response is more nuanced, as many studies document inhibition by IGF1 signalling[46] while separate studies have demonstrated non-responsiveness[47] or even enhancement[48]. This is an important consideration as inflammation drives the senescent state where ECs are growth arrested and unresponsive to extracellular signalling. Again, IGF1 inhibits oxidative-stress mediated senescence, but has been implicated in promoting radiation-induced senescence.[49,50] In addition, macrophage act as essential cellular chaperones in mediating anastomosis.[51]

IGF1, like VEGF, also upregulates endothelial nitric oxide synthase (eNOS) activity through PI3K.[52,53] IGF1 synergistically augments the VEGF-induced angiogenic response through the MAPK pathway.[39] IGF1 is a potent anabolic factor, and promotes mitochondrial function.[54] IGF1 also directly modulates inflammation response of both macrophage and ECs. Physiological response to the development of tissue ischemia includes the upregulation of angiogenic growth factor activity;[55] this may include activation of latent factors sequestered in the ECM as well as de novo synthesis. In in vitro monocultures of ECs, the vascular networks that form rapidly regress. In part, this is due to lysophosphatidic acid (LPA) in the serum that induces destabilization.[56] Inclusion of IGF1 prolongs Erk activity, a signalling pathway recently demonstrated to stabilize nascent vessels. LPA may be important for initial destabilization or remodelling of existing vessels in the early stages of angiogenic sprouting, but continued signalling is deleterious. IGF1-promoted Erk signalling overrides this, at least in the short-term (hours). Such destabilization does not occur in co-cultures that include stromal cells such as pericytes or MSCs, as they accelerate LPA metabolism.[57]

In addition, MSCs secrete IGF1,[35] which may also contribute to the vessel stabilization seen in co-cultures. However, our study demonstrated that augmentation with exogenous IGF1 clearly provided significant additional long-term vessel stabilization. In our experimental vasculogenesis models, we supplemented the co-cultures with genetically engineered cells that produce IGF1 or provided recombinant protein in the medium. In normal vasculature, IGF1 is significantly expressed only by mural cells; the low levels of protein detected in ECs is thought to have been sequestered from serum.[19,58,59] Both cell types, however, are fully capable of responding to IGF1 signalling as they both abundantly express the receptor.[41,42] Furthermore, some of the effects documented in this study may secondary, as IGF1 stimulation can induce synthesis of additional angiogenic growth factors and/or their receptors including VEGF, HGF, and FGF. It is unlikely that IGF1 supplementation functioned directly as a chemoattractant in our studies as it was homogeneously distributed in the cultures. It could, however, have induced secretion of a chemoattractant by a responding cell type that would then present in the requisite gradient.

Both methods of providing IGF1 proved beneficial in vitro, although only HEK-IGF1 provided a similar effect in vivo. HEK-IGF1-containing cultures were also noticeably more robust by most in vitro metrics. The exception was network survival as both methods of IGF1 supplementation caused significant enhanced network persistence. While networks in standard conditions declined precipitously after 19 days in culture, those with either HEK-IGF1 or rIGF1 were still stabile and viable at 36 days. Inclusion of the growth factor also resulted in denser networks, with those containing HEK-IGF1 being greater than rIGF1. The average length of the vessels was longer, although the number of bifurcations was similar. Interestingly, the diameters of the resulting vessels of HEK-IGF1-containing cultures were noticeably larger as well, often several cells wide. This suggests a possible role for IGF1 in arteriogenesis (enlargement of existing vessels), an important but still relatively poorly understood process.[14,15,60,61] Although the mechanism for the apparent toxicity resulting from the highest levels on both MSCs and ECs was not examined in our study, similar concentrations of IGF1 induce apoptosis in other cell types through internalization of the IGF1 receptor and down-regulation of its associated signalling.[62-64]

These results suggest many additional follow up studies to further understand the roles and mechanisms of IGF1 during angiogenesis. From the aspect of therapeutic development of cell therapy, potential benefits from simple pre-exposure to the growth factor prior to network formation and implantation should be determined. A detailed study of anastomosed vasculature should examine long-term in vivo persistence and function. Dissecting some of the specific responses to IGF1 by MSCs and ECs could be done in monocultures; others will require co-cultures expressing mutant or dominant negative IGF1 receptor. In particular, the determination of whether the size of functional vessels can be modulated with IGF1 will be of significant interest.

ACKNOWLEDGEMENTS

This work was sponsored by a grant to CMN from the Stanley H. Durwood Foundation and the Harvard Stem Cell Institute. CCF received a research scholarship from the Charité – Universitätsmedizin Berlin and a scholarship from the Biomedical Sciences Exchange Program of the International Academy of Life Sciences.

CONFLICT OF INTEREST

The authors hereby disclose no conflicts of interest.

ORCID

Claudia C. Friedrich http://orcid.org/0000-0003-3241-6556
Yunfeng Lin http://orcid.org/0000-0003-1224-6561

REFERENCES

1. WHO. The top 10 causes of death. World Health Organization; 2015 [January 17, 2017]. http://www.who.int/mediacentre/factsheets/fs310/en/.
2. Melero-Martin JM, De Obaldia ME, Kang SY, et al. Engineering robust and functional vascular networks in vivo with human adult and cord blood-derived progenitor cells. *Circ Res*. 2008;103:194-202.
3. Tsigkou O, Pomerantseva I, Spencer JA, et al. Engineered vascularized bone grafts. *Proc Natl Acad Sci U S A*. 2010;107:3311-3316.
4. Amini AR, Laurencin CT, Nukavarapu SP. Differential analysis of peripheral blood- and bone marrow-derived endothelial progenitor cells for enhanced vascularization in bone tissue engineering. *J Orthop Res*. 2012;30:1507-1515.
5. Maeng YS, Choi HJ, Kwon JY, et al. Endothelial progenitor cell homing: prominent role of the IGF2-IGF2R-PLCbeta2 axis. *Blood*. 2009;113:233-243.
6. Joensuu K, Uusitalo L, Alm JJ, Aro HT, Hentunen TA, Heino TJ. Enhanced osteoblastic differentiation and bone formation in co-culture of human bone marrow mesenchymal stromal cells and peripheral blood mononuclear cells with exogenous VEGF. *Orthop Traumatol Surg Res*. 2015;101:381-386.
7. Muscari C, Gamberini C, Basile I, et al. Comparison between culture conditions improving growth and differentiation of blood and bone marrow cells committed to the endothelial cell lineage. *Biol Proced Online*. 2010;12:9023.
8. Schar MO, Diaz-Romero J, Kohl S, Zumstein MA, Nesic D. Platelet-rich concentrates differentially release growth factors and induce cell migration in vitro. *Clin Orthop Relat Res*. 2015;473:1635-1643.
9. Rivron NC, Liu JJ, Rouwkema J, de Boer J, van Blitterswijk CA. Engineering vascularised tissues in vitro. *Eur Cell Mater*. 2008;15:27-40.
10. Collinson DJ, Donnelly R. Therapeutic angiogenesis in peripheral arterial disease: can biotechnology produce an effective collateral circulation? *Eur J Vasc Endovasc Surg*. 2004;28:9-23.
11. Lee WY, Wei HJ, Wang JJ, et al. Vascularization and restoration of heart function in rat myocardial infarction using transplantation of human cbMSC/HUVEC core-shell bodies. *Biomaterials*. 2012;33:2127-2136.
12. Nelson MA, Passeri J, Frishman WH. Therapeutic angiogenesis: a new treatment modality for ischemic heart disease. *Heart Dis*. 2000;2:314-325.
13. Silvestre JS, Smadja DM, Levy BI. Postischemic revascularization: from cellular and molecular mechanisms to clinical applications. *Physiol Rev*. 2013;93:1743-1802.
14. Carmeliet P. Mechanisms of angiogenesis and arteriogenesis. *Nat Med*. 2000;6:389-395.
15. Semenza GL. Vasculogenesis, angiogenesis, and arteriogenesis: mechanisms of blood vessel formation and remodeling. *J Cell Biochem*. 2007;102:840-847.
16. Zhou C, Cai X, Grottkau BE, Lin Y. BMP4 promotes vascularization of human adipose stromal cells and endothelial cells in vitro and in vivo. *Cell Prolif*. 2013;46:695-704.
17. Lin S, Xie J, Gong T, et al. TGFbeta signalling pathway regulates angiogenesis by endothelial cells, in an adipose-derived stromal cell/endothelial cell co-culture 3D gel model. *Cell Prolif*. 2015;48:729-737.
18. Bach LA. Endothelial cells and the IGF system. *J Mol Endocrinol*. 2015;54:R1-R13.
19. Delafontaine P, Song YH, Li Y. Expression, regulation, and function of IGF-1, IGF-1R, and IGF-1 binding proteins in blood vessels. *Arterioscler Thromb Vasc Biol*. 2004;24:435-444.
20. Lepenies J, Wu Z, Stewart PM, Strasburger CJ, Quinkler M. IGF-1, IGFBP-3 and ALS in adult patients with chronic kidney disease. *Growth Horm IGF Res*. 2010;20:93-100.
21. Friedrich N, Alte D, Volzke H, et al. Reference ranges of serum IGF-1 and IGFBP-3 levels in a general adult population: results of the Study of Health in Pomerania (SHIP). *Growth Horm IGF Res*. 2008;18:228-237.
22. Francis GL, Ross M, Ballard FJ, et al. Novel recombinant fusion protein analogues of insulin-like growth factor (IGF)-I indicate the relative importance of IGF-binding protein and receptor binding for enhanced biological potency. *J Molec Endocrinol*. 1992;8:213-223.
23. Prockop DJ, Azizi SA, Colter D, Digirolamo C, Kopen G, Phinney DG. Potential use of stem cells from bone marrow to repair the extracellular matrix and the central nervous system. *Biochem Soc Trans*. 2000;28:341-345.
24. Cai X, Lin Y, Friedrich CC, et al. Bone marrow derived pluripotent cells are pericytes which contribute to vascularization. *Stem Cell Rev*. 2009;5:437-445.
25. Rubinson DA, Dillon CP, Kwiatkowski AV, et al. A lentivirus-based system to functionally silence genes in primary mammalian cells, stem cells and transgenic mice by RNA interference. *Nat Genet*. 2003;33:401-406.
26. Adamo ML, Ben-Hur H, LeRoith D, Roberts CT Jr. Transcription initiation in the two leader exons of the rat IGF-I gene occurs from disperse versus localized sites. *Biochem Biophys Res Commun*. 1991;176:887-893.
27. Graham FL, Smiley J, Russell WC, Nairn R. Characteristics of a human cell line transformed by DNA from human adenovirus type 5. *J Gen Virol*. 1977;36:59-74.
28. Melero-Martin JM, Bischoff J. Chapter 13. An in vivo experimental model for postnatal vasculogenesis. *Methods Enzymol*. 2008;445:303-329.
29. Lin RZ, Melero-Martin JM. Bioengineering human microvascular networks in immunodeficient mice. *J Vis Exp*. 2011;53:e3065.
30. Abramoff MD, Magalhaes PJ, Ram SJ. Image processing with image. *J Biophotonics Int*. 2004;11:36-42.
31. Brunner E, Domhof S, Langer F. *Nonparametric analysis of longitudinal data in factorial experiments*. New York, NY: Wiley; 2002. Vol. XVII, 261 p.
32. Au P, Tam J, Fukumura D, Jain RK. Bone marrow-derived mesenchymal stem cells facilitate engineering of long-lasting functional vasculature. *Blood*. 2008;111:4551-4558.
33. Ehrbar M, Djonov VG, Schnell C, et al. Cell-demanded liberation of VEGF121 from fibrin implants induces local and controlled blood vessel growth. *Circ Res*. 2004;94:1124-1132.
34. Dor Y, Djonov V, Abramovitch R, et al. Conditional switching of VEGF provides new insights into adult neovascularization and pro-angiogenic therapy. *EMBO J*. 2002;21:1939-1947.
35. Conti E, Musumeci MB, De Giusti M, et al. IGF-1 and atherothrombosis: relevance to pathophysiology and therapy. *Clin Sci (Lond)*. 2011;120:377-402.
36. Cao Y, Hong A, Schulten H, Post MJ. Update on therapeutic neovascularization. *Cardiovasc Res*. 2005;65:639-648.
37. Grant M, Jerdan J, Merimee TJ. Insulin-like growth factor-I modulates endothelial cell chemotaxis. *J Clin Endocrinol Metab*. 1987;65:370-371.
38. Nakao-Hayashi J, Ito H, Kanayasu T, Morita I, Murota S. Stimulatory effects of insulin and insulin-like growth factor I on migration and tube formation by vascular endothelial cells. *Atherosclerosis*. 1992;92:141-149.
39. Smith LE, Shen W, Perruzzi C, et al. Regulation of vascular endothelial growth factor-dependent retinal neovascularization by insulin-like growth factor-1 receptor. *Nat Med*. 1999;5:1390-1395.
40. Chiu CJ, Conley YP, Gorin MB, et al. Associations between genetic polymorphisms of insulin-like growth factor axis genes and risk

for age-related macular degeneration. *Invest Ophthalmol Vis Sci*. 2011;52:9099-9107.
41. Bar RS, Boes M. Distinct receptors for IGF-I, IGF-II, and insulin are present on bovine capillary endothelial cells and large vessel endothelial cells. *Biochem Biophys Res Commun*. 1984;124:203-209.
42. Du J, Meng XP, Delafontaine P. Transcriptional regulation of the insulin-like growth factor-I receptor gene: evidence for protein kinase C-dependent and -independent pathways. *Endocrinology*. 1996;137:1378-1384.
43. Arnqvist HJ, Bornfeldt KE, Chen Y, Lindstrom T. The insulin-like growth factor system in vascular smooth muscle: interaction with insulin and growth factors. *Metabolism*. 1995;44(10 Suppl. 4):58-66.
44. Liu W, Liu Y, Lowe WL Jr. The role of phosphatidylinositol 3-kinase and the mitogen-activated protein kinases in insulin-like growth factor-I-mediated effects in vascular endothelial cells. *Endocrinology*. 2001;142:1710-1719.
45. Vincent AM, Feldman EL. Control of cell survival by IGF signaling pathways. *Growth Horm IGF Res*. 2002;12:193-197.
46. Liu SJ, Zhong Y, You XY, Liu WH, Li AQ, Liu SM. Insulin-like growth factor 1 opposes the effects of C-reactive protein on endothelial cell activation. *Mol Cell Biochem*. 2014;385:199-205.
47. Back K, Islam R, Johansson GS, Chisalita SI, Arnqvist HJ. Insulin and IGF1 receptors in human cardiac microvascular endothelial cells: metabolic, mitogenic and anti-inflammatory effects. *J Endocrinol*. 2012;215:89-96.
48. Che W, Lerner-Marmarosh N, Huang Q, et al. Insulin-like growth factor-1 enhances inflammatory responses in endothelial cells: role of Gab1 and MEKK3 in TNF-alpha-induced c-Jun and NF-kappaB activation and adhesion molecule expression. *Circ Res*. 2002;90:1222-1230.
49. Higashi Y, Pandey A, Goodwin B, Delafontaine P. Insulin-like growth factor-1 regulates glutathione peroxidase expression and activity in vascular endothelial cells: Implications for atheroprotective actions of insulin-like growth factor-1. *Biochim Biophys Acta*. 2013;1832:391-399.
50. Panganiban RA, Day RM. Inhibition of IGF-1R prevents ionizing radiation-induced primary endothelial cell senescence. *PLoS ONE*. 2013;8:e78589.
51. Fantin A, Vieira JM, Gestri G, et al. Tissue macrophages act as cellular chaperones for vascular anastomosis downstream of VEGF-mediated endothelial tip cell induction. *Blood*. 2010;116:829-840.
52. Wang Y, Nagase S, Koyama A. Stimulatory effect of IGF-I and VEGF on eNOS message, protein expression, eNOS phosphorylation and nitric oxide production in rat glomeruli, and the involvement of PI3-K signaling pathway. *Nitric Oxide*. 2004;10:25-35.
53. Michell BJ, Griffiths JE, Mitchelhill KI, et al. The Akt kinase signals directly to endothelial nitric oxide synthase. *Curr Biol*. 1999;9:845-848.
54. Sadaba MC, Martin-Estal I, Puche JE, Castilla-Cortazar I. Insulin-like growth factor 1 (IGF-1) therapy: mitochondrial dysfunction and diseases. *Biochim Biophys Acta*. 2016;1862:1267-1278.
55. Folkman J. Angiogenesis in cancer, vascular, rheumatoid and other disease. *Nat Med*. 1995;1:27-31.
56. Jacobo SM, Kazlauskas A. Insulin-like growth factor 1 (IGF-1) stabilizes nascent blood vessels. *J Biol Chem*. 2015;290:6349-6360.
57. Motiejunaite R, Aranda J, Kazlauskas A. Pericytes prevent regression of endothelial cell tubes by accelerating metabolism of lysophosphatidic acid. *Microvasc Res*. 2014;93:62-71.
58. Gajdusek CM, Luo Z, Mayberg MR. Sequestration and secretion of insulin-like growth factor-I by bovine aortic endothelial cells. *J Cell Physiol*. 1993;154:192-198.
59. Tucci M, Nygard K, Tanswell BV, Farber HW, Hill DJ, Han VK. Modulation of insulin-like growth factor (IGF) and IGF binding protein biosynthesis by hypoxia in cultured vascular endothelial cells. *J Endocrinol*. 1998;157:13-24.
60. Lahteenvuo JE, Lahteenvuo MT, Kivela A, et al. Vascular endothelial growth factor-B induces myocardium-specific angiogenesis and arteriogenesis via vascular endothelial growth factor receptor-1- and neuropilin receptor-1-dependent mechanisms. *Circulation*. 2009;119:845-856.
61. Buschmann I, Schaper W. Arteriogenesis versus angiogenesis: two mechanisms of vessel growth. *News Physiol Sci*. 1999;14:121-125.
62. Rosenfeld RG, Dollar LA. Characterization of the somatomedin-C/insulin-like growth factor I (SM-C/IGF-I) receptor on cultured human fibroblast monolayers: regulation of receptor concentrations by SM-C/IGF-I and insulin. *J Clin Endocrinol Metab*. 1982;55:434-440.
63. Rosenfeld RG, Hintz RL. Characterization of a specific receptor for somatomedin C (SM-C) on cultured human lymphocytes: evidence that SM-C modulates homologous receptor concentration. *Endocrinology*. 1980;107:1841-1848.
64. Chi MM, Schlein AL, Moley KH. High insulin-like growth factor 1 (IGF-1) and insulin concentrations trigger apoptosis in the mouse blastocyst via down-regulation of the IGF-1 receptor. *Endocrinology*. 2000;141:4784-4792.

How to cite this article: Friedrich CC, Lin Y, Krannich A, Wu Y, Vacanti JP, Neville CM. Enhancing engineered vascular networks in vitro and in vivo: The effects of IGF1 on vascular development and durability. *Cell Prolif*. 2018;51:e12387. https://doi.org/10.1111/cpr.12387

Engineered vascularized bone grafts

Olga Tsigkou[a,b], Irina Pomerantseva[a,b], Joel A. Spencer[c,d], Patricia A. Redondo[a,b], Alison R. Hart[a,b], Elisabeth O'Doherty[a,b], Yunfeng Lin[a], Claudia C. Friedrich[a,b], Laurence Daheron[a], Charles P. Lin[c], Cathryn A. Sundback[a,b], Joseph P. Vacanti[a,b], and Craig Neville[a,b,1]

[a]Center for Regenerative Medicine, [b]Department of Surgery, and [c]Advanced Microscopy Program, Center for Systems Biology and Wellman Center for Photomedicine, Massachusetts General Hospital, Harvard Medical School, Boston, MA 02114; and [d]Department of Biomedical Engineering, Tufts University, Science and Technology Center, 4 Colby Street, Medford, MA 02155

Edited by Stephen F Badylak, University of Pittsburgh Medical Center, Pittsburgh, PA, and accepted by the Editorial Board December 17, 2009 (received for review June 1, 2009)

Clinical protocols utilize bone marrow to seed synthetic and decellularized allogeneic bone grafts for enhancement of scaffold remodeling and fusion. Marrow-derived cytokines induce host neovascularization at the graft surface, but hypoxic conditions cause cell death at the core. Addition of cellular components that generate an extensive primitive plexus-like vascular network that would perfuse the entire scaffold upon anastomosis could potentially yield significantly higher-quality grafts. We used a mouse model to develop a two-stage protocol for generating vascularized bone grafts using mesenchymal stem cells (hMSCs) from human bone marrow and umbilical cord-derived endothelial cells. The endothelial cells formed tube-like structures and subsequently networks throughout the bone scaffold 4–7 days after implantation. hMSCs were essential for stable vasculature both in vitro and in vivo; however, contrary to expectations, vasculature derived from hMSCs briefly cultured in medium designed to maintain a proliferative, nondifferentiated state was more extensive and stable than that with hMSCs with a TGF-β-induced smooth muscle cell phenotype. Anastomosis occurred by day 11, with most hMSCs associating closely with the network. Although initially immature and highly permeable, at 4 weeks the network was mature. Initiation of scaffold mineralization had also occurred by this period. Some human-derived vessels were still present at 5 months, but the majority of the graft vasculature had been functionally remodeled with host cells. In conclusion, clinically relevant progenitor sources for pericytes and endothelial cells can serve to generate highly functional microvascular networks for tissue engineered bone grafts.

endothelial cell | mesenchymal stem cell | pericyte | vasculogenesis

Bone grafting is required to correct deficits arising from congenital defects, trauma, and disease. Autologous grafts are considered the gold standard with the best clinical outcome. They are vascularized and contain vital cells and growth factors that facilitate remodeling to form a strong unified structure with the host site, but significant limitations associated with autologous grafts include availability of donor tissue (restricting size and shape) and requirement of an additional surgical procedure entailing added patient suffering and increased operating time and cost.

Autologous bone marrow aspirate is used to seed synthetic and allogeneic grafts for spinal fusion and nonunion of long bone fractures (1, 2). The marrow is a rich source of cytokine-secreting cells that promotes both bone formation and angiogenesis; however, the neovasculature derives from the recipient tissue, with negligible cellular contribution from the transplanted marrow (1). Only the periphery of the graft is efficiently vascularized. Because the inner cell mass must rely upon mass transport for oxygen and metabolic requirements (3), a central zone of necrosis frequently occurs that results in a shell of ossification at the surface, with shallow penetration. The size, strength, and rate of remodeling of such constructs are directly limited by constraints to oxygen diffusion in supporting interior cell populations, restricting utility of nonautologous grafts primarily to small structures and bone extenders.

Endothelial cells will spontaneously form microcapillary-like networks with lumens in vitro when cultured in the presence of specific growth factors such as VEGF (4). Coculturing with an additional cell type to serve as mural cells and inclusion of ECM are necessary to maintain and mature the networks (5–11). The ability to precisely control in vitro experimental conditions directly led to identifying the mechanisms of many fundamental aspects of this process over the past several decades (5–7, 10–14). Several groups have recently shown that microvascular structures that are preformed in vitro by using endothelial and smooth muscle progenitor cells can anastomose with the host vasculature when implanted in a nude mouse model (15–20). In this study we demonstrate that human mesenchymal stem cells (hMSCs) coimplanted with endothelial cells (ECs) in a fibronectin-containing collagen gel act as a source of perivascular cells and generate a stable functional vasculature within a porous scaffold. The potential of MSCs both as a source for the osteogenic component (cells attached to the surface of the scaffold) and as perivascular and vessel stabilizing cells is explored. The osteoprogenitor nature of hMSCs and their potential to differentiate into the osteogenic lineage has been extensively exploited for bone regenerative therapy; thus, characterizing their role in vasculogenesis could provide unique solutions for successful bone tissue engineering. Efficient incorporation of such vascular networks in bone grafts in a clinical setting could potentially greatly increase their utility and reduce the reliance on autologous harvesting of bone.

Results

Vascularized Bone Graft Model. We developed a two-step scaffold seeding protocol (Fig. 1) in order to provide the hMSCs with a 3D porous scaffold that resembles trabecular bone structure on which to differentiate into osteoblasts. We first seeded the hMSCs intended for bone formation and allowed them to attach and grow on the surface of the scaffold for a week. During this period, an osteoinductive medium was used. The scaffolds were then seeded with collagen-fibronectin gel containing fluorescently labeled human umbilical vein endothelial cells (HUVECs) and hMSCs and incubated overnight in endothelial cell medium EGM-2. The cell/scaffold constructs were then either grown in vitro or implanted subcutaneously in mice for analysis. A detailed protocol and analysis of the resulting bone scaffolds is described below.

Author contributions: O.T., I.P., and C.N. designed research; O.T., I.P., J.A.S., P.A.R., A.R.H., E.O., Y.L., and C.C.F. performed research; L.D., C.P.L., and C.A.S. contributed new reagents/analytic tools; O.T., I.P., J.P.V., and C.N. analyzed data; and O.T. and C.N. wrote the paper.

The authors declare no conflict of interest.

This article is a PNAS Direct Submission. S.F.B. is a guest editor invited by the Editorial Board.

[1]To whom correspondence should be addressed. E-mail: neville@helix.mgh.harvard.edu.

This article contains supporting information online at www.pnas.org/cgi/content/full/0905445107/DCSupplemental.

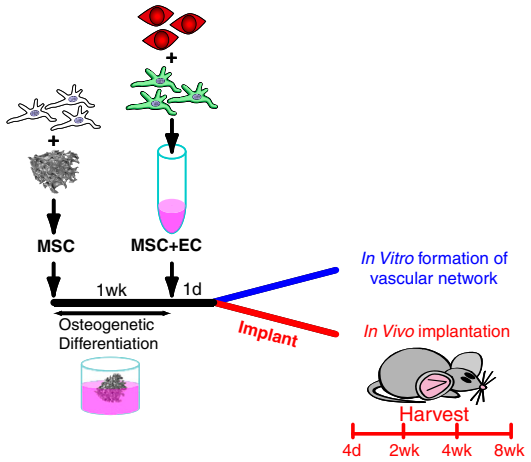

Fig. 1. Protocol timeline. Unlabeled hMSCs were seeded and allowed to attach to the bone scaffold. Medium containing osteoinductive agents was used to commit these cells to the bone lineage, after which it was replaced with a hydrogel containing labeled ECs (red) and additional hMSCs (25% labeled green) to serve as pericytes. The scaffold was continued to be cultured in vitro or implanted the following day.

Formation of Vascular Network Within the 3D Porous Scaffold in Vitro. Scaffolds were fabricated with interconnected porosity to replicate the structure of trabecular bone from the copolymer (85:15 molar ratio) poly(DL-lactide-co-glycolide) (PLGA) (Fig. 2*A*). A light vacuum was used to ensure homogeneous seeding of suspended cells throughout the scaffold. The ability of the scaffold to support the formation of a 3D vascular network throughout the interconnected pores was then evaluated. tdTomato-labeled ECs and eGFP-labeled hMSCs were mixed at a ratio 4:1 in the collagen-fibronectin gel and either cultured in endothelial (EGM-2) medium in a multiwell plate or applied to the PLGA scaffold. Fluorescent microscopy demonstrated the presence of an extensive vascular network within the collagen-fibronectin gel (Fig. 2*B*) that was stable for several weeks. A continuous three-dimensional network of HUVEC-hMSC engineered vessels formed throughout the porosity within the PLGA scaffold also remained stable for greater than a month in vitro (Fig. 2*C*). Furthermore, the eGFP-labeled hMSCs had migrated to line the tubular structures formed by the tdTomato-labeled HUVECs and acquired a flattened, elongated morphology with stellate processes (Movie S1).

Preinduction of hMSCs into Pericytes. During vasculogenesis, mural wall cells are recruited to the newly formed endothelial cell network and direct its maturation through both soluble factors and direct contact (21). Multiple studies utilizing vasculogenesis and angiogenesis models have demonstrated that contact and communication between ECs and smooth muscle cells (SMCs)/pericytes are required for vascular maturation (22, 23). We reasoned that predifferentiation of hMSCs to smooth muscle prior to addition to the vascular component may accelerate formation and maturation of the network. In addition to hMSCs grown in standard culture conditions, we utilized hMSCs that had been grown for 5 days in standard medium supplemented with 1 ng/mL of TGF-β, a well-established inducer of smooth muscle phenotype (24). For comparison purposes, we simultaneously cultured hMSCs for 5 days in a commercial low serum medium (MesenPro) specifically formulated to maintain hMSCs in an undifferentiated proliferative state. As expected, TGF-β induced a SMC phenotype as evidenced by an increase in expression for several smooth muscle markers (Fig. 2*D*), whereas the low serum conditions caused a small decrease relative to standard hMSC medium.

The ability of each hMSC population to assist HUVECs in forming and maintaining a network when cocultured in a collagen-fibronectin gel was then evaluated in vitro (Fig. 2*E–H*). Endothelial cultures without hMSCs (Fig. 2*E*) formed short-lived multicellular cords that were much shorter and wider than those formed by hMSC-containing cultures; they were already regressing and falling apart by day 6 with the HUVECs subsequently dying. All hMSC-containing cultures formed extensive vascular networks, although with noticeable differences. Constructs containing the TGF-β-induced hMSCs were delayed in tube formation, with ECs only starting to coalesce at day 5. Both standard

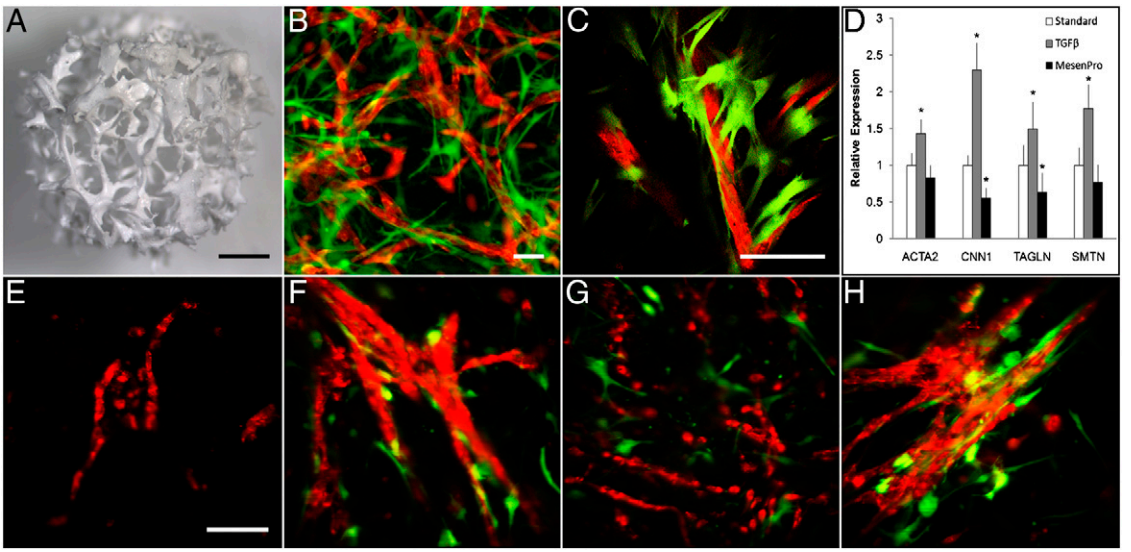

Fig. 2. hMSCs contribute to in vitro formation of a 3D vascular network within a porous scaffold. (*A*) The bone scaffold was synthesized of the biocompatible polymer (85:15) PLGA, by using sucrose leaching to generate interconnected pores averaging 1000 μm. (*B*) Stable network containing HUVECs and hMSCs in fibronectin-containing collagen gel at 21 days postseeding. (*C*) Physical interaction of hMSCs with EC network formed in the PLGA scaffold at 28 days postseeding. (*D*) Relative transcriptional response of the smooth muscle markers smooth muscle actin (ACTA2), calponin (CNN1), SM22 (TAGLN), and smoothelin (SMTN) to the 5-day preconditioning treatment. (*E–H*) In vitro formation of networks by HUVECs imaged with confocal microscopy at 10 days (*E*) without hMSCs, (*F*) with standard condition hMSCs, (*G*) with hMSCs cultured with TGF-β, and (*H*) hMSCs cultured in low serum MesenPro medium. (Scale bars: *A* = 1 mm; *B* = 50 μm; *C* = 100 μm, *E–H* = 100 μm. $^*P < 0.05$.)

medium and MesenPro-precultured hMSCs, however, formed extensive networks rapidly. At day 5, most hMSCs were closely associated with ECs; however, the MesenPro-derived hMSCs were more numerous, indicating that they continued to rapidly proliferate even after being switched to medium optimized for EC culture. More interestingly, this population of hMSCs also made far more extensive contact with the ECs, often stretching between bifurcated branches. Tubes with extensive hMSC coverage were often quite large.

Formation of Engineered Vessels Within the 3D Porous Scaffold in Vivo. To determine whether cocultures of HUVECs-hMSCs are able to self-assemble in vivo in the scaffold and anastomose with the host vasculature to become functional blood vessels, constructs were implanted subcutaneously in immunodeficient mice. At various time periods between 4 days and 5 months after implant, the scaffolds were examined. Intravital microscopy confirmed the formation of vascular networks within the scaffolds (Fig. 3*A–D*). In agreement with previous observations (22, 25, 26), when constructs with HUVECs alone were implanted, circular structures formed by day 4 after implantation, but the engineered vessels appeared counterfeit, remained immature, and eventually regressed. Implanted constructs generally showed relative behavior similar to in vitro culture, with endothelial-only scaffolds showing poor survival and marginal lumen formation and no evidence of anastomosis. Here, we found that HUVECs coseeded with hMSCs were capable of vasculogenesis. However, the density and persistence of the engineered neovasculature were substantially different depending on hMSC pretreatment. hMSC-containing scaffolds had vascular structures forming by day 4 (Fig. 3*E–L*) and extensive association of hMSCs by week 4. Scaffolds utilizing MesenPro-treated hMSCs again produced the most extensive networks intimately surrounded by hMSCs. In addition, immunohistochemical staining demonstrated multiple vessels positive for the human-specific endothelial marker CD31 that were evenly distributed throughout the scaffold. Furthermore, by day 11 blood cells were found in the vessels that stained positively with antihuman CD31 indicating the connection of the engineered vessels with the host vasculature (Fig. 3*M–T*). Adjacent serial sections of an explanted scaffold

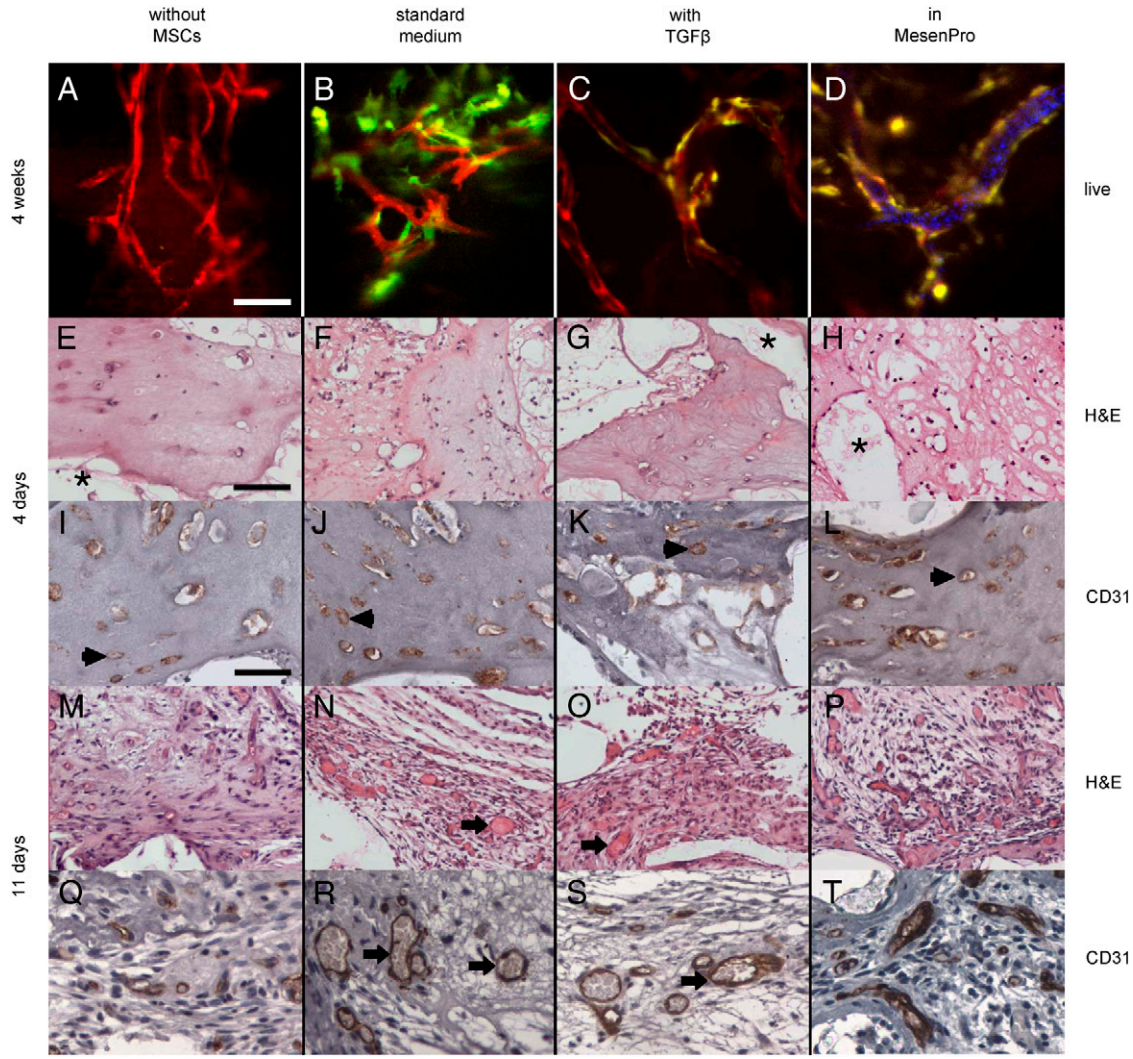

Fig. 3. Formation of engineered vessels in vivo. (*A–D*) Networks formed by HUVECs imaged with confocal laser-scanning microscopy at 4 weeks (*A*) without hMSCs, (*B*) with standard condition hMSCs, (*C*) with hMSCs cultured with TGF-β, and (*D*) with hMSCs cultured in low serum MesenPro medium. For (*D*) only, maximum intensity projection of 30 consecutive frames (1 sec) was used to demonstrate flow of DiD-labeled blood cells. H&E and human-specific CD31 immunohistochemical staining of scaffolds explanted 4 (*E–L*) and 11 (*M–T*) days after implantation. Acellular regions (*) derive from scaffold. EC-derived tubular structures have formed by 4 days (arrowheads) but do not contain blood cells indicating that they are not yet functional. By 11 days, the structures were larger with more robust CD31 staining, and most lumens were filled with blood cells (arrows). The symbols mark only a representative sample of indicated structures. (Scale bars: *A–D* = 100 μm; *E–T* = 200 μm.)

were stained with CD31 to identify the human-derived vessels and the pericyte markers smooth muscle actin and calponin (Fig. 4). The hMSCs localized to the vessels were expressing the smooth muscle markers; although they made extensive contact with the ECs, coverage appeared incomplete as is typical of most microvasculature.

Functionality of the Engineered Vessels. In order to test for permeability of anastomosed vessels, the fluorescent dye Evans blue was injected systemically through the tail vein of the mice. At 2 weeks postimplantation, graft EC-derived vessels with associated hMSCs were patent and functional, as the lumens of the networks were clearly delineated. However, after several minutes, significant accumulation of background fluorescence occurred in all graft conditions indicating that the vessels were still immature and leaky (Fig. 5*A*). The assay was repeated at 8 weeks postimplantation on additional implants, and only very minimal leakage was detectable even 5 hours post injection, indicating that the endothelium had further matured to develop functional tight junctions (Fig. 5*B*). Occasional small pools of blood resulting from minor trauma caused by in vivo imaging 2 weeks postimplantation indicated the fragility of the structures; after this period, there was no evidence of any hemorrhagic event during imaging, indicating that the maturing vessels more closely resemble normal rather than tumor pathology. Inosculation points were also visible where the engineered vessels had anastomosed with the host vasculature (Fig. 5*C*). Nascent, immature vessels often support only irregular blood flow; therefore, to further evaluate the functionality of the engineered vessels we injected DiD-labeled mouse blood cells systemically and subsequently visualized flow through both the graft and the nearby host vasculature. The rate of flow was indistinguishable (Fig. 5*D* and Movie S2). Confocal images taken at 4 weeks postimplantation were used to determine graft vessel density (Fig. 5*E*) and mean diameter (Fig. 5*F*). Without hMSCs, tubular networks were fragmentary and meager and did not appear patent. Vessels derived from TGF-β-treated hMSCs produced vessels of a slightly larger diameter relative to standard medium conditions but had a lower overall vessel density. hMSCs precultured in MesenPro produced vascular networks with both a higher vessel density and a larger diameter than those of all other tested conditions.

Induction of Osteogenic Lineage. After 8 weeks, scaffolds were harvested and frozen sections were prepared and analyzed by von Kossa staining for evidence of calcium production and consequent bone formation. Extensive calcium phosphate deposition was detected that was restricted to the surface of the scaffold pores (Fig. 6*A*). No significant staining was apparent in the pore spaces that would indicate that the vascular component containing hMSCs contributed to bone formation. Coculture of ECs with hMSCs has been shown to have a close reciprocal relation and can induce bone formation in the absence of external osteogenic stimuli (27). We therefore repeated the scaffold seeding procedure, but during the 1-week culture period we omitted osteogenic inducers from the culture medium, and then the fibronectin-containing collagen gel with ECs and MSCs was added and implanted the following day. Explanted scaffolds had significant mineralization at 8 weeks (Fig. 6*B*), although less than the osteo-induced samples. Parallel scaffolds without the vascular component produced a very modest staining for calcium (Fig. 6*C*). As the von Kossa technique sometimes detects non-calcium-containing mineral deposits (e.g., urates), the presence of calcium was confirmed by Alizarin red staining (Fig. 6*D*). Scaffold surfaces were also positive for osteocalcin, a late marker of osteoblast differentiation (Fig. 6*E*, magnified in Fig. 6*F*).

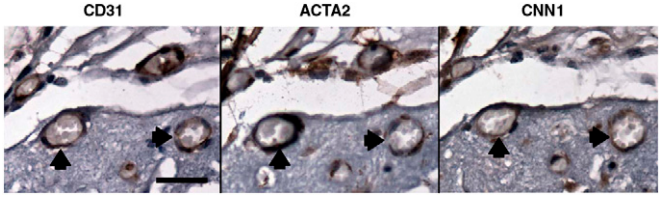

Fig. 4. Perivascular localization of hMSCs. A seeded scaffold containing HUVECs and MesenPro-treated MSCs was explanted after 4 weeks and embedded in paraffin. Serial sections cut from a region containing several transverse vessels (two of which are marked by arrowheads) were immunohistologically stained to identify human-derived structures: a human-specific antibody for PE-CAM (CD31) stained graft-derived endothelium, vascular-associated MSCs stained positive for the mural markers smooth muscle actin (ACTA2) and calponin (CNN1). Numerous erythrocytes within lumens indicate that the vasculature has anastomosed and is functional. Positive signals are brown with hematoxylin counterstaining. (Scale bar: 25 μm.).

Discussion

New bone formation in bone grafts occurs only in the presence of a vascular network within the implant, with the greatest amounts of newly laid down bone occurring in the most vascularized areas (28). For metabolically active tissues such as newly formed bone to grow beyond the oxygen diffusion limit of a couple hundred microns, formation of new blood vessels is required (3). Numerous strategies for vascularization involve highly sophisticated scaffolds and local delivery of angiogenic factors to enhance ingrowth of vessels from the host (29). Because of the considerable amount of time required for angiogenesis, the use of larger bone grafts is not often feasible as necrosis develops in the core with only a shell of bone at the surface. Thus the ability to promote rapid vascularization of bone grafts in a clinically relevant manner could vastly expand the utility of synthetic bone grafts.

The development of a mature and functional vasculature, however, does not depend only on migration and proliferation of endothelial cells but requires cooperation and symbiosis between them and mural cells (pericytes in small and SMCs in larger-sized vessels) (23, 26, 30). In addition, ECM is required in order to provide both structural support for the cellular component and sites to sequester important growth factors and other signaling molecules (10–13). Many studies have demonstrated that formation of stable and functional vascular networks necessitates the coimplantation of ECs with perivascular cells, a role that has been undertaken by human saphenous vein SMCs or mesenchymal precursor cells such as the mouse embryonic cell line 10T1/2 (24, 31). Furthermore, it is suggested that 10T1/2 cells differentiate into SMCs or pericytes through heterotypic interactions with ECs (23, 24, 26). Recently, the perivascular/pericyte origin of bone marrow MSCs (32, 33) has been identified, and the ability of these cells to differentiate to SMCs and stabilize nascent blood vessels (22, 34, 35) is being characterized.

Here we demonstrated that hMSCs specifically assume the role of perivascular cells and act as a potent stabilizer of the engineered blood vessels formed in the porous bone scaffold. Their differentiation state prior to coimplantation with ECs, however, is an important parameter that supports the network, because the population that remained in an undifferentiated proliferated state formed stronger, more mature networks. The hMSCs fulfill at least two roles in supporting the vasculogenesis process, synthesis of trophic factors (22, 23) and contributing the mural component (9, 19, 21, 24, 25), neither of which is well understood at present. Both in vitro and in vivo, the tubular networks formed by monocultures of ECs such as HUVECs are not stable. Inclusion of mesenchymal-derived cells that can serve as pericytes such as the 10T1/2 cell line, embryonic and dermal fibroblasts, or hMSCs generates networks that are more robust and can anastomose to form functional vessels in vivo (5, 7, 9, 11, 28). Furthermore, it is suggested that 10T1/2 cells differentiate into SMCs or pericytes through heterotypic interactions with ECs (10, 11, 13). Treatment with TGF-β is a well-established protocol to generate a

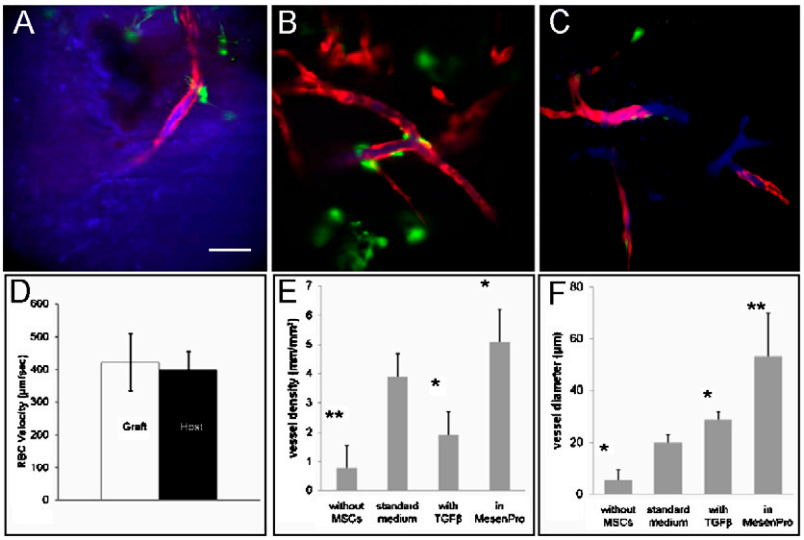

Fig. 5. Assessment of functionality of the engineered vessels within the porous scaffold. At 2 weeks, tail vein injection of Evans blue was used to visualize flow through the grafts by intravital microscopy in order to verify anastomosis and assess vessel permeability (*A*). The assay was repeated at 8 weeks postimplantation on additional implants with a second vascular probe, Qtracker800. In this case only very minimal leakage was detected. (*C*) Points of anastomosis, where dye-labeled serum flowing through the graft (red) and adjacent host vasculature clearly indicate that the engineered vessels have anastomosed with the mouse vessels. (*D*) Vibrant DiD-labeled RBC flow rates through graft and neighboring host vessels were calculated. Vessel density (*E*) and average diameter (*F*) in grafts with indicated hMSCs 4 weeks after implanting. $^{*}P < 0.05$, $^{**}P < 0.01$ compared with standard medium conditions. (Scale bar: *A*–*C* = 100 μm.)

more mature smooth muscle phenotype (24). We found that transcription of several genes expressed in smooth muscle, including the late marker smoothelin, was up-regulated after a relatively brief culture period in medium containing additional TGF-βand expected that these cells would better support vasculogenesis. However, the resulting networks were inferior to those generated by cells that had not been treated with the cytokine. Although the resulting networks did anastomose and support blood flow, they were noticeably less complex. The TGF-β-treated hMSCs were tightly associated with the endothelium but were smaller and fewer in number and so generated vessels with relatively sparse pericytes. In contrast, MesenPro-treated hMSCs generated structures with very extensive mural coverage. MesenPro supports proliferation, whereas TGF-β is a potent growth inhibitor; the impact of this preconditioning persisted even after implantation. Both the phenotype and the relative number of pericytes influence native microvascular properties (e.g., leakiness, degree of branching, and vessel density). These parameters will undoubtedly be important in constructing functional vasculature in engineered tissue as well.

As previously reported (14), the hMSCs implanted with ECs differentiated to the osteoblasts lineage without prior induction, although mineralization occurred at reduced levels. It is not yet known whether this was because a smaller number of cells committed to the lineage or differentiation lagged. The osteogenic model we chose, ectopic bone formation in an immunodeficient mouse, uniquely allowed us to generate vascularized tissue by using clinically relevant human cell sources. Complementary studies for evaluating the effects of vasculogenesis on load-bearing bone grafts need to be performed in a large animal model but will first require developing autologous cell sources.

Characterization of the dynamics of graft vessel remodeling, particularly with respect to hMSC and EC proliferation and persistence, is ongoing. In our current model, the vasculature generated by the implanted cells was gradually replaced by host vasculature. For clinical purposes, long-term maintenance of the engineered vasculature may not be necessary or even desirable if it can be replaced by patient-supported angiogenesis. Osteoblasts and pericytes are readily generated from autologous bone marrow-derived cells; all potential autologous sources of EC progenitors are currently significantly more difficult to isolate and expand. This is particularly true for the older patient population. If vasculogenesis of the implanted engineered tissue were to function as a bridge to support initial metabolic needs until it is replaced by angiogenic ingrowth, any required immunosuppression resulting from the use of nonautologous endothelial cell sources could be temporary. In our model, network formation occurred rapidly, but anastomosis was first detected eleven days postimplantation for all hMSC-containing scaffolds. Although the vasculature at this stage was immature and leaky to the fluorescent indicators, it was functional and without cellular extravasation. Providing separate hMSC populations that have been individually optimized for specific functions (bone formation, trophic factor production, pericytes) could give a significant advantage in accelerating vasculogenesis.

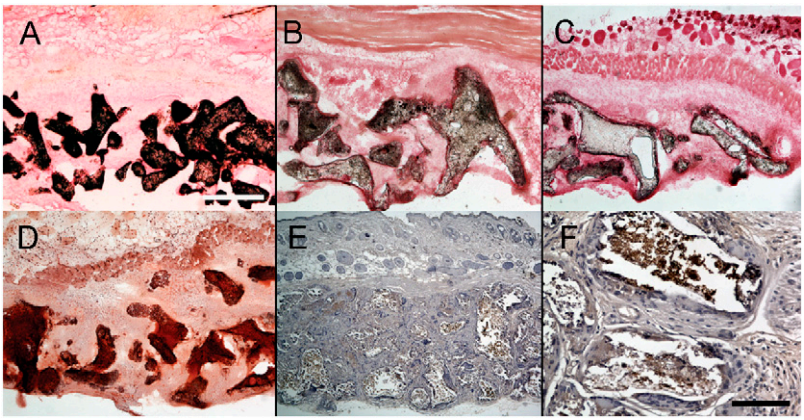

Fig. 6. Osteogenic induction. At 8 weeks, scaffolds that had been seeded with standard condition osteoinduced hMSCs were explanted and calcium deposits stained with von Kossa. Calcium deposition was extensive and restricted to the pore surfaces of the scaffolds. Vascularized scaffolds (*B*) in which the initial seeding for attached hMSCs had not undergone prior in vitro osteogenic induction had more extensive mineralization than avascular scaffolds (*C*) but less than (*A*). A section from a scaffold (*A*) also stained with Alizarin red (*D*). This scaffold was also immunopositive for the late marker of osteoblast differentiation, osteocalcin (brown with hematoxylin counterstaining) (*E*, magnified in *F*). (Scale bars: *A*–*E* = 500 μm; *F* = 100 μm.)

Materials and Methods

Fabrication of PLGA 3D Porous Scaffolds. Five-millimeter-diameter porous bone scaffolds were fabricated from PLGA (85/15) by using the sucrose leaching technique. For detailed information, see *SI Methods*.

Cell Isolation and Culture. Bone marrow samples were obtained according to guidelines established by the Massachusetts General Hospital Institutional Review Board from patients undergoing hip replacement surgery. hMSC cultures were established as previously described (36) and maintained in mesenchymal stem cell growth medium (MSCGM) (Cambrex). All experiments were performed with hMSCs having less than six cell passages. For osteogenic induction, hMSC-seeded scaffolds were cultured in osteoinductive medium (MSCGM with 50 μg/mL L-ascorbic acid 2-phosphate, 10 mM β-glycerol phosphate, and 10^{-8} M dexamethasone). When indicated, 1 ng/mL of TGF-β was added to MSCGM; MesenPro RS Medium was obtained from Invitrogen. HUVECs were maintained in 0.1% gelatin-coated plates in EGM-2 medium (Cambrex). Lentivirus was used to fluorescently label hMSCs (eGFP) and HUVECs (tdTomato) in order to visualize vascular structures; details are provided in *SI Methods*.

Tissue Engineered Blood Vessel Model Within PLGA Scaffold. The engineered blood vessels within the PLGA scaffold were prepared by mixing 1×10^6 EC and 2.5×10^5 MSCs and suspended in 1 mL of type-1 collagen (PureCol; Advanced BioMatrix) and fibronectin (Invitrogen) gel solution prepared as previously described (26). Then 100 μL of gel with cells was added over PLGA scaffolds applying a slight vacuum to ensure removal of any trapped air in the center of the scaffold. Constructs were maintained in culture in EGM-2 endothelial cell medium for the duration of the in vitro experiments or overnight prior to implantation in vivo.

In Vivo Imaging. An immunodeficient mouse model was used in order to support in vivo growth of bone scaffolds with human cells. All procedures were approved by the Institutional Animal Care and Use Committee of the Massachusetts General Hospital and performed according to the National Institutes of Health Guidelines for the Care and Use of Laboratory Animals. Constructs were implanted subcutaneously in the backs of severe combined immunodeficient mice (NOD.CB17; Jackson Laboratory). The custom-built video-rate laser-scanning confocal microscope (37) used for in vivo imaging is described in *SI Methods*.

Whole blood from a Balb/C mouse (Jackson Laboratory) was diluted 10× with RPMI 1640 cell culture media (Mediatech) plus 0.1% BSA (Sigma-Aldrich). The cells were stained with 100 μM Vibrant DiD for 30 minutes at 37 °C and then washed with PBS, and up to 1×10^8 cells were injected retroorbitally. Flow of DiD-labeled cells was captured in live video mode. Lengths of individual engineered and native vessels were measured by manual tracing of perfused vessels by using ImageJ software (38) and speed determined by tracking individual cells across isolated frames. For display purposes, color levels and contrast of individual images and movies were adjusted. Average vessel density and calculated average diameter were determined on images derived from maximum intensity projections of 4 consecutive *z* slices by using ImageJ.

Gene Expression and Histochemical Staining. Detailed information is included in *SI Methods*.

ACKNOWLEDGMENTS. We thank Katelyn McGovern (Massachusetts General Hospital) for assistance with analyzing confocal images and Dr. Patrick Au (Massachusetts General Hospital) for assistance with preparing the engineered blood vessel model. This work was sponsored by a grant from the Stanley H. Durwood Foundation and the Harvard Stem Cell Institute. Imaging studies were supported by the Massachusetts General Hospital Advanced Microscopy Program start-up fund.

1. Muschler GF, Nakamoto C, Griffith LG (2004) Engineering principles of clinical cell-based tissue engineering. *J Bone Joint Surg Am*, 86-A(7):1541–1558.
2. Muschler GF, et al. (2003) Spine fusion using cell matrix composites enriched in bone marrow-derived cells. *Clin Orthop Relat Res*, 407:102–118.
3. Folkman J, Hochberg M (1973) Self-regulation of growth in three dimensions. *J Exp Med*, 138(4):745–753.
4. Folkman J, Haudenschild C (1980) Angiogenesis in vitro. *Nature*, 288(5791):551–556.
5. Sato N, et al. (1987) Development of capillary networks from rat microvascular fragments in vitro: The role of myofibroblastic cells. *Microvasc Res*, 33(2):194–210.
6. Berthod F, Germain L, Tremblay N, Auger FA (2006) Extracellular matrix deposition by fibroblasts is necessary to promote capillary-like tube formation in vitro. *J Cell Physiol*, 207(2):491–498.
7. Supp DM, Wilson-Landy K, Boyce ST (2002) Human dermal microvascular endothelial cells form vascular analogs in cultured skin substitutes after grafting to athymic mice. *FASEB J*, 16(8):797–804.
8. Vernon RB, Sage EH (1999) A novel, quantitative model for study of endothelial cell migration and sprout formation within three-dimensional collagen matrices. *Microvasc Res*, 57(2):118–133.
9. Black AF, Berthod F, L'Heureux N, Germain L, Auger FA (1998) In vitro reconstruction of a human capillary-like network in a tissue-engineered skin equivalent. *FASEB J*, 12(13):1331–1340.
10. Kubota Y, Kleinman HK, Martin GR, Lawley TJ (1988) Role of laminin and basement membrane in the morphological differentiation of human endothelial cells into capillary-like structures. *J Cell Biol*, 107(4):1589–1598.
11. Montesano R, Orci L, Vassalli P (1983) In vitro rapid organization of endothelial cells into capillary-like networks is promoted by collagen matrices. *J Cell Biol*, 97(5 Pt 1):1648–1652.
12. Peters MC, Isenberg BC, Rowley JA, Mooney DJ (1998) Release from alginate enhances the biological activity of vascular endothelial growth factor. *J Biomater Sci-Polym Ed*, 9(12):1267–1278.
13. Hoying JB, Williams SK (1996) Effects of basic fibroblast growth factor on human microvessel endothelial cell migration on collagen I correlates inversely with adhesion and is cell density dependent. *J Cell Physiol*, 168(2):294–304.
14. Ingber DE, Folkman J (1989) Mechanochemical switching between growth and differentiation during fibroblast growth factor-stimulated angiogenesis in vitro: Role of extracellular matrix. *J Cell Biol*, 109(1):317–330.
15. Levenberg S, et al. (2005) Engineering vascularized skeletal muscle tissue. *Nat Biotechnol*, 23(7):879–884.
16. Nor JE, et al. (2001) Engineering and characterization of functional human microvessels in immunodeficient mice. *Lab Invest*, 81(4):453–463.
17. Shepherd BR, et al. (2004) Rapid perfusion and network remodeling in a microvascular construct after implantation. *Arterioscler Thromb Vasc Biol*, 24(5):898–904.
18. Tremblay PL, Hudon V, Berthod F, Germain L, Auger FA (2005) Inosculation of tissue-engineered capillaries with the host's vasculature in a reconstructed skin transplanted on mice. *Am J Transplant*, 5(5):1002–1010.
19. Rouwkema J, Westerweel PE, de Boer J, Verhaar MC, van Blitterswijk CA (2009) The use of endothelial progenitor cells for prevascularized bone tissue engineering. *Tissue Eng Pt A*, 15(8):2015–2027.
20. Rouwkema J, de Boer J, Van Blitterswijk CA (2006) Endothelial cells assemble into a 3-dimensional prevascular network in a bone tissue engineering construct. *Tissue Eng*, 12(9):2685–2693.
21. von Tell D, Armulik A, Betsholtz C (2006) Pericytes and vascular stability. *Exp Cell Res*, 312(5):623–629.
22. Au P, Tam J, Fukumura D, Jain RK (2008) Bone marrow-derived mesenchymal stem cells facilitate engineering of long-lasting functional vasculature. *Blood*, 111(9):4551–4558.
23. Wang ZZ, et al. (2007) Endothelial cells derived from human embryonic stem cells form durable blood vessels in vivo. *Nat Biotechnol*, 25(3):317–318.
24. Hirschi KK, Rohovsky SA, D'Amore PA (1998) PDGF, TGF-beta, and heterotypic cell-cell interactions mediate endothelial cell-induced recruitment of 10T1/2 cells and their differentiation to a smooth muscle fate. *J Cell Biol*, 141(3):805–814.
25. Au P, et al. (2008) Differential in vivo potential of endothelial progenitor cells from human umbilical cord blood and adult peripheral blood to form functional long-lasting vessels. *Blood*, 111(3):1302–1305.
26. Koike N, et al. (2004) Tissue engineering: Creation of long-lasting blood vessels. *Nature*, 428(6979):138–139.
27. Kaigler D, et al. (2005) Endothelial cell modulation of bone marrow stromal cell osteogenic potential. *FASEB J*, 19(6):665–667.
28. Deleu J, Trueta J (1965) Vascularisation of bone grafts in the anterior chamber of the eye. *J Bone Joint Surg Br*, 47:319–329.
29. Young S, et al. (2009) Dose effect of dual delivery of vascular endothelial growth factor and bone morphogenetic protein-2 on bone regeneration in a rat critical-size defect model. *Tissue Eng Pt A*, 15(9):2347–2362.
30. Nguyen LL, D'Amore PA (2001) Cellular interactions in vascular growth and differentiation. *Int Rev Cytol*, 204:1–48.
31. Jain RK (2003) Molecular regulation of vessel maturation. *Nat Med*, 9(6):685–693.
32. Caplan AI (2008) All MSCs are pericytes?. *Cell Stem Cell*, 3:229–230.
33. Crisan M, et al. (2008) A perivascular origin for mesenchymal stem cells in multiple human organs. *Cell Stem Cell*, 3(3):301–313.
34. Gong Z, Calkins G, Cheng EC, Krause D, Niklason LE (2009) Influence of culture medium on smooth muscle cell differentiation from human bone marrow-derived mesenchymal stem cells. *Tissue Eng Pt A*, 15(2):319–330.
35. Melero-Martin JM, et al. (2008) Engineering robust and functional vascular networks in vivo with human adult and cord blood-derived progenitor cells. *Circ Res*, 103(2):194–202.
36. Colter DC, Class R, DiGirolamo CM, Prockop DJ (2000) Rapid expansion of recycling stem cells in cultures of plastic-adherent cells from human bone marrow. *Proc Natl Acad Sci USA*, 97(7):3213–3218.
37. Veilleux I, Spencer JA, Biss DP, Côté D, Lin CP (2008) In vivo cell tracking with movie rate multimodality laser scanning microscopy. *IEEE J Sel Top Quant*, 14:10–18.
38. Collins TJ (2007) ImageJ for microscopy. *Biotechniques*, 43(Suppl 1):25–30.

Supporting Information

Tsigkou et al. 10.1073/pnas.0905445107

SI Text
Supporting Methods

Fabrication of Poly(DL-lactide-co-glycolide) (PLGA) 3D Porous Scaffolds. Three-dimensional scaffolds were fabricated to resemble the structure of trabecular bone, with porosity ranging from 850 to 1180 μm. PLGA (85/15) (Alkermes), with an intrinsic viscosity of 0.8 dL/g at 30 °C in chloroform, was dissolved in dimethyl sulfoxide. The 1% wt/vol PLGA solution was poured over packed glucose particles, and the polymer solution was frozen at −20 °C for 30 min. The resulting scaffolds were immersed in stirred water for 24 hr to precipitate the PLGA, extract the sugar, and remove residual solvent. After vacuum drying, the foams were cut into 5-mm-diameter and 3-mm-high cylinders by using a dermal biopsy punch (Acuderm). The scaffolds were sterilized in 70% ethanol for 30 min, extensively rinsed with PBS, and then incubated in DMEM for 1 hr at 37 °C prior to cell seeding.

Lentivirus Packaging and Transduction. Cell cultures were transduced with lentivirus to express the fluorescent proteins eGFP human mesenchymal stem cells (hMSCs) and tdTomato human umbilical vein endothelial cells (HUVECs) to facilitate lineage tracing and imaging. The vector pLL3.7eGFP was the kind gift of Luk Van Parijs (Massachusetts Institute of Technology); pLL3.7tdTomato was made by replacing the open reading frame of eGFP with a fragment encoding tdTomato (1). The vectors were packaged by using the previously described lentivirus system (2). Cultures were infected in an overnight incubation with concentrated virus (multiplicity of infection 5) followed by extensive washing with PBS the following day. After 48 hr, the transduction efficiency was determined by fluorescence microscopy and FACS analysis (Becton Dickinson). Efficiency was over 90% for HUVECs and 25% for hMSCs. Unsorted labeled cultures were used for seeding the vascular component of the scaffolds.

In Vivo Imaging. The in vivo fate of the fluorescently labeled ECs and hMSCs in the scaffolds was tracked at various time points with a custom-built video-rate laser-scanning confocal microscope, as previously described (3). The scaffolds were imaged with either a 30× 0.9 N.A. water immersion objective (LOMO) or a 60× 1.2 N.A. water immersion objective (Olympus). eGFP, tdTomato, and Qtracker800 quantum dots (Invitrogen) were excited with a 491-nm continuous wave laser (Cobalt) and detected through a 520 ± 20-nm band pass filter (Semrock), a 593 ± 20-nm band pass filter (Semrock), and a 770-nm long pass filter (Omega Optical) by using three separate photomultiplier tubes (model R3896; Hamamatsu Photonics). Vibrant DiD (Invitrogen) and Evans blue (Sigma-Aldrich) were excited by using a 635-nm continuous wave laser (Coherent) and detected through a 695 ± 27.5-nm band pass filter (Omega Optical) by using a fourth photomultiplier tube.

Gene Expression. Total RNA was extracted by using the RNeasy Mini Kit (QIAGEN Sciences), and quality and concentration were determined by absorbance. One-half microgram was converted to cDNA by using MMLV reverse transcriptase (New England Biolabs). qPCR was performed with human-specific oligonucleotides by using the Brilliant II SYBR Green QPCR Master Mix (Stratagene) on a Mx 3005 instrument (Stratagene). Human GAPDH was used to normalize for cDNA conversion efficiency and quality. Each assay was repeated in triplicate and the mean and standard error calculated. Normalized results are reported with an expression in standard medium assigned a value of 1.

Primers Used for qPCR. ***GAPDH.*** CAACGGATTTGGTCGTATTGG
GCAACAATATCCACTTTACCAGAGTTAA

Smooth muscle actin. CTGTTCCAGCCATCCTTCAT
CGGCTTCATCGTATTCCTGT

Smoothelin. GGAGAACTGGCTGCACTCTC
GAAACCTCTGCCTGCTGTTC

SM22. AACAGCCTGTACCCTGATGG
ATGACATGCTTTCCCTCCTG

Calponin. TCCAAATATGACCCCCAGAA
CCCACTCTCAAACAGGTCGT

Statistical Analysis. The data were expressed as means ± SEM and evaluated by one-way ANOVA; a P value <0.05 was considered a statistically significant difference. Gene expression: TGF-β or MesenPro vs. standard medium. Vessel morphology: no hMSCs, TGF-β, or MesenPro vs. standard medium.

Histochemical Staining. Excised constructs were fixed in 10% neutral buffered formalin and routinely processed and embedded in paraffin. Transverse sections (4 μm) cut from the center of the construct were prepared by deparaffinization and hydration and used for hematoxylin and eosin staining and immunohistochemistry. Prior to immunostaining, sections were incubated at 95 °C for 30 min in target antigen retrieval buffer (DAKO) for epitope recovery. Sections were incubated for 1 hr at room temperature with primary antibodies mouse antihuman CD31 (1:25; Millipore), mouse antismooth muscle actin (1:50; DAKO), mouse anticalponin (1:50; DAKO), and rabbit antiosteocalcin (1:100; Santa Cruz Biotechnology). Immunohistochemical staining was carried out by using the appropriate DAKO EnVision kit (HRP, DAB+) according to the manufacturer's instructions.

For von Kossa and Alizarin red staining, excised implants were retrieved, embedded in O.C.T. Compound (Sakura Finetek), and frozen on dry ice. Transverse sections (10–15 μm) were cut with a cryotome from the center of the construct, and sections were left to air dry at room temperature and fixed with 4% paraformaldehyde. Alizarin red (Sigma-Aldrich) solution and von Kossa Staining Kit (American Master Tech Scientific) were used according to the manufacturer's instructions.

1. Melero-Martin JM, et al. (2008) Engineering robust and functional vascular networks in vivo with human adult and cord blood-derived progenitor cells. *Circ Res* 103 (2):194–202.
2. Colter DC, Class R, DiGirolamo CM, Prockop DJ (2000) Rapid expansion of recycling stem cells in cultures of plastic-adherent cells from human bone marrow. *Proc Natl Acad Sci USA* 97(7):3213–3218.
3. Veilleux I, Spencer JA, Biss DP, Côté D, Lin CP (2008) In vivo cell tracking with video rate multimodality laser scanning microscopy. *IEEE J Sel Top Quant* 14:10–18.

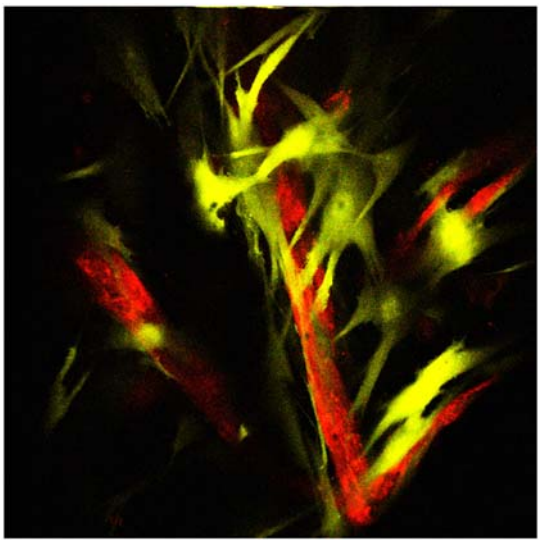

Movie S1. Scaffolds were imaged after 3 weeks of in vitro culture. HUVEC-hMSC engineered vessels formed continuously throughout the interconnected pores of the scaffold. The eGFP-labeled hMSCs migrated to align along the tdTomato-labeled HUVECs and acquired a flattened, elongated morphology with numerous stellate processes.

Movie S1 (MOV)

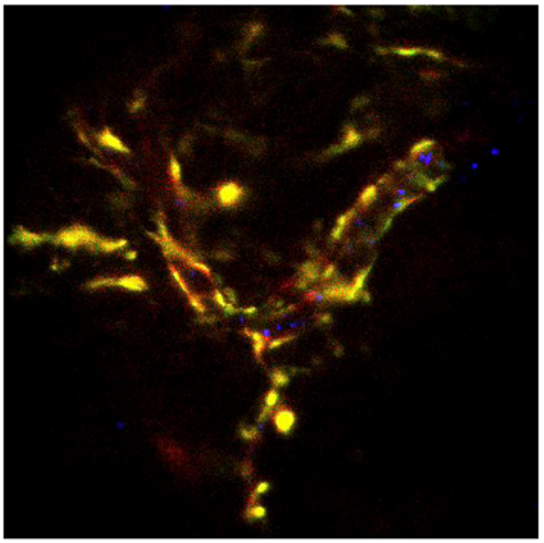

Movie S2. To evaluate the functionality of the engineered vessels of implanted scaffolds, DiD membrane-labeled blood cells were systemically injected. Flow was then imaged at both the graft and nearby host vasculature. Shown is a graft seeded with both HUVECs and MesenPro-treated hMSCs, 3 weeks post-implantation.

Movie S2 (AVI)

Stem Cell Rev and Rep (2009) 5:437–445
DOI 10.1007/s12015-009-9097-6

Bone marrow Derived Pluripotent Cells are Pericytes which Contribute to Vascularization

Xiaoxiao Cai · Yunfeng Lin · Claudia C. Friedrich · Craig Neville · Irina Pomerantseva · Cathryn A. Sundback · Parul Sharma · Zhiyuan Zhang · Joseph P. Vacanti · Peter V. Hauschka · Brian E. Grottkau

Published online: 2 October 2009

Abstract Pericytes are essential to vascularization, but the purification and characterization of pericytes remain unclear. Smooth muscle actin alpha (α-SMA) is one maker of pericytes. The aim of this study is to purify the α-SMA positive cells from bone marrow and study the characteristics of these cells and the interaction between α-SMA positive cells and endothelial cells. The bone marrow stromal cells were harvested from α-SMA-GFP transgenic mice, and the α-SMA-GFP positive cells were sorted by FACS. The proliferative characteristics and multilineage differentiation ability of the α-SMA-GFP positive cells were tested. A 3-D culture model was then applied to test their vascularization by loading α-SMA-GFP positive cells and endothelial cells on collagen-fibronectin gel. Results demonstrated that bone marrow stromal cells are mostly α-SMA-GFP positive cells which are pluripotent, and these cells expressed α-SMA during differentiation. The α-SMA-GFP positive cells could stimulate the endothelial cells to form tube-like structures and subsequently robust vascular networks in 3-D culture. In conclusion, the bone marrow derived pluripotent cells are pericytes and can contribute to vascularization.

Keywords Bone marrow stromal cells · Pericytes · Multilineage differentiation · Endothelial cells · Vascularization.

Study conducted at the Pediatric Orthopaedic Laboratory for Tissue Engineering, Mass General Hospital for Children, Boston, MA, USA.

X. Cai · Y. Lin (✉)
State Key Laboratory of Oral Diseases,
West China College of Stomatology, Sichuan University,
Chengdu 610041 People's Republic of China
e-mail: yunfenglin@scu.edu.cn

X. Cai · P. Sharma · Z. Zhang · P. V. Hauschka
Department of Orthopaedic Surgery, Children's Hospital Boston,
Harvard Medical School,
Boston, MA, USA

Y. Lin · C. C. Friedrich · C. Neville · I. Pomerantseva ·
C. A. Sundback · J. P. Vacanti
Center for Regenerative Medicine,
Massachusetts General Hospital, Harvard Medical School,
Boston, MA 02114 USA

Y. Lin · B. E. Grottkau (✉)
Department of Orthopaedic Surgery, Mass General Hospital
for Children and the Pediatric Orthopaedic Laboratory
for Tissue Engineering, Harvard Medical School,
Boston, MA, USA
e-mail: bgrottkau@partners.org

Introduction

Currently regeneration medicine approaches are being developed to reconstruct and restore the function of damaged or diseased tissues [1]. The basic principle involves an appropriate seeding cell source and a biocompatible and biodegradable scaffold to produce a construct that structurally and functionally mimics the target site [2]. Vascularization is a formidable obstacle for the application of tissue-engineered constructs, because the inner part of the construct cannot get enough oxygen and nutrients in the early stage, which causes the central zone of necrosis. Engineered tissues must have the ability to generate an early vascular network which can quickly connect with the host vasculature to supply adequate nutrients, oxygen, and eliminate waste [3, 4].

Blood vessels are composed of endothelial cells and supporting cells. The supporting cells are called pericytes/smooth muscle cells which express α-smooth muscle actin and form the external wall of the blood vessels [5]. Several groups have recently shown that microvascular structures

can be pre-formed in vitro using endothelial and smooth muscle progenitor cells [6–9]. The formation of mature and functional vasculature not only requires migration and connection of endothelial cells but also the cooperation and symbiosis of pericytes [10–12] Several studies have demonstrated that formation of robust and functional vascular networks required the co-implantation of endothelial cells and mesenchymal stem/progenitor cells [3, 4]. In a recent issue of Cell Stem Cell, Crisan et al. [7] documents a subpopulation of human perivascular cells that express both pericytes and mesenchymal stem cell (MSCs) markers in situ [13]. They have proved that blood vessel walls harbor a reserve of progenitor cells that may be integral to the origin of the elusive MSCs and other related adult stem cells[7].

In this study, we utilized a transgenic mouse model which uses smooth muscle alpha actin (α-SMA) promoter to direct the expression of green fluorescent protein (GFP) [14, 15] So purified α-SMA-GFP positive cells can be obtained from the transgenic mouse, and the proliferative characters and multilineage differentiation ability of the α-SMA-GFP positive cells were tested. Then the purified bone marrow derived α-SMA-GFP positive cells were co-cultured with endothelial cells in a collagen-fibronectin gel and act as a source of perivascular cells to generate vascular network in vitro. Our findings support earlier studies suggesting that the bone marrow mesenchymal stem cells originate from pericytes [7].

Materials and Methods

Experimental Mouse Model

In order to harvest purified α-SMA-GFP positive cells from bone marrow, we utilized a transgenic mouse model which uses smooth muscle alpha actin promoter to direct the expression of enhanced GFP [14, 15]. The transgenic mice were provided by the Bone Biology Research Laboratory, Department of Orthopaedic Surgery, Children's Hospital Boston.

Isolation of Bone Marrow Stromal Cells from α-SMA-GFP Transgenic Mouse

Bone marrow stem cells were collected from 8-week-old male α-SMA-GFP transgenic mice weighing 20~25 g, as previously described [16]. Briefly, mice were anesthetized by an intramuscular injection of Nembutal at 25 mg/ kg. The complete tibia and femurs were obtained and both ends of the metaphysis were removed. Sterile D-Hanks solution with 100 units/ml heparin was slowly injected into the bone marrow cavity to collect the bone marrow stromal cells. Bone marrow stromal cells were cultured in a-MEM containing 10% fetal bovine serum and maintained in a humidified atmosphere of 5% CO_2 at 37°C.

FACS Sorting of Bone Marrow Derived α-SMA-GFP Positive Cells

Different passages of bone marrow stromal cells were sent to FACS sorting to analyze the percentage of α-SMA-GFP positive cells. The cells were sorted into two groups: GFP positive and negative groups. The sorted α-SMA-GFP positive cells should be perivascular cells which mainly consist of pericytes and smooth muscle cells, because the GFP gene was directed by the smooth muscle alpha actin promoter which was one of the markers of pericytes and smooth muscle cells. The purified α-SMA-GFP positive cells were seeded on the plastic tissue culture dishes in control medium. These cells were maintained in a humidified atmosphere of 5% CO_2 at 37°C and passaged 3 times prior to multilineage differentiation.

Human Umbilical Vein Endothelial Cells preparation and Label

Human Umbilical Vein Endothelial Cells (HUVECs) were labeled with DsRed by lentivirus vector with an efficiency of well over 90%. HUVECs were maintained in 0.1% gelatin coated plates in endothelial cell growth medium (EGM-2, Lonza).

Multilineage Differentiation of Purified Bone Marrow Derived α-SMA-GFP Positive Cells

After culture and expansion in the control medium, the α-SMA-GFP positive cells were trypsinized and reseeded onto 24 well plates at a density of 10^5 cells per well. The cells were incubated in the control medium for 2 days to adhere to the plates and then the medium was transferred with specific medium containing the components listed in Table 1 to induce multilineage differentiation of bone marrow derived pericytes [17]. The cells cultured in the control medium (α-MEM, 10% FBS) were set as control. Differentiated phenotypes of variant lineages were viewed and compared by fluorescent microscopy and histochemical staining.

Histochemical Staining

The adipogenic differentiation was assessed by Oil Red O staining. The cells were rinsed in PBS and fixed in 4% paraformaldehyde for 15 min, then stained with 1% Oil Red O for 10 min. The cells were differentiated with 60% isopropanol and washed with 70% ethanol. Then the cells were observed under the fluorescent microscope for red lipid drops [18].

Table 1 Lineage-specific differentiation induced by medium supplementation

Lineage	Medium	Serum	Supplementation
Osteogenesis	α-MEM	FBS (10%)	50 μM ascorbate-2-phosphate, 10 mM β -glycerophosphate, 0.01 μM 1,25-dihydroxyvitamin D3, 1% antibiotic /antimycotic
Chondrogenesis	α-MEM	FBS (10%)	10 ng/ml TGF-β1, 100 nM dexamethasone, 6.25 μg/ml insulin, 50 nM ascorbate-2-phosphate, 110 mg/L sodium pyruvate, 1% antibiotic /antimycotic
Adipogenesis	α-MEM	FBS (10%)	1 μM dexamethasone, 10 μM insulin, 200 μM indomethacin, 0.5 mM isobutyl-methylxanthine (IBMX), 1% antibiotic /antimycotic
Control	α-MEM	FBS (10%)	1% antibiotic /antimycotic

The mineralization nodules of osteogenic lineages were stained with alizarin red S (AR-S). The cells were rinsed in PBS and incubated with 40 mM AR-S (pH 4.2) with agitation for 10 min. Then they were rinsed by PBS and observed through a microscope.

After the α-SMA-GFP positive cells were placed into chondrogenic medium for 7 days, the cells were trypsinized and pelleted by centrifugation at 1200 g for 5 min. The resultant pellet was cultured for another 2 weeks. The pellet frozen sections were stained in toluidine blue for 10 seconds and washed in water and differentiated in 0.2% uranyl nitrate until the background appeared colorless.

RNA Isolation and Reverse Transcription-Polymerase Chain Reactiontr

Total RNA was extracted using RNeasy Mini Kit (QIAGEN Sciences, Gaithersburg MD), and quality and concentration determined by absorbance. One-half microgram was converted to cDNA using MMLV reverse transcriptase (New England Biolabs, Beverly MA). PCR amplification of target messages RNA was performed by TaKaRa PCR kit (TaKaRa, Jap). PCR oligonucleotide primers were listed in Table 2. The products were electrophoresed on 2% agarose gels, stained with ethidium bromide and visualized with Quantity One software (BIO-RAD).

3-D Collagen/Fibronectin Gels Preparation and Formation of Vascular Network In Vitro

Collagen/fibronectin gels were prepared as previously described with minor modifications [19]. The number and ratio of α-SMA-GFP positive cells to endothelial cells used to load the gels was determined by prior experiments. HUVECs and α-SMA-GFP positive cells were mixed at a ratio of 4:1 (HUVECs: α-SMA-GFP positive cells) and suspended in gel which included 1.5 mg/ml collagen gel (PureCol), 90 μg/ml human plasma fibronectin (Gibco), 25 mM HEPES (Gibco), 38.5% Complete EGM-2 (Lonza), with the final cell concentration 2×10^6 cells/ml. The control group had only HUVECs. The cell suspensions were polymerized in a 48-well plate (100 μl/well) for 30 minutes at 37°C. The gels were then covered with 250 μl complete EGM-2 medium. The culture medium was replaced every 3 days.

Results

Morphological Features and Proliferation Characters of α-SMA-GFP Positive Cells and HUVECs

Approximately 1×10^6 nucleated cells were derived from the bone marrow of each α-SMA-GFP transgenic mouse. The primary bone marrow stromal cells demonstrated two cell types which had different morphology (Fig. 1a–c): A majority of the cells were small and spindle-like cells which were GFP negative (Fig. 1c red arrow); a smaller population were large, flat cells which were GFP positive. The GFP positive cells consisted of pericytes and smooth muscle cells which expressed the α-smooth muscle actin

Table 2 Specific primers for PCR amplification with expected fragments size and optimal annealing temperature

Gene	Primers
OSX	F: 5'-CACTCACACCCGGGAGAAGA-3'
	R: 5'-GGTGGTCGCTTCGGGTAAA-3'
OCN	F: 5'-AACGTCCTGGTCACCCTGTATG-3'
	R: 5'-GATCTTCTTCACCCGCAGCTT-3'
PPAR-γ	F: 5'- GACCACTCGCATTCCTTT-3'
	R:5'- CCACAGACTCGGCACTCA-3'
LPL	F: 5'- AGGGTGAGGAATCTAATG-3'
	R: 5'-CAGGTGTTTCAACCGCTA-3'
SOX9	F: 5'- GTTGATCTGAAGCGAGAGGG 3'
	R: 5'-CATTGACGTCGAAGGTCTCA 3'
Col-II	F: 5'- AAGACCCAGACTGCCTCAAC 3'
	R: 5'-TTGGCCCTAATTTTCCACTG 3'
GAPDH	F: 5'-CTCACTGGCATGGCCTTCCG -3'
	R: 5'- ACCACCCTGTTGCTGTAGCC-3'

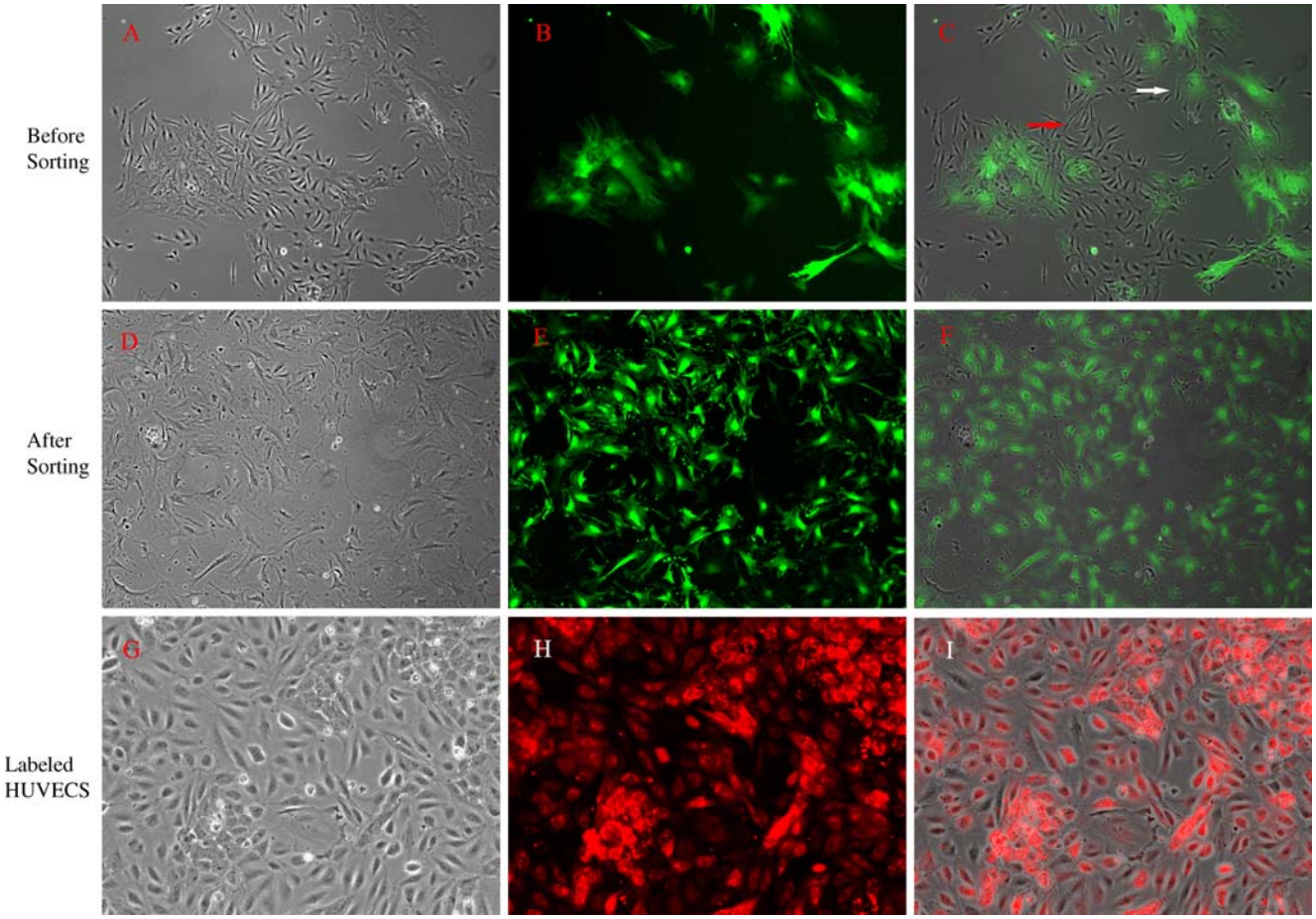

Fig. 1 The primary bone marrow stromal cells of α-SMA-GFP transgenic mouse had different morphologies **a–c**, big population of the cells were small and spindle-like which are GFP negative (C *red arrow*); small population were huge and flat cells which were GFP positive (C *white arrow*). The sorted α-SMA-GFP positive cells were complete "green" which were very huge and flat **d–f**. Human Umbilical Vein Endothelial Cells (HUVECs) were labeled with DsRed and the efficiency was well over 90% (G–I)

(Fig. 1c white arrow). The primary bone marrow stromal cells were sorted into GFP positive cells and negative cells by FACS. The sorted GFP positive cells were completely "green" (Fig. 1d–f). Human Umbilical Vein Endothelial Cells (HUVECs) were labeled with DsRed with an efficiency well over 90% (Fig. 1g–i).

Different passages of bone marrow stromal cells from α-SMA-GFP transgenic mice were analyzed by FACS to determine the percentage of GFP positive cells (pericytes and smooth muscle cells). According to the FACS results: in the primary passage (passage 0) of bone marrow stromal cells, the α-SMA-GFP positive cells represented 17±3.45%, in passage 1, the percentage was 32±5.85%; in passage 2, the percentage was 58±8.61%; in the passage 3, the percentage was 89±7.53% (Fig. 2a).

The numbers of sorted GFP positive and negative cells were counted at different time points to construct the growth curve. The initial number of GFP positive cells and negative cells were both 1×10^4. At day 3 the GFP positive cells proliferated to $1.8\pm0.2\times10^4$ and the negative cells to $1.2\pm0.1\times10^4$. At day 6, the GFP positive cells numbered $3.2\pm0.3\times10^4$ and the negative cells numbered $1.6\pm0.2\times10^4$. At day 9, there were $5.6\pm0.5\times10^4$ GFP positive cells and $2.2\pm0.3\times10^4$ negative cells. At day 12, the GFP positive cells numbered $8.7\pm0.8\times10^4$ and the negative cells $3.2\pm0.4\times10^4$. According to the growth curve, GFP positive cells (pericytes and smooth muscle cells) proliferated much faster than the negative cells (Fig. 2b).

Multilineage Differentiation of Bone Marrow Derived α-SMA-GFP Positive Cells

Adipogenesis

Seven days after culture in adipogenic medium, the morphology of α-SMA-GFP positive cells changed into rounded and lipid drop accumulation were observed. Two weeks after induction, there were more and more lipid-filled cells (Fig. 3a). The lipids showed black on green

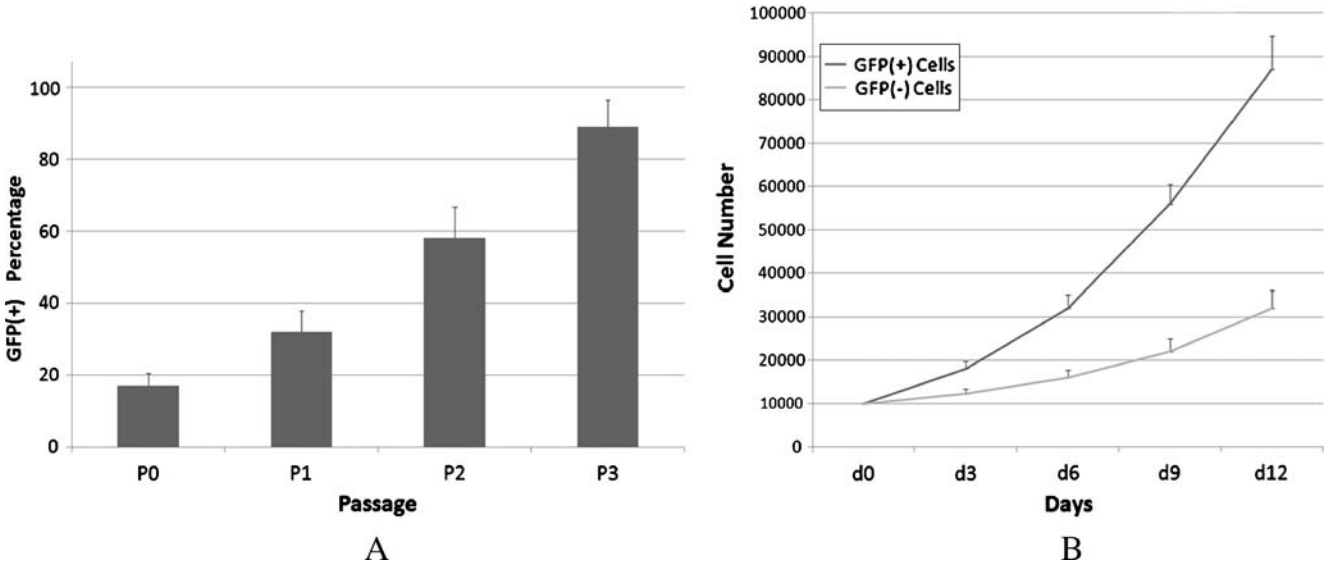

Fig. 2 The percentage of α-SMA-GFP positive cells in different passages of bone marrow stromal cells and the growth curve of α-SMA-GFP positive cells and negative cells. In the primary passage of bone marrow stromal cells, the α-SMA-GFP positive cells took part of 17±3.45%, in the passage 1, the percentage of α-SMA-GFP positive cells was 32±5.85%; in passage 2, the percentage was 58±8.61%; in the passage 3, the percentage was 89±7.53% **a**. The numbers of sorted α-SMA-GFP positive and negative cells were counted at different time points to draw the growth curve. According to the growth curve, α-SMA-GFP positive cells proliferated much faster than the negative cells **b**

fluorescence microscopic images while GFP remained positive during adipogenesis (Fig. 3b). The adipogenic differentiation was confirmed by positive Oil Red O staining with lipid drops demonstrating red on fluorescence microscopic images (Fig. 3c). The merged picture proves the α-SMA-GFP positive cells continue expressing GFP during adipogenesis (Fig. 3d). The α-SMA-GFP positive cells cultured in the control medium (α-MEM, 10%FBS) were set as control. There were no lipid drops observed in the control group. The expression of PPAR-γ and LPL was

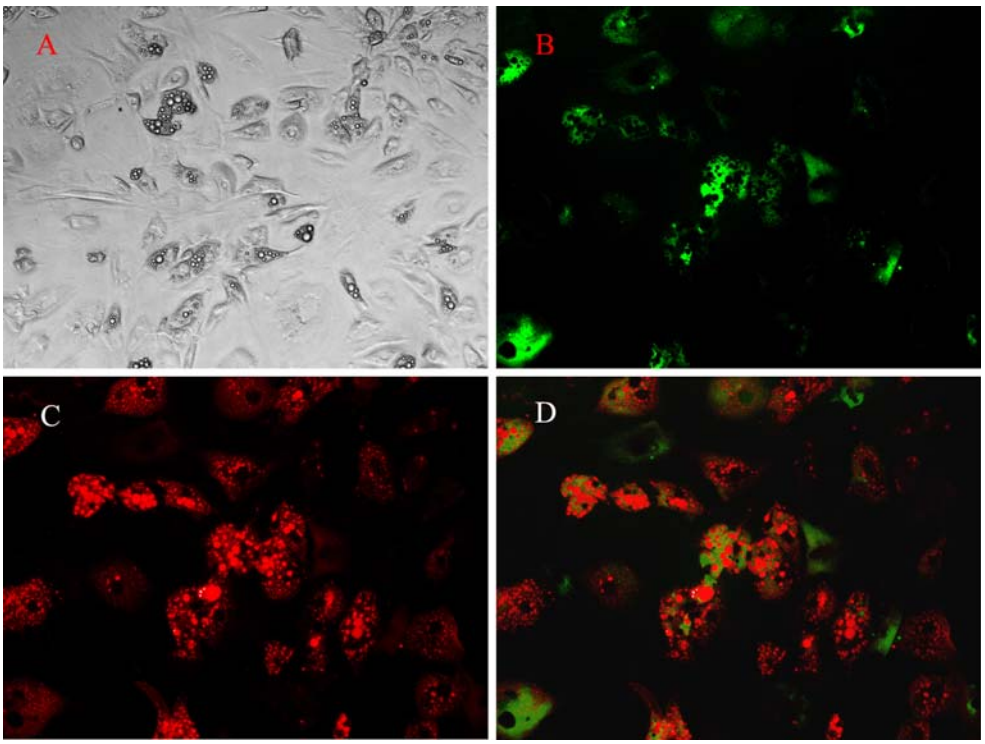

Fig. 3 Adipogenic differentiation of bone marrow derived α-SMA-GFP positive cells. **a** α-SMA-GFP positive cells were incubated two weeks in inductive medium and lipid-filled cells could be observed through light microscopic images. **b** α-SMA-GFP positive cells expressed GFP during the adipogenesis, the lipids appeared black on green fluorescence microscopic images. **c** Adipogenic differentiated α-SMA-GFP positive cells were stained positively with Oil Red O, the lipid drop showed red on red fluorescence microscopic images. **d** The merged picture proved the α-SMA-GFP positive cells still expressed the GFP during the adipogenesis

positive in induced α-SMA-GFP positive cells with no expression in the control group (Fig. 6).

Chondrogenesis

In order to prove their chondrogenic differentiation ability, α-SMA-GFP positive cells were placed in chondrogenic medium for 7 days. The cells changed their appearance from fibroblast-like into flat and multi-angled (Fig. 4a). While GFP remained positive throughout the chondrogenesis (Fig. 4b). The merged picture shows that all of the chondrogenic differentiated α-SMA-GFP positive cells also expressed the GFP. These results prove that α-SMA-GFP positive cells persisted expressing α-SMA during chodrogenic differentiation (Fig. 4c). The toluidine blue staining demonstrated that most of the cells were surrounded by proteoglycan (Fig. 4d). RT-PCR analysis of SOX9 and Col-II was positive in induced α-SMA-GFP positive cells and not observed in the control group (Fig. 6).

Osteogenesis

Bone marrow derived α-SMA-GFP positive cells were placed in osteogenic medium. After culture for 21 days, the cells became osteoblast-like in morphology, with mineralized nodules observed (Fig. 5a). At the same time, the GFP remained positive throughout osteogenesis (Fig. 5b). The merged pictures showed all of the osteogenic differentiated α-SMA-GFP positive cells also expressed the GFP; these results proved the α-SMA-GFP positive cells retained their ability to express α-SMA during osteogenic differentiation (Fig. 5c). The mineralized nodular structures were assessed by Alizarin Red-S staining (Fig. 5d). As osteogenic specific genes, OSX and OCN were observed in differentiated α-SMA-GFP positive cells and not observed in the control group (Fig. 6).

Formation of Vascular Network within the 3D Collagen/Fibronectin Gels

The ability of α-SMA-GFP positive cells to assist HUVECs in forming and maintaining a network was evaluated in vitro by loading into a 3-D collagen-fibronectin gel (Fig 7). The gels were cultured and observed under fluorescent microscopy to demonstrate the presence of an extensive network. On the second day of 3-D culture, the HUVECs began to elongate and contact with others (Fig. 7a). The α-SMA-GFP positive cells distributed along the HUVECs (Fig. 7b, c). On day 4, the HUVECs began to form tube-like structures and connected to each other (Fig. 7e); the

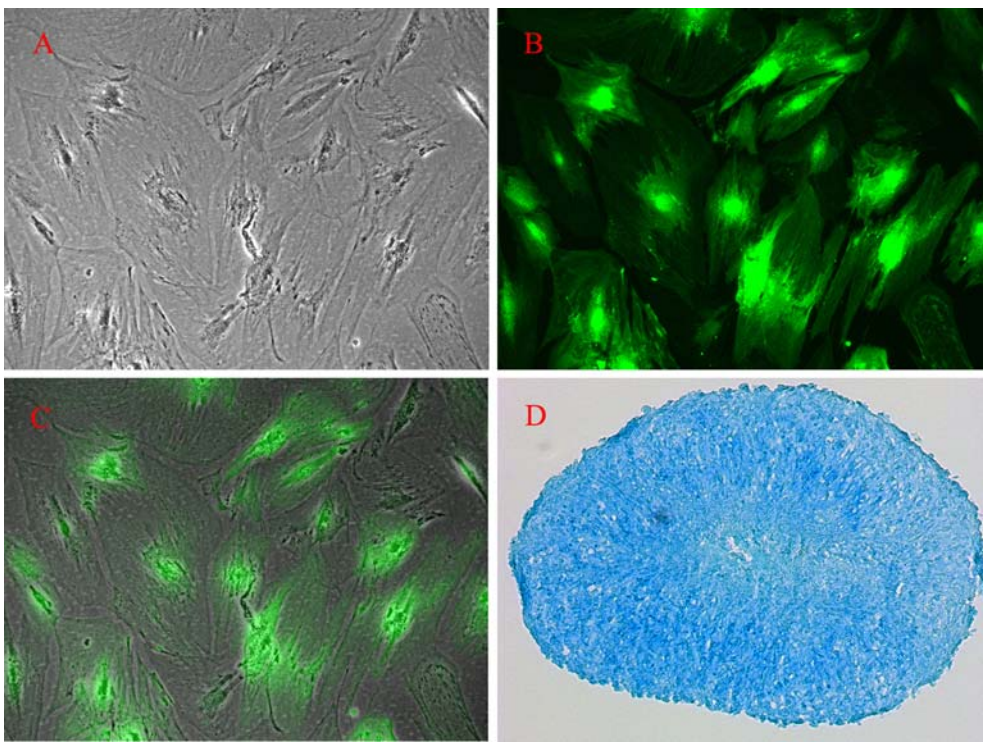

Fig. 4 Chondrogenic differentiation of α-SMA-GFP positive cells. **a** After chondrogenic induction, the cells changed their appearance from fibroblast-like into flat and multi-angle. **b** GFP was still positive during chondrogenesis. **c** The merged picture shows all of the chondrogenic differentiated α-SMA-GFP positive cells also express the GFP. **d** The toluidine blue staining of the α-SMA-GFP positive cell pellet proved the cells differentiated into chondrocytes. Most of the cells were surrounded by proteoglycan (×200)

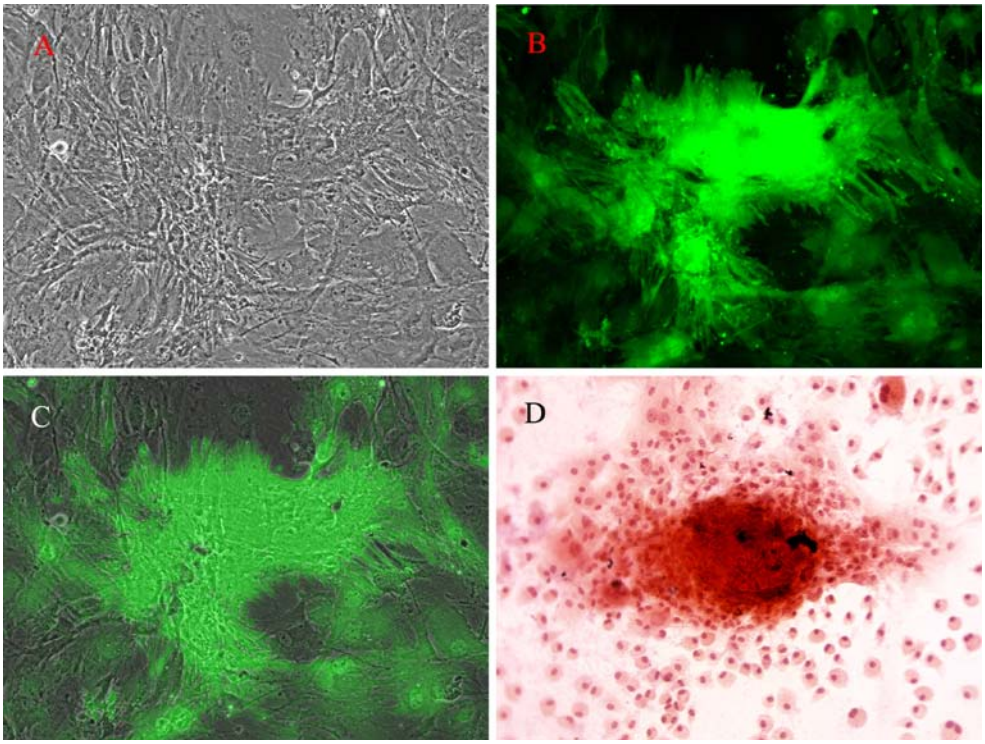

Fig. 5 Osteogenic differentiation of α-SMA-GFP positive cells. (A) After cultured in osteogenic medium for 21 days, the morphology changed from fibroblast-like to a multilateral and cuboidal form, which showed a tightly packed arrangement. **b** α-SMA-GFP positive cells still expressed GFP during osteogenic differentiation. **c** The merged picture shows that all of the osteogenic differentiated α-SMA-GFP positive cells still expressed GFP. **d** Mineralized nodule staining was positive by alizarin red S. (×200)

α-SMA-GFP positive cells proliferated quickly and distributed around the tubes (Fig. 7f, g). On day 7, the networks were primarily formed by HUVECs (Fig. 7i); the α-SMA-GFP positive cells became more condensed around the networks (Fig. 7j, k). On day 14, the robust network of HUVECs demonstrated many branches (Fig. 7m), the numbers of α-SMA-GFP positive cells were increasingly evident (Fig. 7n, o). HUVECs and α-SMA-GFP positive cells formed vessels within the 3D gel and remained stable for more than one month in vitro. Furthermore, the α-SMA-GFP positive cells had migrated to line the tubular structures formed by the HUVECs and acquired a flattened, elongated morphology with stellate processes. In the control group, HUVECs cultures without α-SMA-GFP positive cells formed small multi-cellular cords at day 1, but they were much shorter and smaller than those formed by α-SMA-GFP positive cells containing cultures; the cords were already regressing and falling apart by day 4. The HUVECs proliferated slowly and could not form vascular networks at day 7 and day 14 (Fig. 7d, h, l, p).

Discussion

Based on recent papers and our previous work, many clues suggest that adult mesenchymal stem cells may reside around the small blood vessel and may be part of the pericytes [7, 20–22]. Crisan et al. proved that mesenchymal stem cells found throughout fetal and adult tissues are members of the pericytes family of cells [7, 13]. In our study, we have found direct proof that the bone marrow derived pluripotent cells express α-SMA which is one of the markers of perivascular cells. We conclude that bone marrow mesenchymal stem cells derive from the perivas-

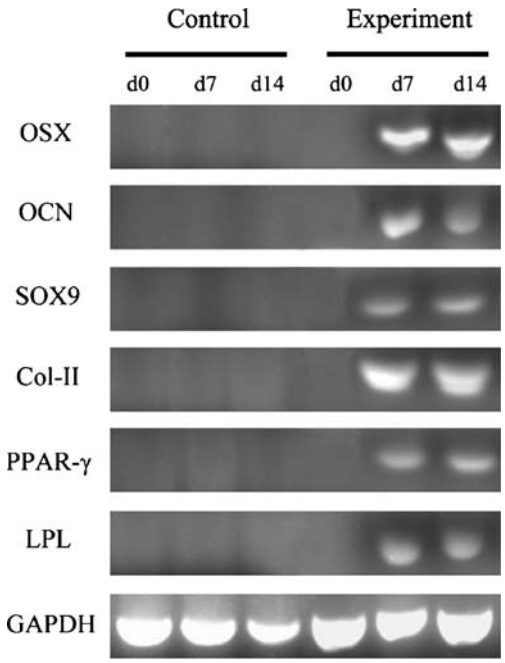

Fig. 6 RT-PCR analysis of multilineage differentiation specific genes. The differentiated α-SMA-GFP positive cells revealed upregulated expression of osteogenic (OSX, OCN), chondrogenic (SOX9, Col-IIα1) and adipogenic (PPAR-γ, LPL) differentiation specific genes. The α-SMA-GFP positive cells cultured in the control medium showed no expression of the above genes

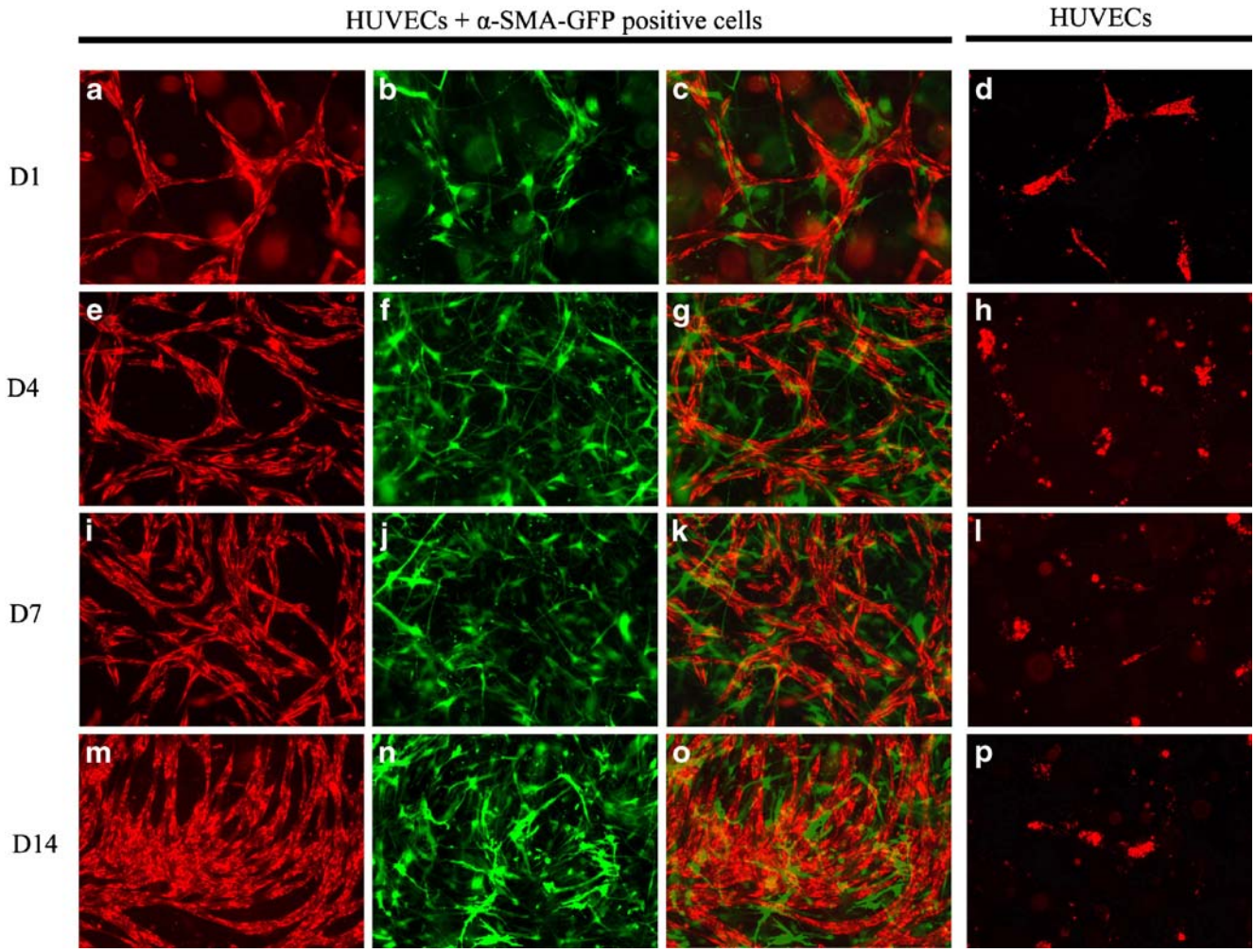

Fig. 7 Formation of vascular network within the 3D Collagen/fibronectin gels In the experiment group, the HUVECs were cultured with α-SMA-GFP positive cells. HUVECs began to elongate and contact with each other at day 1 **a**, the α-SMA-GFP positive cells distributed along the HUVECs **b, c**. At day 4, the HUVECs began to form tube-like structures and connect to each other **e**; the α-SMA-GFP positive cells proliferated quickly and distributed around the tubes **f**, **g**. At day 7, the networks were primarily formed by HUVECs **i**; the α-SMA-GFP positive cells became denser around the networks **j**, **k**. At day 14, the robust network of HUVECs and many branches were observed **m**, the numbers of α-SMA-GFP positive cells were increasingly abundant **n**, **o**. In the control group, HUVECs cultures without α-SMA-GFP positive cells formed short-lived multi-cellular cords at day 1 **d**, but they were much shorter and smaller than those formed by pericytes-containing cultures; the HUVECs proliferated slowly and could not form vascular network at day 4, day 7 and day 14 **h, l, p**

cular cells and quite probably are pericytes. But not all of the pericytes can be stem cells. So we assume that only part of the pericyte population are mesenchymal stem cells. But now we can use FACS to enrich bone marrow stem cells by some typical markers of pericytes, such as Desmin, α-SMA CD146, NG2, and PDGF-Rβ and so on [7]. We are now trying to find more specific surface proteins of bone marrow mesenchymal stem cells to further study these pericytes.

Vascularization is a process of blood vessel formation occurring by endothelial progenitor cells differentiation, migration and connection in response to stimulations (such as growth factors and cell contact) to form new blood vessels [23]. During vascularization, pericytes are recruited to surround the endothelial cells and stimulate them to proliferate and contact with each other. The pericytes still help endothelial cells to form networks and direct their maturation through direct contact and interactions [23]. The pericytes fulfill at least two important roles in assisting the vascularization: synthesis of growth factors [24, 25] and formation of the mural wall of new blood vessels [3, 7, 16, 26], both mechanisms of which are unclear at present. A number of studies have proved that direct contact and communication between ECs and pericytes/smooth muscle cells are essential to vascularization [7, 12]. The 3-D collagen gel has previously been used to create models of bone tissue engineering [19, 27]. Here we utilized the 3-D collagen-fibronectin construct to support the vascularization of α-SMA-GFP positive cells and endothelial cells. Further

work is ongoing to determine whether pre-vascularized structures can survive implantation and are able to anastomose quickly with the host vascular network.

Acknowledgements This work was funded by the Anthony and Constance Franchi Fund for Pediatric Orthopaedics at the MassGeneral Hospital for Children, The Peabody Foundation Inc., the National Natural Science Foundation of China (30801304), Foundation for the Author of National Excellent Doctoral Dissertation of PR China (FANEDD 200977) and Program for New Century Excellent Talents in University (NCET-08-0373).

References

1. Langer, R., & Vacanti, J. P. (1993). Tissue engineering. *Science, 260*(5110), 920–6.
2. Caplan, A. I. (2000). Tissue engineering designs for the future: new logics, old molecules. *Tissue Eng, 6*(1), 1–8.
3. Melero-Martin, J. M., De Obaldia, M. E., Kang, S. Y., et al. (2008). Engineering robust and functional vascular networks in vivo with human adult and cord blood-derived progenitor cells. *Circ Res, 103*(2), 194–202.
4. Traktuev, D. O., Prater, D. N., Merfeld-Clauss, S., et al. (2009). Robust functional vascular network formation in vivo by cooperation of adipose progenitor and endothelial cells. *Circ Res, 104*(12), 1410–20.
5. Armulik, A., Abramsson, A., & Betsholtz, C. (2005). Endothelial/pericyte interactions. *Circ Res, 97*(6), 512–23.
6. Levenberg, S., Rouwkema, J., Macdonald, M., et al. (2005). Engineering vascularized skeletal muscle tissue. *Nat Biotechnol, 23*(7), 879–84.
7. Crisan, M., Yap, S., Casteilla, L., et al. (2008). A perivascular origin for mesenchymal stem cells in multiple human organs. *Cell Stem Cell, 3*(3), 301–13.
8. Shepherd, B. R., Chen, H. Y., Smith, C. M., Gruionu, G., Williams, S. K., & Hoying, J. B. (2004). Rapid perfusion and network remodeling in a microvascular construct after implantation. *Arterioscler Thromb Vasc Biol, 24*(5), 898–904.
9. Tremblay, P. L., Hudon, V., Berthod, F., Germain, L., & Auger, F. A. (2005). Inosculation of tissue-engineered capillaries with the host's vasculature in a reconstructed skin transplanted on mice. *Am J Transplant, 5*(5), 1002–10.
10. Koike, N., Fukumura, D., Gralla, O., Au, P., Schechner, J. S., & Jain, R. K. (2004). Tissue engineering: creation of long-lasting blood vessels. *Nature, 428*(6979), 138–9.
11. Nguyen, L. L., & D'Amore, P. A. (2001). Cellular interactions in vascular growth and differentiation. *Int Rev Cytol, 204*, 1–48.
12. Wu, Y., Wang, J., Scott, P. G., & Tredget, E. E. (2007). Bone marrow-derived stem cells in wound healing: a review. *Wound Repair Regen, 15*(Suppl 1), S18–26.
13. Caplan, A. I. (2008). All MSCs are pericytes? *Cell Stem Cell, 3*(3), 229–30.
14. Kalajzic, Z., Li, H., Wang, L. P., et al. (2008). Use of an alpha-smooth muscle actin GFP reporter to identify an osteoprogenitor population. *Bone, 43*(3), 501–10.
15. Yokota, T., Kawakami, Y., Nagai, Y., et al. (2006). Bone marrow lacks a transplantable progenitor for smooth muscle type alpha-actin-expressing cells. *Stem Cells, 24*(1), 13–22.
16. Cai, X., Lin, Y., Ou, G., et al. (2007). Ectopic osteogenesis and chondrogenesis of bone marrow stromal stem cells in alginate system. *Cell Biol Int, 31*(8), 776–83.
17. Lin, Y., Chen, X., Yan, Z., et al. (2006). Multilineage differentiation of adipose-derived stromal cells from GFP transgenic mice. *Mol Cell Biochem, 285*(1–2), 69–78.
18. Wu L, Cai X, Dong H, et al. Serum regulates adipogenesis of mesenchymal stem cells via MEK/ERK dependent PPARgamma expression and phosphorylation. J Cell Mol Med 2009.
19. Verseijden F, Posthumus-van Sluijs S, Pavljasevic P, Hofer S, van Osch G, Farrell E. Adult human bone marrow- and adipose tissue-derived stromal cells support the formation of prevascular-like structures from endothelial cells in vitro. Tissue Eng Part A 2009.
20. Lin, Y. F., Jing, W., Wu, L., et al. (2008). Identification of osteo-adipo progenitor cells in fat tissue. *Cell Prolif, 41*(5), 803–12.
21. Tang, W., Zeve, D., Suh, J. M., et al. (2008). White fat progenitor cells reside in the adipose vasculature. *Science, 322*(5901), 583–6.
22. Rodeheffer, M. S., Birsoy, K., & Friedman, J. M. (2008). Identification of white adipocyte progenitor cells in vivo. *Cell, 135*(2), 240–9.
23. von Tell, D., Armulik, A., & Betsholtz, C. (2006). Pericytes and vascular stability. *Exp Cell Res, 312*(5), 623–9.
24. Caplan, A. I. (2009). Why are MSCs therapeutic? New data: new insight. *J Pathol, 217*(2), 318–24.
25. Haynesworth, S. E., Baber, M. A., & Caplan, A. I. (1996). Cytokine expression by human marrow-derived mesenchymal progenitor cells in vitro: effects of dexamethasone and IL-1 alpha. *J Cell Physiol, 166*(3), 585–92.
26. Rouwkema, J., de Boer, J., & Van Blitterswijk, C. A. (2006). Endothelial cells assemble into a 3-dimensional prevascular network in a bone tissue engineering construct. *Tissue Eng, 12*(9), 2685–93.
27. Akita, M., Murata, E., Merker, H. J., & Kaneko, K. (1997). Formation of new capillary-like tubes in a three-dimensional in vitro model (aorta/collagen gel). *Ann Anat, 179*(2), 137–47.

5 Curriculum vitae

Der Lebenslauf wurde aus Datenschutzgründen in der elektronischen Version entfernt.

Der Lebenslauf wurde aus Datenschutzgründen in der elektronischen Version entfernt.

Der Lebenslauf wurde aus Datenschutzgründen in der elektronischen Version entfernt.

6 Vollständige Publikationsliste

6.1 Publikationen der Promotion

1. Friedrich C, Lin Y, Krannich A, Wu Y, Vacanti JP, Neville CM, Enhancing engineered vascular networks *in vitro* and *in vivo*: The effects of IGF1 on vascular development and durability, Cell Prolif. 2017 Nov 7. doi: 10.1111/cpr.12387. [Epub ahead of print].

2. Tsigkou O, Pomerantseva I, Spencer JA, Redondo PA, Hart AR, O'Doherty E, Lin Y, Friedrich C, Daheron L, Lin CP, Sundback CA, Vacanti JP, Neville C, Engineered vascularized bone grafts, Proc Natl Acad Sci U S A. 2010 Feb 23;107(8):3311-6. doi: 10.1073/pnas.0905445107. Epub 2010 Feb 2. PMID: 20133604

3. Cai Y, Lin Y, Friedrich C, Neville C, Pomerantseva I, Sundback CA, Zhang Z, Vacanti JP, Hauschka PV, Grottkau BE, Bone marrow derived pluripotent cells are pericytes which contribute to vascularization, Stem Cell Review, 2009 Dec;5(4):437-45. doi: 10.1007/s12015-009-9097-6. Erratum in: Stem Cell Rev. 2009 Dec;5(4):435-6. PMID: 20058207

4. Grottkau BE, Chen XR, Friedrich C, Yang XM, Jing W, Wu Y, Cai XX, Liu YR, Huang YD, Lin YF, DAPT enhances the apoptosis of human tongue carcinoma cells, Int J Oral Sci. 2009 Jun;1(2):81-9. doi: 10.4248/ijos.08025. PMID: 20687300

6.2 Publizierte Abstracts

1. Friedrich C, Lin Y, Neville CM, Salanova M, Vacanti JP, Blottner D. Enhancing engineered vascular networks *in vitro* and *in vivo*. The effects of IGF1 on vascular development. 9th World Congress for Microcirculation 2010. PS1-84.

2. Friedrich C, Breaking the Wall of Engineered Organs 2.0. Falling Walls Lab 2013. 15.

7 Danksagung

An dieser Stelle möchte ich mich herzlich bedanken bei all denjenigen, die mich auf dem Weg zur Promotion unterstützt haben. Der wohl größte Dank gilt meinen Mentoren, Dozenten, Kollegen und Freunden, die mich begleitet, inspiriert, beraten und in schwereren Zeiten moralisch unterstützt haben. Mein besonderer Dank Herrn Prof. Dr. med. Hilmar Stolte, meinem verstorbenen Doktorvater, der mich wissenschaftlich und menschlich sehr beeinflusst hat. Auch Herrn Dr. Joseph P. Vacanti danke ich für seine immerwährende Unterstützung und herausragende wissenschaftliche Inspiration. Herrn Dr. Craig M. Nevilles jahrelange außerordentlich kompetente fachliche Betreuung meiner Projekte und Unterstützung der Publikationspromotion weiß ich sehr zu schätzen. Für die freundschaftliche und kollegiale Zusammenarbeit, den regen fachlichen Austausch sowie die strategische Entwicklung meines Forschungsprojektes danke ich Herrn Prof. Yunfeng Lin und dem Team des Laboratory of Tissue Engineering and Organ Fabrication am Massachusetts General Hospital sehr herzlich. Herrn Prof. Dr. rer. nat. Otmar Huber und Herrn Prof. Dr. rer. nat. Dieter Blottner danke ich für die Möglichkeit, in ihren Laboren zahlreiche molekularbiologische und auch immunhistochemische Methoden kennengelernt und gefestigt zu haben. Darüber hinaus möchte ich mich sehr herzlich bedanken bei Herrn PD Dr. med. Andreas Weimann für die vielen fachlichen Anregungen und die Unterstützung rund um das Promotionsvorhaben. Herrn Prof. Dr. med. Michael Walter danke ich sehr für die hilfreichen Anregungen und die Unterstützung beim Feinschliff des Manteltextes. Herrn Dr. med. Ijad Madisch danke ich für die konstruktiven und einsichtsreichen Gespräche über das gemeinsame Forschungsfeld sowie die Empfehlung an und Vermittlung des Labors. Auch danke ich Frau Prof. Dr. med. Claudia Spies, Herrn PD Dr. med. Falk von Dincklage und Herrn Prof. Dr. med. Roland Francis für die fachliche und auch moralische Unterstützung und die konstruktiven Dialoge. Ein besonderer Dank gilt weiterhin meinem dritten Doktorvater, Herrn PD Dr. med. Moritz Schmelzle, der mir in außerordentlichem Maße in den Endzügen meiner Publikationspromotion zur Seite gestanden hat. Zudem möchte ich noch meinen Eltern danken für alles und auch meinen früheren Lehrern des Gymnasium Steglitz, die mich weit über die Schule und das Studium hinaus begleitet haben. Namentlich erwähnen möchte ich insbesondere Herrn Dr. Rosumek und Herrn Faller, ohne die mir viele Facetten der alten Sprachen und damit des Denkens, der Gesellschaft, der Philosophie und auch zahlreiche Weisheiten des Lebens verborgen geblieben wären sowie Herrn Heß und Herrn Dr. Gey für die exzellente Betreuung und Vorbereitung auf das Studium. Zuletzt möchte ich mich auch bei allen anderen bedanken, die mich unterstützt haben und aus Platzgründen keine namentliche Erwähnung finden können. Ihre Unterstützung wird dennoch sehr geschätzt.